

Dielectric continuum methods for quantum chemistry

John M. Herbert*

Department of Chemistry and Biochemistry, The Ohio State University, Columbus, Ohio, USA

March 15, 2022

Abstract

This review describes the theory and implementation of implicit solvation models based on continuum electrostatics. Within quantum chemistry this formalism is sometimes synonymous with the polarizable continuum model, a particular boundary-element approach to the problem defined by the Poisson or Poisson-Boltzmann equation, but that moniker belies the diversity of available methods. This work reviews the current state-of-the art, with emphasis on theory and methods rather than applications. The basics of continuum electrostatics are described, including the nonequilibrium polarization response upon excitation or ionization of the solute. Nonelectrostatic interactions, which must be included in the model in order to obtain accurate solvation energies, are described as well. Numerical techniques for implementing the equations are discussed, including linear-scaling algorithms that can be used in classical or mixed quantum/classical biomolecular electrostatics calculations. Anisotropic models that can describe interfacial solvation are briefly described.

Contents

1	Overview	2
2	Continuum Electrostatics	4
2.1	Poisson's equation	4
2.2	Solute cavity	7
2.3	Polarizable continuum models	10
2.4	Comparison of ASC-PCMs	15
3	Implementation	16
3.1	Matrix equations for PCMs	16
3.2	Discretization	19
3.3	Isodensity and self-consistent cavity surfaces	22
3.4	Linear-scaling algorithms	24
4	Solvation Energies	26
4.1	SM _x and SASA-based models	28
4.2	Physics-based models	31

*herbert@chemistry.ohio-state.edu

5	Nonequilibrium Solvation	36
5.1	Conceptual overview	36
5.2	State-specific approach	38
5.3	Linear response approach	47
6	Anisotropic Solvation	48
7	Closing remarks	50
	References	51

1 Overview

The use of dielectric continuum models in quantum chemistry dates to the mid-1970s,^{1–6} to when the field itself was still in its infancy. In their simplest form, these models describe the solvent in terms of a single parameter ε_s , the (static) dielectric constant, a dimensionless quantity equal to the electric permittivity relative to vacuum and ranging (for simple liquids) from $\varepsilon_s \approx 2$ for non-polar solvents such as benzene and hexane, up to $\varepsilon_s = 78$ for water and $\varepsilon_s = 110$ for formamide. This constant describes the solvent’s ability to screen a charge, and the Coulomb interaction between charges Q_1 and Q_2 separated by a distance r is modified from $V(r) = Q_1 Q_2 / 4\pi \varepsilon_0 r$ in the gas phase, to an attenuated version $V(r) = Q_1 Q_2 / 4\pi \varepsilon_0 \varepsilon_s r$ within the dielectric medium. The continuum description represents the ultimate in coarse-graining, reducing the solvent to a single parameter, which has obvious utility in a quantum chemistry calculation whose cost rises steeply with system size. Within a continuum description, there is no need for sampling over solvent degrees of freedom (*e.g.*, solvent reorganization in response to an electron transfer event that modifies the solute’s charge distribution), because this averaging is implicitly encoded into the value of ε_s . While advantageous from the standpoint of cost, limitations of the continuum description are equally apparent: “specific” solvation effects such as hydrogen bonding are not captured, and dielectric continuum theory alone does not describe nonelectrostatic interactions including dispersion and Pauli repulsion. Without the latter, there is nothing to imbue the molecules with finite size, necessitating *ad hoc* introduction of a “solute cavity” to define the interface between the atomistic solute and the continuum solvent, as depicted in Fig. 1.

Some of the aforementioned limitations can be overcome, in principle, by admission of a small number of explicit solvent molecules into the atomistic part of the calculation, in what is often called a “semicontinuum” or a “cluster + continuum” approach.⁸ As such, the continuum description serves as a flexible and highly useful starting point for the description of solvation effects in quantum chemistry. Introduction of continuum solvation models into quantum chemistry was led by the group of Tomasi in Pisa,^{9–16} who refer to this approach as the *polarizable continuum models* (PCM). That terminology will be introduced in Section 2.3, to refer to a particular class of continuum solvation models that replace the three-dimensional partial differential equations of continuum electrostatics with a two-dimensional boundary element problem, defined on the surface of a cavity representing the interface between atomistic solute and continuum solvent. Although PCMs are ubiquitous in quantum chemistry, they are not the only continuum solvation models that are used in the field and not the only ones discussed herein. In any case, the combination of a quantum-mechanical (QM) description of the solute sets up a *self-consistent reaction-field* (SCRF) problem in which the solute’s charge distribution both polarizes, and is polarized by, its environment. The two effects must be iterated to self-consistency.

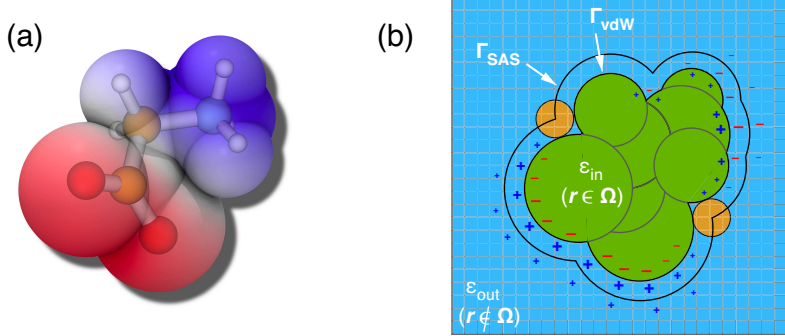


Fig. 1: (a) Zwitterionic tautomer of glycine ($-\text{O}_2\text{CCH}_2\text{NH}_3^+$) in a molecular cavity constructed from atom-centered spheres. Coloring reflects the sign and magnitude of the molecular electrostatic potential evaluated at the cavity surface, $\varphi^\rho(\mathbf{s})$ for $\mathbf{s} \in \Gamma$. (b) Schematic illustration of the same molecular cavity (in green) embedded in a dielectric medium (in blue), illustrating how the continuum polarizes in response to the solute's electrostatic potential. The orange probe sphere illustrates how the atomic radii that define the van der Waals (vdW) cavity surface might be augmented to afford a “solvent-accessible surface” (SAS). The region interior to the solute cavity is designated as Ω , and for a sharp dielectric interface one sets $\epsilon(\mathbf{r}) \equiv \epsilon_{\text{in}}$ for $\mathbf{r} \in \Omega$. If the solute is described using quantum chemistry then the natural choice is $\epsilon_{\text{in}} = 1$. Outside of the cavity, the permittivity function $\epsilon(\mathbf{r})$ takes the value ϵ_{out} , which is usually the static dielectric constant of the solvent, ϵ_s . Panel (b) is adapted from Ref. 7; copyright 2008 John Wiley & Sons.

The remainder of this review is organized as follows. Section 2 provides the elementary specification of the continuum electrostatics problem, starting from the Poisson and Poisson-Boltzmann equations. The mechanics of turning that formalism into a computationally-tractable model are discussed in Section 3, with an emphasis on the smooth discretization approach developed by this author’s group.^{17–21} The focus here is on continuum solvation models in quantum chemistry but the formalism in Sections 2 and 3 is perfectly applicable to biomolecular implicit solvent calculations, in which a macromolecular solute is described using a classical force field.¹⁹ Section 3 also introduces the various flavors of PCM that can be found in the literature and discusses how they can be understood in one another’s context. It should be noted that the solution of Poisson’s equation, or equivalently the apparent surface charge PCM problem, specifies only the *electrostatic* contribution to the solvation energy. Other contributions including cavitation, dispersion, Pauli repulsion, and hydrogen bonding must be included in order to predict free energies of solvation ($\Delta_{\text{solv}}\mathcal{G}$) in reasonable agreement with experiment. Section 4 introduces models for these nonelectrostatic contributions and provides an overview of the accuracy that can be expected for $\Delta_{\text{solv}}\mathcal{G}$. Section 5 introduces several “nonequilibrium” formulations of the continuum electrostatics problem, which are used to describe the continuum’s response to a sudden change in the solute’s charge density, as in photoexcitation or photoionization. This provides the machinery to compute solvent effects on vertical excitation, ionization, or fluorescence energies. Finally, Section 6 discusses modifications to the isotropic continuum model that are necessary in order to describe anisotropic solvation environments, such as the air/water interface or the solid-state/aqueous interface.

This review is focused on the theoretical framework and computational mechanics of continuum solvation models, not on applications. While some limited data to describe the performance of the models are provided, for a complete overview of continuum solvation methods in action, the reader is directed to several general reviews,^{8,13–15,22–24} as well as specialized ones concerning the application of PCMs to specific types of spectroscopy.^{25–31} In lieu of a great deal of data, the present work

provides copious references to the primary literature.

2 Continuum Electrostatics

This section reviews the basic electrostatic formalism that underlies continuum solvation theory. The physical model is defined by Poisson's equation in three-dimensional space (Section 2.1) but is not fully specified without a surface to demarcate the boundary of the atomistic region (Section 2.2). The *polarizable continuum models* that were introduced into quantum chemistry by Tomasi and co-workers^{6,9,13} are introduced in Section 2.3, and stem from a reformulation of the Poisson problem as a boundary-element of “apparent surface charge” problem. There are several variants, and these are compared side-by-side in Section 2.4.

2.1 Poisson's equation

The basic tenet of dielectric continuum theory is an assumption that the electric response of matter can be coarse-grained in the form of a dipole density \mathbf{P} that defines the polarization of the medium. In the presence of this dielectric medium, the role of the electric field $\mathbf{E}(\mathbf{r})$ in vacuum is supplanted by the electric displacement field (or electric induction),

$$\mathbf{D}(\mathbf{r}) = \mathbf{E}(\mathbf{r}) + 4\pi\mathbf{P}(\mathbf{r}) = \varepsilon(\mathbf{r})\mathbf{E}(\mathbf{r}) . \quad (2.1)$$

The electric permittivity $\varepsilon(\mathbf{r})$ is defined by the manner in which polarization $\mathbf{P}(\mathbf{r})$ is induced by the external field $\mathbf{E}(\mathbf{r})$, and Eq. (2.1) amounts to the definition of a *linear* dielectric material whose polarization is proportional to field strength. Nonlinear susceptibilities are harder to describe within a continuum formalism and have received less attention.¹³ Whereas a fully general discussion of (linear) dielectric materials would allow for a permittivity that is a function of frequency also (or even a nonlocal function of space and/or time, in some formulations),^{32–34} the ground-state SCRF problem does not require this generality, and unless otherwise specified, ε will mean the *static* (zero-frequency) dielectric constant, ε_s . (The continuum electrostatics community has stubbornly defied the suggestion³⁵ that “dielectric constant” is obsolete and should be replaced by “relative electric permittivity”.) For an anisotropic medium, ε would take the form of a 3×3 tensor rather than scalar, which could be used to model a liquid crystal in which the electric susceptibility depends on the orientation of the applied field.^{36,37} This review will not consider such cases, although a different form of anisotropic solvation is considered in Section 6. Herein, ε is a scalar.

That said, Eq. (2.1) does express the permittivity as a scalar-valued *function*, $\varepsilon(\mathbf{r})$, rather than simply a dielectric *constant*. This allows for a situation such as that depicted in Fig. 1(b), wherein a “solute cavity” (two-dimensional surface $\mathbf{\Gamma}$) defines an interface between the continuum solvent and an atomistic region, the latter of which shall be described using quantum chemistry. Within the cavity, inter-particle Coulomb interactions are included explicitly in the Hamiltonian and thus $\varepsilon = 1$ in this region. Outside of the cavity, the permittivity function takes on a value equal to the (static) dielectric constant of the solvent, *e.g.*, $\varepsilon = 78$ for water. Given a charge density $\rho(\mathbf{r})$ for the solute, including both nuclei and electrons, Maxwell's equation for the displacement field $\mathbf{D}(\mathbf{r})$ is

$$\hat{\nabla} \cdot \mathbf{D}(\mathbf{r}) = 4\pi\rho(\mathbf{r}) . \quad (2.2)$$

Recognizing that the electric field is $\mathbf{E}(\mathbf{r}) = -\hat{\nabla}\varphi(\mathbf{r})$, where $\varphi(\mathbf{r})$ is the *electrostatic potential*, Eq. (2.2) can be written in the more familiar form of *Poisson's equation*,

$$\hat{\nabla} \cdot [\varepsilon(\mathbf{r}) \hat{\nabla}\varphi(\mathbf{r})] = -4\pi\rho(\mathbf{r}) . \quad (2.3)$$

All of these equations are expressed in Gaussian electrostatic units, where $4\pi\epsilon_0 = 1$.³⁸

Poisson's equation is the mathematical starting point for continuum electrostatics. Given the charge density $\rho(\mathbf{r})$ from an electronic structure calculation, Eq. (2.3) is solved for $\varphi(\mathbf{r})$ throughout space, including both the atomistic region and the surrounding dielectric medium. This potential can be separated into two parts,

$$\varphi(\mathbf{r}) = \varphi^\rho(\mathbf{r}) + \varphi_{\text{rxn}}(\mathbf{r}) , \quad (2.4)$$

where the first term is the electrostatic potential generated by the solute's charge density,

$$\varphi^\rho(\mathbf{r}) = \int \frac{\rho(\mathbf{r}')}{\|\mathbf{r} - \mathbf{r}'\|} d\mathbf{r}' , \quad (2.5)$$

whereas the “reaction field” contribution $\varphi_{\text{rxn}}(\mathbf{r})$ arises from polarization of the continuum, resulting in an additional charge density $\rho_{\text{pol}}(\mathbf{r})$. Having obtained $\rho(\mathbf{r})$ from Schrödinger's equation and then $\varphi(\mathbf{r})$ by solving Eq. (2.3), the electrostatic solvation energy can be expressed variously as^{18,39}

$$\mathcal{G}_{\text{elst}} = \frac{1}{2} \int \varphi_{\text{rxn}}(\mathbf{r}) \rho(\mathbf{r}) d\mathbf{r} = \frac{1}{2} \int \varphi^\rho(\mathbf{r}) \rho_{\text{pol}}(\mathbf{r}) d\mathbf{r} . \quad (2.6)$$

This is sometimes alternatively called the *polarization energy* (\mathcal{G}_{pol}),¹⁸ but we will use the term *electrostatic energy* ($\mathcal{G}_{\text{elst}}$) as that is the nomenclature typically encountered in the literature on dielectric materials.³⁸ Unlike the theory of intermolecular interactions,⁴⁰ it makes little sense in the present context to consider electrostatics separate from polarization but the reader may, if desired, substitute the phrase “electrostatics + polarization” whenever “electrostatics” is used herein. The quantity $\mathcal{G}_{\text{elst}}$ is a *free* energy insofar as the dielectric formalism implicitly accounts for the averaging over solvent degrees of freedom, and the factor of 1/2 in Eq. (2.6) reflects the fact that the interaction energy is reduced, by precisely half its value, on account of the work required to polarize the environment.^{9,18,41,42}

From the point of view of electronic structure theory, $\mathcal{G}_{\text{elst}}[\epsilon, \rho]$ is a functional of both the permittivity function $\epsilon(\mathbf{r})$ and the solute's charge density $\rho(\mathbf{r})$. The total (free) energy is

$$\mathcal{G}_0[\Psi] = \langle \Psi | \hat{\mathcal{H}}_{\text{vac}} | \Psi \rangle + \mathcal{G}_{\text{elst}}[\epsilon, \rho] , \quad (2.7)$$

where the first term represents the electronic energy *in vacuo*. (It is written here in a form that suggests wave function quantum mechanics but could be replaced by a density functional.) This can equivalently be expressed as a total energy functional

$$\mathcal{G}_0[\Psi] = \langle \Psi | \hat{\mathcal{H}}_{\text{vac}} + \frac{1}{2} \hat{\mathcal{R}}_0 | \Psi \rangle \quad (2.8)$$

where $\hat{\mathcal{R}}_0$ is a reaction-field operator that generates the integral in Eq. (2.6). Minimization of $\mathcal{G}_0[\Psi]$, or $\mathcal{G}_0[\rho]$ in density functional theory (DFT), in conjunction with Poisson's equation to obtain the electrostatic potential that defines $\hat{\mathcal{R}}_0$, defines the SCRF problem. Provided that the electronic structure model satisfies a variational principle, as it does for self-consistent field (SCF) models, then the total energy defined by Eq. (2.7) satisfies a variational principle as well,^{18,43}

Equation (2.3) is sometimes called the “generalized” form of Poisson's equation, with the “ordinary” form being

$$\epsilon \hat{\nabla}^2 \varphi(\mathbf{r}) = -4\pi\rho(\mathbf{r}) . \quad (2.9)$$

The distinction is that the permittivity function $\epsilon(\mathbf{r})$ in Eq. (2.3) is replaced in Eq. (2.9) by a scalar, ϵ . It is the latter equation that is often taken to define the continuum electrostatics problem, but this requires additional specification because $\epsilon = 1$ for the atomistic interactions. Some sort of

molecular surface is needed to delineate the boundary with the continuum, as shown in Fig. 1 where the cavity is defined by a union of atom-centered spheres. Given a cavity surface, Eq. (2.9) is shorthand for Eq. (2.3) with the permittivity function

$$\varepsilon(\mathbf{r}) = \begin{cases} \varepsilon_{\text{in}}, & \mathbf{r} \in \Omega \\ \varepsilon_{\text{out}}, & \mathbf{r} \notin \Omega \end{cases} . \quad (2.10)$$

Note that $\varphi(\mathbf{r})$ is continuous across the cavity surface but its derivative is not.⁹ In general it makes sense to take $\varepsilon_{\text{in}} = 1$ although larger values (commonly $\varepsilon_{\text{in}} = 2\text{--}4$,^{7,44,45} but in some cases $\varepsilon_{\text{in}} = 10\text{--}20$ ^{45\text{--}48}) have sometimes been used in biomolecular electrostatics calculations, in an effort to approximate a “dielectric constant of protein”. (However, the very concept that such a “constant” exists has been vociferously criticized.^{44,49\text{--}52}) If the solute is described using quantum mechanics, however, then any choice other than $\varepsilon_{\text{in}} = 1$ represents an inconsistent treatment of the Coulomb interactions unless the Coulomb operators that define \mathcal{H}_{vac} are modified, which is seldom done.

Although we have introduced it as a quantum-mechanical SCRF problem that must be solved in tandem with the electronic structure problem, Eq. (2.3) is also used in classical electrostatics calculations for biomolecules,^{53\text{--}56} where $\rho(\mathbf{r})$ is comprised of classical point charges (or higher-order multipoles^{57,58}) that come from a force field, *e.g.*,

$$\rho(\mathbf{r}) = \sum_A^{\text{atoms}} Q_A \delta(\mathbf{r} - \mathbf{R}_A) . \quad (2.11)$$

For biomolecular applications, one is often interested in an aqueous solvent containing some concentration of dissolved ions. The continuum analogue of that situation is described by the *Poisson-Boltzmann equation*,^{7,59\text{--}62}

$$\hat{\nabla} \cdot [\varepsilon(\mathbf{r}) \hat{\nabla} \varphi(\mathbf{r})] = -4\pi [\rho(\mathbf{r}) + \rho_{\text{ions}}(\mathbf{r})] , \quad (2.12)$$

in which the right side of Eq. (2.3) has been augmented with a term that accounts for a thermal distribution of dissolved ions.^{7,60} Whereas the solute’s charge density $\rho(\mathbf{r})$ reflects atomistic modeling, using either a classical force field or else an electronic structure calculation, the density $\rho_{\text{ions}}(\mathbf{r})$ of “mobile” ions is treated statistically.^{60,63} For an electrolyte with dissolved ion concentrations $\{c_i\}$, whose ionic charges are denoted $\{q_i\}$, the statistical charge density for the ions is⁷

$$\rho_{\text{ions}}(\mathbf{r}) = \sum_i^{\text{ions}} q_i c_i \lambda_i(\mathbf{r}) \exp\left(\frac{-q_i \varphi(\mathbf{r})}{k_B T}\right) . \quad (2.13)$$

The *ion accessibility function* $\lambda_i(\mathbf{r})$ represents some type of step function that serves to exclude the ions from the atomistic region. With this form for the density of mobile ions, Eq. (2.12) is sometimes known as the *size-modified* version of the (nonlinear) Poisson-Boltzmann equation.^{7,64} In the case of a 1:1 electrolyte with monovalent ions ($q_1 = e = -q_2$), Eq. (2.13) reduces to

$$\rho_{\text{ions}}(\mathbf{r}) = -2c \lambda(\mathbf{r}) \sinh\left(\frac{e \varphi(\mathbf{r})}{k_B T}\right) . \quad (2.14)$$

At the physiological ionic strengths, the hyperbolic sine function can be linearized without significant error,^{65,66} resulting in a linearized Poisson-Boltzmann equation,^{7,62}

$$\hat{\nabla} \cdot [\varepsilon(\mathbf{r}) \hat{\nabla} \varphi(\mathbf{r})] = -4\pi \rho(\mathbf{r}) + \kappa^2 \lambda(\mathbf{r}) \varphi(\mathbf{r}) , \quad (2.15)$$

where

$$\kappa = \left(\frac{8\pi e^2 c}{k_B T} \right)^{1/2}. \quad (2.16)$$

The dissolved ions screen electrostatic interactions over a length scale $\sim \kappa^{-1}$ known as the *Debye screening length*, such that the potential that appears in Debye-Hückel theory is the attenuated Coulomb potential $e^{-\kappa r}/(\epsilon_s r)$.^{7,60,67,68}

Within the biomolecular electrostatics community there has been significant discussion regarding the accuracy of the linearization approximation, with studies noting that the nonlinear form [Eq. (2.12), with Eq. (2.13) for $\rho_{\text{ions}}(\mathbf{r})$] affords better agreement with explicit solvent simulations when the ionic strength is high.^{66,69} Deficiencies in the Poisson-Boltzmann model itself—even even in its nonlinear form and especially for polyvalent ions—have also been pointed out.⁷⁰ It is therefore worth noting that for the small solutes that characterize most quantum chemistry applications, the effect of the mobile ions on $\mathcal{G}_{\text{elst}}$ is quite modest,^{64,68} although there are effects on activity coefficients.^{64,71} These effects are presumably magnified for a solute the size of a protein, but the intermediate size regime has hardly been explored.

Methods for solving the partial differential equations introduced in this section will be introduced below. First, however, we need to discuss one more aspect of the model problem itself, namely, the definition a surface that establishes the boundary between atomistic solute and continuum solvent.

2.2 Solute cavity

For the case of a sharp dielectric boundary, Eq. (2.3) has an analytic solution if the cavity surface is spherical and contains the entire charge density $\rho(\mathbf{r})$. For a solute consisting of a single point charge, Q , centered in a spherical cavity of radius \bar{R} in a medium with dielectric constant ϵ , this solution affords the well-known “Born model” for ion solvation,^{72,73}

$$\Delta \mathcal{G}_Q = -\frac{Q^2}{2\bar{R}} \left(\frac{\epsilon - 1}{\epsilon} \right). \quad (2.17)$$

Here, $\Delta \mathcal{G}$ indicates the change in $\mathcal{G}_{\text{elst}}$ from its gas-phase value of zero to the solution-phase value obtained from Eq. (2.6). Replacing the point charge Q by a point dipole μ , the solvation energy is

$$\Delta \mathcal{G}_\mu = -\frac{(\epsilon - 1)\mu^2}{(2\epsilon + 1)\bar{R}^3}. \quad (2.18)$$

(This result is often attributed to Onsager,⁷⁴ although it was derived a few years earlier by Bell.⁷⁵) The dipole solvation energy can alternatively be written $\Delta \mathcal{G}_\mu = -\frac{1}{2}(\boldsymbol{\mu} \cdot \mathbf{E}_{\text{rxn}})$, where

$$\mathbf{E}_{\text{rxn}} = \underbrace{\frac{1}{\bar{R}^3} \left(\frac{2(\epsilon - 1)}{2\epsilon + 1} \right)}_{g_1(\epsilon, \bar{R})} \boldsymbol{\mu} = g_1(\epsilon, \bar{R}) \boldsymbol{\mu} \quad (2.19)$$

is the “reaction field” induced by $\boldsymbol{\mu}$.⁴¹ If $\boldsymbol{\mu}$ is polarizable ($\boldsymbol{\mu} = \boldsymbol{\mu}_0 + \boldsymbol{\alpha} \cdot \mathbf{E}$), then Eq. (2.19) provides the earliest example of a SCRF model.⁴¹ Historically, this model was used to formulate a microscopic theory for the dielectric constant of a polar liquid,^{74,76,77} going beyond the mean-field description contained in the Clausius-Mossotti equation.^{78,79} These attempts were not particularly quantitative,⁷⁷ and for modern purposes a dipolar description of the solute constitutes a needless approximation.

The aforementioned results for ΔG were quickly generalized by Kirkwood,^{80–82} and later by others,^{57,83–87} to an arbitrary multipole in a spherical cavity, with the general result

$$G_{\text{elst}} = -\frac{1}{2} \sum_{\ell \geq 0} \underbrace{\left[\frac{(\ell+1)(\varepsilon-1)}{\ell + (\ell+1)\varepsilon} \right]}_{g_\ell(\varepsilon, \bar{R})} \frac{1}{\bar{R}^{2\ell+1}} \sum_{m=-\ell}^{\ell} |\langle \Psi | \hat{T}_{\ell m} | \Psi \rangle|^2 \quad (2.20)$$

where the $\hat{T}_{\ell m}$ are spherical multipole operators.^{88,89} Since then, analytic results for ellipsoidal cavities,^{82,84} off-center charges,⁸¹ and higher-order off-center multipoles⁸⁷ have also been derived, along with formulas for the interaction of multipoles contained in disjoint spheres with a dielectric medium in between.⁹⁰ Insofar as an arbitrary charge distribution $\rho(\mathbf{r})$ has a single-center multipole expansion, these results provide an analytic solution for a charge density of arbitrary complexity in a spherical or ellipsoidal cavity, assuming there is no penetration of $\rho(\mathbf{r})$ into the continuum region. (The latter effect, known as *volume polarization*,^{91–97} is discussed below.) The multipole expansion method has been called a “generalized Kirkwood” solvation model,⁵⁷ and using multipolar formulas for $\hat{\mathcal{R}}_0$ in Eq. (2.8), it can be turned into a generalized Kirkwood SCRF for quantum chemistry. Multipolar methods are reviewed elsewhere,^{9,98} but have effectively been rendered obsolete by the polarizable continuum methods described in Section 2.3. In the absence of volume polarization, these approaches also afford an exact (albeit numerical) solution to the continuum electrostatics problem, yet can be used in conjunction with molecule-shaped cavities.

A spherical cavity may make sense if a large number of explicit solvent molecules are included in the atomistic solute region, and such approaches are known as *solvent boundary potential* methods.^{99–101} These have been developed as replacements for periodic boundary conditions in both QM/MM simulations^{102–108} and in fully quantum-mechanical calculations.^{109–112} Spherical cavities make little sense for single molecules, however, and it is clear from Eq. (2.17) that ΔG will be quite sensitive to the cavity radius. This is especially problematic if that cavity does not correspond closely to the size of the molecule itself, and results in Section 3.3 demonstrate that even for realistic “molecule-shaped” cavities, solvation energies are quite sensitive to cavity construction.

Examples of some molecule-shaped cavity constructions are provided in Fig. 2. A simple union of atom-centered spheres is often called a *van der Waals* (vdW) cavity surface. The atomic radii might simply be empirical parameters of the model,¹¹³ or alternatively covalent radii extracted from crystal structures,^{114,115} or based on calculations of atomic size.¹¹⁶ In the latter two cases these radii represent close-contact distances, meaning that an implicit or continuum solvent should not be allowed to approach all the way to the vdW radii of the solute atoms. This exclusion effect has been treated in several ways, most commonly by scaling the atomic vdW radii by a factor $\alpha > 1$. A scaling factor $\alpha = 1.2$ was chosen early on,¹¹⁷ and factors $\alpha \approx 1.1–1.2$ have since become standard choices, albeit with little theoretical justification to choose one value over another within a modest range. Alternatively, and with somewhat better justification, the atomic vdW radii can be augmented by a “probe radius” representing the assumed size of a solute molecule, which can be extracted from the liquid structure of the solvent. For example, $R_{\text{probe}} = 1.4 \text{ \AA}$ is often used for water, representing half the distance to the first peak in the oxygen–oxygen radial distribution function.¹¹⁸ Values for water as small as $R_{\text{probe}} = 0.2 \text{ \AA}$ have also been used, however, in an effort to match solvation energy benchmarks from simulations with explicit solvent.¹¹⁹ The cavity surface generated using atomic radii $R_{\text{vdW}} + R_{\text{probe}}$ is known as the *solvent-accessible surface* (SAS), which was first introduced as a means to measure accessible surface area in proteins and is often used to define the ion accessibility function $\lambda(\mathbf{r})$ in Eq. (2.15). Note that it does not make sense to augment a *scaled* vdW radius with a probe radius, as this double counts the size of the exclusion layer.

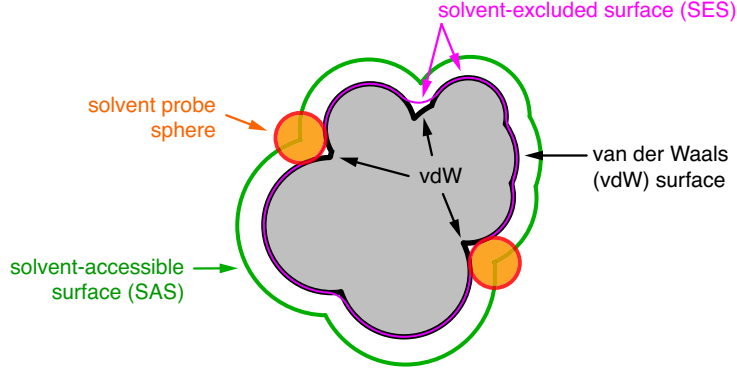


Fig. 2: Illustration of cavity surface definitions using a set of atomic spheres (in gray) whose envelope defines the vdW surface (in black). The solvent-accessible surface (in green) is defined either by augmenting the atomic radii by a probe radius (R_{probe} , taken here to be smaller than the vdW radii), or equivalently as the center point of the probe sphere as it rolls over the vdW surface. The solvent-excluded surface (SES, in magenta, sometimes called the “molecular surface”) is traced out by arcs of the probe that connect points of contact between the probe and the vdW surface. The SES eliminates the cusps in the vdW surface that otherwise appear along seams of intersection between atom-centered spheres.

Both the vdW surface and the SAS exhibit cusps where atomic spheres intersect. These cusps are eliminated by *solvent-excluded surface* (SES) that is generated by the probe sphere as it rolls over the vdW surface; see Fig. 2. (In principle, this procedure could be applied to eliminate cusps in the SAS as well, but that is less often done because cusps in the SAS are less problematic, numerically speaking.²¹) The center of the probe sphere traces out the SES while its points of contact with the vdW surface, combined with the concave arcs of the probe sphere that smooth over the cusps, constitute the SES. (The SES is also known as the Connolly surface,¹²⁰ or sometimes simply the “molecular surface”,¹²¹ as it is probably the closest approximation to the true shape of the molecule. However, these names have sometimes been used interchangeably or ambiguously in the literature, and in particular the term “Lee-Richards surface”¹²² has been used to mean either the SAS and the SES.^{21,119,123} (The notation used here is standard in the quantum chemistry literature.¹²⁴) The SES has an analytic construction,^{21,120} although it has most often been constructed numerically, for visualization purposes.

To a greater or lesser degree each of these cavity definitions seems physically reasonable, but beyond that there is little theoretical justification for any of them, and no guarantee that small changes in one or more atomic radii will not have a significant impact on computed observables.^{97,125} It has been suggested that the “optimal” atomic radius for a given atom likely ought to vary as a function of its partial atomic charge,^{126,127} but this effect is generally handled empirically, if at all. “United-atom” models, in which hydrogen atoms are not given explicit spheres and the radii of the other atoms are increased to compensate,¹²⁶ are also in widespread use. A more justifiable definition of the solute cavity surface might involve an isocontour of the molecular electron density $\rho(\mathbf{r})$,^{94,96,128–130} as it is the density that is ultimately responsible for molecular size and shape.¹³¹ Isodensity cavity definitions are considered in Section 3.3.

With the introduction of a molecule-shaped cavity, one must forego analytic solution of Poisson’s equation. A variety of numerical algorithms have been introduced, either for classical biomolecular applications,^{132–142} or else for quantum electronic structure calculations.^{39,64,143–145} Numerically, Eq. (2.3) and its Poisson-Boltzmann analogue are partial differential equations (for φ) that require

discretization of three-dimensional space, which must extend well into the continuum region due to the $(\varepsilon_s r)^{-1}$ asymptotic decay of $\varphi(\mathbf{r})$. This necessitates the use of multiresolution techniques for efficiency.^{39,55,62,132,134,142} Worth mentioning also is the Langevin dipoles model,^{146–148} which discretizes the continuum solvent using a three-dimensional grid of point dipoles, and is therefore a direct realization of the conceptual notion that \mathbf{P} is a dipole density.

As compared to these approaches, each of which requires discretization of three-dimensional space, a much more efficient two-dimensional formulation of the continuum electrostatics problem is often feasible. The transformation of Eq. (2.3) from a partial differential equation in three dimensions to an integral equation in two dimensions (over the cavity surface Γ) defines the class of methods known as *polarizable continuum models* (PCMs),^{13,15,19} which we next describe.

2.3 Polarizable continuum models

In quantum chemistry, PCMs are so widely used as to be nearly synonymous with continuum solvation itself. This popularity stems from efficiency, which in turn derives from a transformation of the volumetric polarization theory of the Poisson or Poisson-Boltzmann equation (Section 2.1) into a surface charge problem that can be solved with numerical methods that are described in Section 3.2. That transformation, and the basic working equations of PCMs, are introduced in this section. Matrix analogues of these integral equations, which define the various PCMs in practice, are introduced in Section 3.1.

Physically speaking, polarization of the continuum extends beyond the solute cavity surface, as indicated pictorially in Fig. 1(b). Transformation of the three-dimensional polarization problem into a two-dimensional problem defined on the cavity surface Γ relies on a characteristic feature of a sharp dielectric interface, namely, a discontinuity in the electric field resulting from a buildup of charge at the interface. This occurs at any dielectric interface, including the one that defines the boundary between atomistic solute and continuum solvent. Let $\mathbf{s} \in \Gamma$ denote a point on the interface (cavity surface), and let \mathbf{n}_s be the outward-pointing unit vector normal to the cavity surface at the point \mathbf{s} . At a sharp interface in the permittivity function $\varepsilon(\mathbf{r})$, as in Eq. (2.10), the normal electric field satisfies a “jump” boundary condition,^{9,92}

$$\varepsilon_{\text{out}} (\mathbf{n}_s \cdot \hat{\nabla}) \varphi(\mathbf{s}) \Big|_{\mathbf{s}=\mathbf{s}^+} = \varepsilon_{\text{in}} (\mathbf{n}_s \cdot \hat{\nabla}) \varphi(\mathbf{s}) \Big|_{\mathbf{s}=\mathbf{s}^-}. \quad (2.21)$$

This ensures that the electric displacement $\mathbf{D}(\mathbf{r}) = \varepsilon(\mathbf{r}) \mathbf{E}(\mathbf{r})$ is continuous across the interface.^{38,41} The notation \mathbf{s}^\pm indicates that these are one-sided derivatives to be evaluated immediately inside ($\mathbf{s}^- \in \Omega$) or outside ($\mathbf{s}^+ \notin \Omega$) of the solute cavity, as φ is only semi-differentiable at the interface.

Polarization of the continuum manifests as a surface charge that accumulates at the boundary between the atomistic and the continuum region in order to satisfy Eq. (2.21), and whose magnitude is proportional to the outward-pointing normal electric field at the dielectric interface.³⁸ Let us call that charge $\sigma(\mathbf{s})$, where $\mathbf{s} \in \Gamma$, so as to distinguish it from a volume charge such as $\rho(\mathbf{r})$, where $\mathbf{r} \in \mathbb{R}^3$. Introducing the notation $\hat{\partial}_s = \mathbf{n}_s \cdot \hat{\nabla}$ to indicate the normal derivative, the surface charge at the dielectric boundary can be expressed in several equivalent ways,^{14,92} two of which are

$$\sigma(\mathbf{s}) = \frac{1}{4\pi} \left(\frac{\varepsilon_{\text{out}} - \varepsilon_{\text{in}}}{\varepsilon_{\text{in}}} \right) \hat{\partial}_s \varphi(\mathbf{s}) \Big|_{\mathbf{s}=\mathbf{s}^+} = \frac{1}{4\pi} \left(\frac{\varepsilon_{\text{out}} - \varepsilon_{\text{in}}}{\varepsilon_{\text{out}}} \right) \hat{\partial}_s \varphi(\mathbf{s}) \Big|_{\mathbf{s}=\mathbf{s}^-}. \quad (2.22)$$

These differ depending on whether the normal electric field is evaluated immediately inside or outside of the cavity. In the usual quantum chemistry case where $\varepsilon_{\text{in}} = 1$ and $\varepsilon_{\text{out}} = \varepsilon_s$, the first form of this equation (in which the field is evaluated within the continuum region) is merely the

definition of the polarization,

$$\mathbf{P} = \left(\frac{\varepsilon_s - 1}{4\pi} \right) \mathbf{E} , \quad (2.23)$$

as obtained from Eq. (2.1). If the entirety of the solute charge $\rho(\mathbf{r})$ is confined within the cavity surface, then Eq. (2.22) is simply a reflection of Gauss' Law. For cavities that are realistic approximations to the size and shape of a molecular solute, however, the tails of a quantum-mechanical charge distribution will penetrate into the continuum region.⁹¹⁻⁹⁷ This outlying or “escaped” charge is discussed in more detail below but will be ignored for now.

It has been argued that the second form of Eq. (2.22), in which the derivative is evaluated inside of the cavity, should be used in order to avoid “self-polarization” of the medium.⁹ Then taking $\varepsilon_{in} = 1$ and $\varepsilon_{out} = \varepsilon_s$ and recognizing that $\mathbf{E} = -\hat{\nabla}\varphi$, one obtains a model

$$\sigma(\mathbf{s}) = -\frac{1}{4\pi} \left(\frac{\varepsilon_s - 1}{\varepsilon_s} \right) \underbrace{[\mathbf{E}^\rho(\mathbf{s}) + \mathbf{E}^\sigma(\mathbf{s})] \cdot \mathbf{n}_s}_{E_\perp(\mathbf{s})} = \frac{1}{4\pi} \left(\frac{\varepsilon_s - 1}{\varepsilon_s} \right) \left(\frac{\partial \varphi}{\partial \mathbf{n}_s} \right)_{\mathbf{s}=\mathbf{s}^-} \quad (2.24)$$

that corresponds to the original PCM introduced by Tomasi and co-workers.^{3-5,9} Here, the induced surface charge density $\sigma(\mathbf{s})$ is proportional to the outward-directed normal electric field, $E_\perp(\mathbf{s}) = \mathbf{E}(\mathbf{s}) \cdot \mathbf{n}_s$, which is separated into two contributions in Eq. (2.24), analogous to how $\varphi(\mathbf{r})$ is partitioned in Eq. (2.4). The contribution $\mathbf{E}^\rho = -\hat{\nabla}\varphi^\rho$ comes from the solute, whose electrostatic potential $\varphi^\rho(\mathbf{r})$ is defined in Eq. (2.4), whereas $\mathbf{E}^\sigma = -\hat{\nabla}\varphi^\sigma$ can be identified as the reaction-field contribution and originates in the electrostatic potential

$$\varphi^\sigma(\mathbf{r}) = \int_{\mathbf{s} \in \Gamma} \frac{\sigma(\mathbf{s})}{\|\mathbf{s} - \mathbf{r}\|} d\mathbf{s} \quad (2.25)$$

that is generated by the surface charge σ . To compute $\varphi^\sigma(\mathbf{r})$, it is only necessary to discretize the cavity surface Γ rather than the whole of three-dimensional space. Historically, Eq. (2.24) was the first example of what has been called an *apparent surface charge* (ASC) formulation of the continuum electrostatics problem. Nowadays the term “ASC model” is essentially synonymous with PCM, as multipolar expansions and other simplified treatments see little use in contemporary quantum chemistry because the model defined by Eq. (2.24) makes it easy to use the exact solute density $\rho(\mathbf{r})$ along with a cavity or arbitrary shape. (Discretization of the surface is considered in Section 3.) For a spherical cavity, Eq. (2.24) is equivalent to the use of the Kirkwood multipolar expansion formulas if the latter are carried to arbitrary order, as can be proven explicitly.¹⁴⁹

In early literature, the model defined by Eq. (2.24) is often called “the” ASC-PCM,⁹ whereas in contemporary literature it is usually called D-PCM,^{13,15} or sometimes the Miertuš-Scrocco-Tomasi model.^{98,150} The somewhat arbitrary decision to use the right side of Eq. (2.22) can be avoided, and a somewhat different version of this model obtained, by noting that the discontinuity in E_\perp at the cavity surface can be expressed as⁹²

$$\hat{\partial}_s \varphi^\sigma(s) \Big|_{s=s^-} = 2\pi\sigma(s) + \hat{\partial}_s \varphi^\sigma(s) \quad (2.26a)$$

$$\hat{\partial}_s \varphi^\sigma(s) \Big|_{s=s^+} = -2\pi\sigma(s) + \hat{\partial}_s \varphi^\sigma(s) . \quad (2.26b)$$

Adding these two equations and combining them with Eq. (2.22) affords a different expression for the surface charge,^{92,149,151}

$$\sigma(s) = \left(\frac{f_\varepsilon}{2\pi} \right) \hat{\partial}_s [\varphi^\rho(s) + \varphi^\sigma(s)] , \quad (2.27)$$

in which the normal derivative is evaluated *at* (rather than *near*) the point $\mathbf{s} \in \Gamma$. The permittivity-dependent prefactor in this expression is

$$f_\varepsilon = \frac{\varepsilon_{\text{out}} - \varepsilon_{\text{in}}}{\varepsilon_{\text{out}} + \varepsilon_{\text{in}}} . \quad (2.28)$$

(For a QM solute the only sensible choice is $\varepsilon_{\text{in}} = 1$, but the more general notation is retained for now, in order to accommodate different values of ε_{in} that are sometimes used in biomolecular electrostatics calculations.^{7,44–48})

The model of Eq. (2.27) can be recast in a convenient form by defining an operator \hat{D}^\dagger that acts on surface functions ($\mathbf{s} \in \Gamma$) according to^{94–96}

$$\hat{D}^\dagger \sigma(\mathbf{s}) = \int_{\Gamma} d\mathbf{s}' \sigma(\mathbf{s}') \frac{\partial}{\partial \mathbf{n}_{\mathbf{s}}} \left(\frac{1}{\|\mathbf{s} - \mathbf{s}'\|} \right) = -E_{\perp}^\sigma(\mathbf{s}) . \quad (2.29)$$

The first equality defines \hat{D}^\dagger and the second follows upon realization that $\partial/\partial \mathbf{n}_{\mathbf{s}} = \mathbf{n}_{\mathbf{s}} \cdot \hat{\nabla}$ can be pulled outside of the integral, leaving $(\mathbf{n}_{\mathbf{s}} \cdot \hat{\nabla})\varphi^\sigma(\mathbf{s}) = -E_{\perp}^\sigma(\mathbf{s})$. The operator \hat{D}^\dagger is often called \hat{D}^* in the literature,^{94–96,152} but is the adjoint of the double-layer operator \hat{D} that is introduced below, and the notation used here is selected to reflect that fact. Using \hat{D}^\dagger to rewrite Eq. (2.27) affords an alternative to Eq. (2.24), namely

$$\left[\left(\frac{2\pi}{f_\varepsilon} \right) \hat{1} - \hat{D}^\dagger \right] \sigma(\mathbf{s}) = -E_{\perp}^\rho(\mathbf{s}) . \quad (2.30)$$

This equation makes clear that the sole ingredient needed to determine the induced surface charge is

$$E_{\perp}^\rho(\mathbf{s}) = -(\mathbf{n}_{\mathbf{s}} \cdot \hat{\nabla})\varphi^\rho(\mathbf{s}) = -\left(\frac{\partial \varphi^\rho}{\partial \mathbf{n}_{\mathbf{s}}} \right) , \quad (2.31)$$

which is the normal electric field due to the solute, evaluated at the cavity surface. Chipman refers to Eq. (2.30) as the *surface polarization for electrostatics* (SPE) method,⁹⁵ but others have called it D-PCM,¹⁵² or simply PCM.¹⁵³

The D-PCM approach, which requires explicit calculation of the electric field at the cavity surface, has largely been superseded by alternative ASC-PCMs that determines $\sigma(\mathbf{s})$ using only electrostatic potentials and not their derivatives, which might be more sensitive to discretization error. The modern approach is known as the *integral equation formalism* (IEF-) PCM,^{152,154} and is based on a reformulation of the continuum electrostatics problem as a boundary-value problem.^{155–157} This reformulation is exact provided that the escaped charge is zero (*e.g.*, for a classical solute), and we continue to defer a discussion of the escaped charge problem. IEF-PCM is formulated in terms of integral operators \hat{S} and \hat{D} that act on surface functions (defined on Γ) to generate the single- and double-layer potentials, respectively. These operators are defined by

$$\hat{S}\sigma(\mathbf{s}) = \int_{\Gamma} d\mathbf{s}' \frac{\sigma(\mathbf{s}')}{\|\mathbf{s}' - \mathbf{s}\|} = \varphi^\sigma(\mathbf{s}) , \quad (2.32)$$

which generates the electrostatic potential associated with the surface charge distribution $\sigma(\mathbf{s})$, and

$$\hat{D}\sigma(\mathbf{s}) = \int_{\Gamma} d\mathbf{s}' \sigma(\mathbf{s}') \underbrace{\frac{\partial}{\partial \mathbf{n}_{\mathbf{s}'}} \left(\frac{1}{\|\mathbf{s}' - \mathbf{s}\|} \right)}_{D(\mathbf{s}, \mathbf{s}')} , \quad (2.33)$$

which generates the double-layer potential, in the language of integral equations.¹⁵² [The operator \hat{D} is the adjoint of \hat{D}^\dagger in Eq. (2.29),¹³ as becomes clear upon reversing the indices of the kernel

$D(\mathbf{s}, \mathbf{s}')$.] Using \hat{S} and \hat{D} , the continuum electrostatics problem can be recast as an integral equation on the surface of the cavity:¹³

$$\left[\left(\frac{2\pi}{f_\varepsilon} \right) \hat{1} - \hat{D} \right] \hat{S} \sigma(\mathbf{s}) = (-2\pi \hat{1} + \hat{D}) \varphi^\rho(\mathbf{s}) . \quad (2.34)$$

Equation (2.34) is the basic working equation of IEF-PCM. In early papers the working equation was formulated somewhat differently, requiring E_\perp^ρ in addition to φ^ρ .^{155–157} That form is sometimes called simply “IEF”,^{95,152} to distinguish it from the IEF-PCM that requires φ^ρ but not its derivative, and should therefore be more stable numerically. Equivalence of the two forms is demonstrated in Ref. 158, and in fact Eq. (2.34) can be cast in a variety of equivalent forms,^{94,95,152} by taking advantage of the fact that $\hat{S} = \hat{S}^\dagger$ and

$$\hat{D} \hat{S} = \hat{S} \hat{D}^\dagger . \quad (2.35)$$

However, except for spherical cavities (for which $\hat{D} = \hat{D}^\dagger$),⁹⁴ the operator identity in Eq. (2.35) is not generally preserved upon discretization,^{20,153} with the practical result that various forms of Eq. (2.34) are *inequivalent* as finite-dimensional matrix equations.^{19,20} These equations are discussed in Section 3.1.

For now, we simply note that Eq. (2.34) is an exact reformulation of the *classical* continuum electrostatics problem, meaning the problem that is defined by Poisson’s equation with a sharp dielectric boundary and where the solute’s charge density $\rho(\mathbf{r})$ is contained entirely within the cavity. That caveat is satisfied if the solute consists of atomic point charges (or higher-order multipoles, including polarizable ones) from a force field. In that case, solution of Eq. (2.34) for $\sigma(\mathbf{s})$ constitutes an exact solution to the electrostatics problem, and the electrostatic solvation energy is¹⁸

$$\mathcal{G}_{\text{elst}} = \frac{1}{2} \int_{\mathbb{R}^3} \varphi^\sigma(\mathbf{r}) \rho(\mathbf{r}) d\mathbf{r} = \frac{1}{2} \int_{\Gamma} \varphi^\rho(\mathbf{s}) \sigma(\mathbf{s}) d\mathbf{s} . \quad (2.36)$$

These are analogous to the two forms of $\mathcal{G}_{\text{elst}}$ that are given in Eq. (2.6), however the second form in Eq. (2.36) requires only surface integration. Using this ASC formulation, in lieu of discretizing three-dimensional space, has significant advantages over the traditional approach to biomolecular electrostatics, which require discretization far enough into the continuum such that $\varphi^\rho(\mathbf{r})$ has decayed to zero. Most contemporary biomolecular electrostatics calculations are also based on finite-difference evaluation of the Laplacian $\hat{\nabla}^2 \varphi(\mathbf{r})$,^{159,160} which leads to problems in obtaining smooth forces for molecular dynamics.^{161–163} Discretization of the action of \hat{D} and \hat{S} on surface functions can be accomplished in a manner that affords inherently smooth forces;^{17–19} see Section 3.2. Especially for biomolecular applications it is worth noting that the IEF-PCM has been adapted to provide a solution to the linearized Poisson-Boltzmann problem,^{68,155,156,164} including the “size-modified” version that accounts for finite size of the mobile ions.⁶⁸ Large biomolecular solutes have been tackled in this way,^{19,165–167} but this requires iterative solvers for the matrix equations that define the PCM. Linear-scaling implementations that can handle biomolecular solutes are discussed in Section 3.4.

For QM solutes, however, there is always escaped charge for realistic cavity sizes, and therefore IEF-PCM is not a fully equivalent substitute for Poisson’s equation. The extent to which this is a problem is unclear from the original derivation of IEF-PCM provided by Cancès *et al.*,^{152,155–157} which does not provide much physical insight, nor does it emphasize the assumption (inherent in the derivation) that there is no outlying charge. That issue was addressed directly by Chipman,^{92–95} who assumes from the start that there is outlying charge and that as a consequence the correct reaction-field potential is not $\varphi^\sigma(\mathbf{r})$ but rather

$$\varphi_{\text{rxn}}(\mathbf{r}) = \varphi^\sigma(\mathbf{r}) + \varphi^\beta(\mathbf{r}) , \quad (2.37)$$

where $\varphi^\sigma(\mathbf{r})$ arises from the accumulation of charge $\sigma(\mathbf{s})$ at the dielectric interface but is accompanied by an additional potential $\varphi^\beta(\mathbf{r})$ due to volume polarization. The latter originates with the tail of the solute's charge density that extends beyond the cavity surface. Including an additional term for φ^β on the right side of Eq. (2.27), and recognizing that $\hat{\partial}_{\mathbf{s}}\varphi^\sigma(\mathbf{s}) = \hat{D}^\dagger\sigma(\mathbf{s})$, an exact equation for the surface charge that includes the effects of volume polarization is⁹⁴

$$\begin{aligned} \left[\hat{1} - \left(\frac{f_\varepsilon}{2\pi} \right) \hat{D}^\dagger \right] \sigma(\mathbf{s}) &= \frac{f_\varepsilon}{2\pi} [\hat{\partial}_{\mathbf{s}} \varphi^\rho(\mathbf{s}) + \hat{\partial}_{\mathbf{s}} \varphi^\beta(\mathbf{s})] \\ &= -\frac{f_\varepsilon}{2\pi} [E_\perp^\rho(\mathbf{s}) + E_\perp^\beta(\mathbf{s})] . \end{aligned} \quad (2.38)$$

The potential $\varphi^\beta(\mathbf{r})$ can be modeled as the electrostatic potential generated by a charge density

$$\beta(\mathbf{r}) = \begin{cases} 0 & \text{for } \mathbf{r} \in \Omega \\ (\varepsilon_{\text{out}}^{-1} - \varepsilon_{\text{in}}^{-1}) \rho(\mathbf{r}) & \text{for } \mathbf{r} \notin \Omega \end{cases} \quad (2.39)$$

that satisfies a vacuum-like Poisson equation,

$$\hat{\nabla}^2 \varphi^\beta(\mathbf{r}) = -4\pi\beta(\mathbf{r}) . \quad (2.40)$$

Equation (2.38) can be solved numerically,⁹¹ to afford an exact solution to the continuum electrostatics problem, in a method that Chipman calls *surface and volume polarization for electrostatics* (SVPE).⁹⁵ This approach is challenging in practice because the volume charge density $\beta(\mathbf{r})$ is discontinuous at the cavity surface, however Eq. (2.38) can be recast into a form that requires only the normal electric field $E_\perp^\rho(\mathbf{s})$ at the cavity surface, along with the solution of the ASC-PCM that is introduced next.⁹⁶ This provides a practical means to access *exact* electrostatics, even in the presence of outlying charge, while staying within a two-dimensional surface integral formalism.

A simplified (if approximate) treatment is possible, which eliminates the normal electric field in Eq. (2.38) and ultimately connects back to IEF-PCM. This model is obtained by introducing an additional surface charge $\alpha(\mathbf{s})$, distinct from $\sigma(\mathbf{s})$, that is defined by the condition

$$\hat{S}\alpha(\mathbf{s}) = \varphi^\beta(\mathbf{s}) , \quad (2.41)$$

meaning that its electrostatic potential $\varphi^\alpha = \hat{S}\alpha$ must reproduce φ^β on the cavity surface.^{91–94} This also ensures that $\varphi^\alpha(\mathbf{r}) = \varphi^\beta(\mathbf{r})$ for all interior points $\mathbf{r} \in \Omega$, and while the two potentials may differ *outside* of the cavity, those contributions are scaled by ε_s^{-1} and therefore less important. (This is confirmed in numerical tests.^{91,97}) Assuming that the true surface charge, augmented to reflect volume polarization, is $\tilde{\sigma}(\mathbf{s}) = \alpha(\mathbf{s}) + \sigma(\mathbf{s})$, the term $\hat{\partial}_{\mathbf{s}} \varphi^\beta(\mathbf{s})$ in Eq. (2.38) can be manipulated into a form that is consistent with the ASC formalism.⁹⁴ The result is a model that Chipman has called *surface and simulation of volume polarization for electrostatics* [SS(V)PE],^{94–96}

$$\underbrace{\hat{S} \left(\hat{1} - \frac{f_\varepsilon}{2\pi} \hat{D}^\dagger \right) \tilde{\sigma}(\mathbf{s})}_{\hat{K}_\varepsilon} = \underbrace{f_\varepsilon \left(\frac{1}{2\pi} \hat{D} - \hat{1} \right) \varphi^\rho(\mathbf{s})}_{\hat{Y}_\varepsilon} . \quad (2.42)$$

Using the identity in Eq. (2.35), this equation is easily rearranged to afford Eq. (2.34) that defines IEF-PCM, and therefore the two models are equivalent at the level of integral operators.^{94,95,158} (They differ in practice, as described in Section 3.1.) Importantly, what the derivation of SS(V)PE makes clear is that the surface charge that is determined by solving Eq. (2.34) implicitly contains the (approximate) effects of volume polarization, which was not evident from the derivation by Cancès and co-workers.^{152,155–157} Chipman's derivation clarifies that both approaches constitute an exact treatment of electrostatic interactions in the limiting case that there is no escaped charge ($\alpha \equiv 0$).

Table 1: Electrostatic solvation energies in toluene ($\varepsilon_s = 2.4$) and in water ($\varepsilon_s = 78.3$), computed with various approaches.^a The SVPE method [Eq. (2.38)] affords the exact result and SPE is the method in Eq. (2.30).

Solute	ε_s	$\mathcal{G}_{\text{elst}}$ (kcal/mol)				Q_{out} (a.u.) ^c	
		SVPE	SS(V)PE	SPE	COSMO ^b		
					$\zeta = 0$	$\zeta = 1/2$	
H ₂ O	2.4	-3.9	-3.9	-4.0	-4.8	-3.9	
CH ₃ CONH ₂	2.4	-5.3	-5.0	-5.2	-5.9	-4.8	
NO ⁺	2.4	-52.2	-52.2	-55.3	-52.5	-43.4	
CN ⁻	2.4	-39.4	-39.4	-35.0	-39.4	-32.5	
H ₂ O	78.3	-8.6	-8.6	-8.7	-8.6	-8.6	-0.06
CH ₃ CONH ₂	78.3	-10.9	-10.8	-11.1	-10.9	-10.8	-0.15
NO ⁺	78.3	-89.5	-89.5	-94.7	-89.5	-88.9	-0.07
CN ⁻	78.3	-67.4	-67.3	-56.8	-67.3	-66.9	-0.17

^aFrom Ref. 95; all calculations used an isodensity cavity with $\rho_0 = 0.001$ a.u.. ^bUsing a renormalization factor $\tilde{f}_\varepsilon(\zeta)$, Eq. (2.45). ^cFrom Ref. 97.

2.4 Comparison of ASC-PCMs

Table 1 presents electrostatic solvation energies ($\mathcal{G}_{\text{elst}}$) for several small molecules and ions, in both a low-dielectric solvent (toluene, $\varepsilon_s = 2.4$) and a high-dielectric solvent (water, $\varepsilon_s = 78$).⁹⁵ The SVPE method [Eq. (2.38)] affords the exact result but SS(V)PE solvation energies are within 0.1 kcal/mol. In comparison, the SPE method of Eq. (2.30), which is equivalent to D-PCM, exhibits noticeable differences, especially for ions. The amount of outlying charge (Q_{out}) is also quantified in Table 1. For future reference we note the obvious definitions

$$Q_{\text{in}} = \int_{\mathbf{r} \in \Omega} \rho(\mathbf{r}) \, d\mathbf{r} \quad (2.43a)$$

$$Q_{\text{out}} = \int_{\mathbb{R}^3} \rho(\mathbf{r}) \, d\mathbf{r} - Q_{\text{in}}. \quad (2.43b)$$

The charge density $\rho(\mathbf{r})$ includes both nuclei and electrons, so $Q_{\text{in}} + Q_{\text{out}} = 0$ for a neutral molecule. The escaped charge is generally $|Q_{\text{in}}| \approx 0.1\text{--}0.2e$ for small solutes.^{91,97}

By arbitrarily dropping the \hat{D} - and \hat{D}^\dagger -dependent terms in Eq. (2.42), one obtains a model $\hat{S}\sigma = -f_\varepsilon\varphi^\rho$ that we rewrite as

$$\hat{S}\sigma(\mathbf{s}) = -\tilde{f}_\varepsilon(\zeta) \varphi^\rho(\mathbf{s}). \quad (2.44)$$

This introduces a parameter ζ into the permittivity factor that was defined in Eq. (2.28), rewriting it as

$$\tilde{f}_\varepsilon(\zeta) = \frac{\varepsilon_s - 1}{\varepsilon_s + \zeta} \quad (2.45)$$

for the usual QM case where $\varepsilon_{\text{in}} = 1$ and $\varepsilon_{\text{out}} = \varepsilon_s$. The model in Eq. (2.44) has a long history and a variety of names, one of which is the *conductor-like screening model* (COSMO).¹⁶⁸ Since the neglected double-layer operator embodies the electric field discontinuity at the cavity surface, this condition is not satisfied when these terms are neglected to obtain Eq. (2.44),^{68,152} and rescaling the surface charge by $\tilde{f}_\varepsilon(\zeta)$ can be seen as an attempt to mimic the effect of the jump boundary condition.

The name COSMO hints at the original derivation of the model in Eq. (2.44): for a conductor ($\varepsilon_s = \infty$), the total electrostatic potential vanishes at the cavity surface and the ASC formulation

of the Poisson problem is simply $\hat{S}\sigma = -\varphi^\rho$.⁹³ A scaling factor $\tilde{f}_\varepsilon(\zeta)$ is then introduced to account for the fact that ε_s is finite, and that there is charge penetration into the medium. The scaling factor [Eq. (2.45)] can be justified based on the normalization condition for the total surface charge, which is^{92,156,169}

$$\int_{\Gamma} \sigma(\mathbf{s}) \, d\mathbf{s} = - \left(\frac{1}{\varepsilon_{\text{in}}} - \frac{1}{\varepsilon_{\text{out}}} \right) Q_{\text{in}}. \quad (2.46)$$

For $\varepsilon_{\text{in}} = 1$ and $\varepsilon_{\text{out}} = \varepsilon_s$, the total surface charge $Q_{\text{surf}} = -[(\varepsilon_s - 1)/\varepsilon_s]Q_{\text{in}}$, and it was originally suggested to take $\zeta = 1/2$ in order to renormalize for outlying charge,¹⁶⁸ although the value $\zeta = 0$ was later recommended for ions,¹⁷⁰ and values $0 \leq \zeta \leq 2$ have also been used.¹⁰ The choice $\zeta = 0$ has variously been called the “generalized COSMO” (GCOSMO) model,^{171–174} or the *conductor-like PCM* (C-PCM).^{175,176} In fact, the normalization condition in Eq. (2.46) forms the basis of various *ad hoc* attempts to rescale the surface charge,^{3,5,177–179} but tests against exact results from Poisson’s equation suggest that none of these schemes is very satisfactory.⁹¹ Charge rescaling also complicates analytic energy gradients.¹⁸⁰

At a practical level, the choice $\zeta = 1/2$ for neutral solutes and $\zeta = 0$ for ions works remarkably well in comparison to the IEF-PCM and SS(V)PE methods, even in low-dielectric solvents. This is suggested by the smattering of data in Table 1 and confirmed by calculations on a much larger data set, for which the statistical difference between these methods is $\lesssim 0.1$ kcal/mol for neutral solutes and ≈ 0.5 kcal/mol for ions, even at $\varepsilon_s = 2$.¹⁷⁰ Some justification for these parameter choices is found in the fact that $\tilde{f}_\varepsilon(0)$ looks like the ε -dependent factor in the Born ion model [Eq. (2.17)], whereas $\tilde{f}_\varepsilon(1/2)$ affords the prefactor in the Bell-Onsager model of dipole solvation [Eq. (2.18)]. With appropriate choice of ζ , COSMO is therefore little different from SS(V)PE or IEF-PCM in practice, and considerably simpler. It can be extended in a straightforward way to solvents with nonzero ionic strength, with or without size exclusion.⁶⁸ For large biomolecular applications in aqueous solvent, there seems little reason *not* to use this approach, in lieu of exact but more complicated models, and as an alternative to finite-difference solution of Poisson’s equation.

3 Implementation

Poisson’s equation with a sharp dielectric interface makes for a cute problem in applied mathematics and there has sometimes been a tendency in that community to analyze its properties, or those of the various cavity surfaces discussed in Section 2.2, at fixed molecular geometries only. This is not useful for chemistry, which requires a potential energy *surface*. Exploration of that surface requires gradients of the total energy functional $\mathcal{G}[\Psi]$, which in turn requires discretization of the integral equations introduced above. In addition, many spectroscopic observables can be formulated as analytic energy derivatives,^{181–183} so a solution-phase theory that encompasses molecular properties requires a differentiable model. Numerical implementation of the models introduced in Section 2 is the topic of this section. We deal specifically with PCMs in Sections 3.1 and 3.2, but admit more general Poisson equation models in Section 3.3. Linear-scaling implementations, which are useful for hybrid QM/MM simulations with PCM boundary conditions, are discussed in Section 3.4.

3.1 Matrix equations for PCMs

In practice, the integral equation that defines any PCM must be discretized in order to obtain a finite-dimensional matrix equation. As such, it is convenient to rewrite the equation that defines SS(V)PE and IEF-PCM as

$$\hat{K}_\varepsilon \sigma(\mathbf{s}) = \hat{Y}_\varepsilon \varphi^\rho(\mathbf{s}), \quad (3.1)$$

Table 2: Matrices that define various PCMs according to $\mathbf{K}_\varepsilon \mathbf{q} = \mathbf{Y}_\varepsilon \mathbf{v}^\rho$ [Eq. (3.2)].

Method	Matrix \mathbf{K}_ε	Matrix \mathbf{Y}_ε
C-PCM ^{a,b}	\mathbf{S}	$-\tilde{f}_\varepsilon(0) \mathbf{1}$
COSMO ^b	\mathbf{S}	$-\tilde{f}_\varepsilon(\zeta) \mathbf{1}$
DESMO ^c	\mathbf{S}	$-\mathbf{1} + (1/\varepsilon)\mathbf{M}$
SS(V)PE ^d	$\mathbf{S} - (f_\varepsilon/4\pi)(\mathbf{DAS} + \mathbf{SAD}^\dagger)$	$-f_\varepsilon[\mathbf{1} - (1/2\pi)\mathbf{DA}]$
IEF-PCM ^d	$\mathbf{S} - (f_\varepsilon/2\pi)\mathbf{DAS}$	$-f_\varepsilon[\mathbf{1} - (1/2\pi)\mathbf{DA}]$

^aAlso known as GCOSMO. ^b $\tilde{f}_\varepsilon(\zeta) = (\varepsilon - 1)/(\varepsilon + \zeta)$. ^c $M_{ij} = \delta_{ij} \varphi_\kappa^\rho(\mathbf{s}_i)/\varphi_0^\rho(\mathbf{s}_i)$.
^d $f_\varepsilon = (\varepsilon - 1)/(\varepsilon + 1)$.

which is simply a restatement of Eq. (2.42). Using various definitions for \hat{K}_ε and \hat{Y}_ε , this equation can encompass a whole family of ASC-PCMs including the simplified C-PCM and COSMO methods (Table 2).^{19,20,95,129}

To discretize Eq. (3.1), one must first generate a surface grid of points $\mathbf{s}_i \in \Gamma$. The surface charge distribution $\sigma(\mathbf{s})$ is thereby replaced by a set of point charges $\{q_i\}$ at the discretization points $\{\mathbf{s}_i\}$. The details of this procedure are discussed in the next section but for now it suffices to introduce a matrix notation

$$\mathbf{K}_\varepsilon \mathbf{q} = \mathbf{Y}_\varepsilon \mathbf{v}^\rho \quad (3.2)$$

for the discretized form of Eq. (3.1), where \mathbf{q} is a vector of surface charges and \mathbf{v}^ρ denotes the molecular electrostatic potential evaluated at the cavity surface, $v_i^\rho = \varphi^\rho(\mathbf{s}_i)$. In this form, surface integrals are replaced by scalar products, *e.g.*, $\mathcal{G}_{\text{elst}} = \frac{1}{2}\mathbf{q} \cdot \mathbf{v}^\rho$ replaces Eq. (2.36). An alternative form of Eq. (3.2) that is sometimes encountered is $\mathbf{q} = \mathbf{Q}_\varepsilon \mathbf{v}^\rho$ where $\mathbf{Q}_\varepsilon = \mathbf{K}_\varepsilon^{-1} \mathbf{Y}_\varepsilon$, but whereas the corresponding operator $\hat{Q}_\varepsilon = \hat{K}_\varepsilon^{-1} \hat{Y}_\varepsilon$ is self-adjoint, this property is generally not preserved by discretization except in the special case of C-PCM and COSMO.¹⁸ This means that the mapping from Eq. (3.1) to Eq. (3.2) is not unique, because discretization fails to preserve the condition $\hat{D}\hat{S} = \hat{S}\hat{D}^\dagger$.²⁰ In matrix form, this implies that $\mathbf{DAS} \neq \mathbf{SAD}^\dagger$ (except for spherical cavities),^{20,153} where \mathbf{A} is a diagonal matrix consisting of the surface area a_i associated with each discretization point \mathbf{s}_i . This leads to an ambiguity in the matrix representation of the operator $\hat{K}_\varepsilon = \hat{S} - (f_\varepsilon/2\pi)\hat{S}\hat{D}^\dagger$ [Eq. (2.42)], since it can be argued that any matrix of the form

$$\mathbf{K}_\varepsilon = \mathbf{S} - \left(\frac{f_\varepsilon}{4\pi} \right) \underbrace{(c_1 \mathbf{DAS} + c_2 \mathbf{SAD}^\dagger)}_{\mathbf{X}}. \quad (3.3)$$

is an equally valid representation, provided that $c_1 + c_2 = 1$.²⁰ The various choices for \mathbf{X} are inequivalent in matrix form. Historically, IEF-PCM has been implemented using $\mathbf{X} = \mathbf{DAS}$ (that is, $c_1 = 1$ and $c_2 = 0$), whereas SS(V)PE was implemented using the symmetrized matrix $(\mathbf{DAS} + \mathbf{SAD}^\dagger)/2$.^{19,95} This is indicated in Table 2, which provides matrix definitions for these and other commonly-encountered PCMs. Precise definitions of the matrices \mathbf{S} and \mathbf{D} that represent the operators \hat{S} and \hat{D} can be found elsewhere.^{18–20,124,129} These depend somewhat upon the discretization algorithm that is selected, but generally S_{ij} represents the Coulomb interaction between q_i and q_j (which is straightforward to discretize except when $i = j$), whereas D_{ij} incorporates the effects of the outward-pointing electric field.

In the absence of outlying charge, the IEF-PCM and SS(V)PE models are exact up to discretization errors, which can be driven to zero in a controlled way. Although this fact follows from

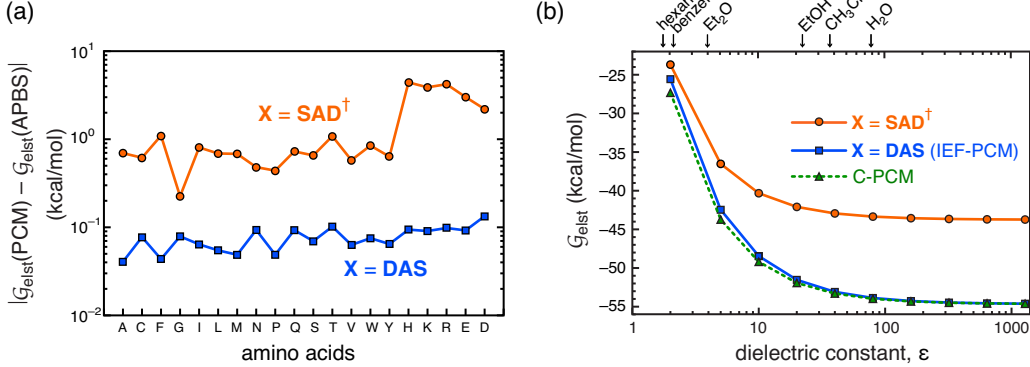


Fig. 3: (a) Comparison of aqueous solvation energies, $|\mathcal{G}_{\text{elst}}(\text{PCM}) - \mathcal{G}_{\text{elst}}(\text{APBS})|$, computed using either an ASC-PCM or else by numerical solution of Poisson’s equation using the APBS software. The data set of solutes consists of amino acids described using atomic partial charges from a force field, so that there is no outlying charge. The traditional implementation of IEF-PCM corresponds to $\mathbf{X} = \mathbf{DAS}$ (see Table 2) but results are also shown for the transpose matrix, \mathbf{SAD}^\dagger , and SS(V)PE is essentially the average of these two choices. (b) Convergence of $\mathcal{G}_{\text{elst}}$ for classical histidine as a function of the solvent’s dielectric constant, using the SwiG discretization scheme described in Section 3.2. Dielectric constants for a few common solvents are indicated along the top axis. Adapted from Ref. 20; copyright 2011 Elsevier.

the derivation in Section 2.3, it is worth emphasizing via numerical calculations. For classical solutes with no outlying charge, which are described using atomic partial charges from a force field, Fig. 3(a) presents a comparison of PCM solvation energies to those obtained by numerical solution of Poisson’s equation,^{19,20} using a standard multiresolution algorithm as implemented in the APBS software.¹⁸⁴ To examine the ambiguity regarding the choice of \mathbf{X} , these calculations test both $\mathbf{X} = \mathbf{DAS}$ (*i.e.*, IEF-PCM) and also $\mathbf{X} = \mathbf{SAD}^\dagger$; the SS(V)PE model should be essentially the average of these two choices. Calculations in Fig. 3 use dense but finite discretization grids, and a small systematic discrepancy is evident between the two choices of \mathbf{X} , indicating a systematic discrepancy between SS(V)PE and IEF-PCM. Numerical values of $\mathcal{G}_{\text{elst}}$ obtained using the IEF-PCM choice of \mathbf{X} agree to within $\lesssim 0.1$ kcal/mol of APBS results, demonstrating the operational equivalence of the ASC and the volumetric implementation of continuum electrostatics. This renders the Kirkwood (multipolar expansion) formulas obsolete, since the requisite formulas are only valid in the absence of escaped charge anyway, and in that case the ASC-PCM formalism furnishes an exact numerical solution to the continuum electrostatics problem, for cavities of arbitrary shape, while also providing a correction for outlying charge.^{94,96,169}

The conductor-like model (C-PCM) represents the high-dielectric limit of IEF-PCM and the two models do indeed become equivalent as $\epsilon \rightarrow \infty$,^{20,68,93} as demonstrated numerically in Fig. 3(b). In practice, there is little difference between the two models already for moderately polar solvents. For $\epsilon > 10$, there seems little justification for the increased complexity of IEF-PCM relative to C-PCM. That said, for non-spherical cavities only the $\mathbf{X} = \mathbf{DAS}$ form of the \mathbf{K}_ϵ matrix achieves the correct conductor limit for finite discretization grids, as demonstrated by both formal and numerical arguments.²⁰ In general, \hat{D}^\dagger proves more challenging to implement as compared to \hat{D} ,^{20,185} so the absence of \hat{D}^\dagger is one reason to prefer the IEF-PCM form with $\mathbf{X} = \mathbf{DAS}$.

It is illustrative to note that C-PCM can be derived in an alternative way,⁶⁸ which also generalizes the method to the Poisson-Boltzmann case in which the solvent contains a dissolved electrolyte.

This can be done by introducing the following *ansatz* for the electrostatic potential:^{19,68}

$$\varphi(\mathbf{r}) = \begin{cases} \varphi_0^\rho(\mathbf{r}) + \varphi_0^\sigma(\mathbf{r}) & \text{for } \mathbf{r} \in \Omega \\ \varphi_\kappa^\rho(\mathbf{r})/\varepsilon & \text{for } \mathbf{r} \notin \Omega \end{cases} . \quad (3.4)$$

Within the solute cavity, this looks like the solute's electrostatic potential ($\varphi_0^\rho \equiv \varphi^\rho$) plus that arising from the apparent surface charge, whereas outside of the cavity the potential is modified to include screening by dissolved ions:

$$\varphi_\kappa^\rho(\mathbf{r}) = \int \rho(\mathbf{r}') \frac{\exp(-\kappa\|\mathbf{r} - \mathbf{r}'\|)}{\|\mathbf{r} - \mathbf{r}'\|} d\mathbf{r}' . \quad (3.5)$$

The screened Coulomb potential $e^{-\kappa r}/(\varepsilon_s r)$ is the form encountered in Debye-Hückel theory,^{7,60,67,68} with screening length κ^{-1} that is defined in Eq. (2.16). C-PCM is immediately recovered by requiring $\varphi(\mathbf{r})$ in Eq. (3.4) to remain continuous across the solute cavity surface.⁶⁸ This simple *ansatz* cannot, however, be made to satisfy the jump boundary condition in Eq. (2.21) and incurs an error of $\mathcal{O}(1/\varepsilon)$.^{19,68} (This is consistent with the fact that C-PCM can be “derived” from IEF-PCM simply by dropping the \hat{D} - and \hat{D}^\dagger -dependent terms from IEF-PCM and rescaling the surface charge to compensate,¹⁵² as described in Section 2.4.) The simple *ansatz* in Eq. (3.4) is easily modifiable to incorporate the effects of an ion exclusion layer (Stern layer) around the solute cavity, as in the size-modified Poisson-Boltzmann equation of Eq. (2.12), where the ion accessibility function $\lambda(\mathbf{r})$ serves the same purpose. In homage to GCOSMO, and in recognition of the fact that this approach generalizes Debye-Hückel theory to cavities of arbitrary shape, this approach has been named the *Debye-Hückel-like screening model* (DESMO).^{19,68}

3.2 Discretization

Having introduced various PCMs in matrix form, we now turn to the details of discretizing the cavity surface. Historically, this has been accomplished using various “tessellation” schemes,¹²⁴ in which small, flat surface elements approximate the curved surface of the cavity. The “GEPOL” algorithm^{186–189} is a popular version of this finite-element approach, and an example of a molecular cavity discretized in this way is presented in Fig. 4(a). This approach has several limitations, however, including the fact that the number of tesserae per atomic sphere cannot be increased arbitrarily and thus the discretization error cannot be systematically driven to zero.²⁰ Furthermore, the solid geometry of the tessellation procedure is complicated, leading to very complex formulas for surface areas¹⁹⁰ and analytic energy gradients.¹⁹¹ (In fact, second derivatives of the tesserae areas a_i were considered sufficiently complicated that they were not originally formulated, and the PCM Hessian was implemented in a semi-analytic way, via finite-difference evaluation of $\partial^2 a_i / \partial x \partial y$.¹⁵³) More recently, these complexities have been overcome by discretizing the surface using atom-centered Lebedev grids,^{17–21,192–194} which are already widely used in density functional theory,^{195–198} and therefore widely available in quantum chemistry codes. An example is depicted in Fig. 4(b), where the outline of the vdW surface is evident even though only the discretization grid points (and the underlying nuclear framework) are shown. Relative to GEPOL and other tessellation schemes, Lebedev grids have the advantage of being systematically improvable so that results can be converged to the infinite-grid limit.^{18,20} Fully analytic Hessians have been formulated and implemented.¹⁹⁹

An important issue faced by both tessellation and quadrature is ensuring that the discretization algorithm produces a smooth potential energy surface as the atoms are displaced. The appearance

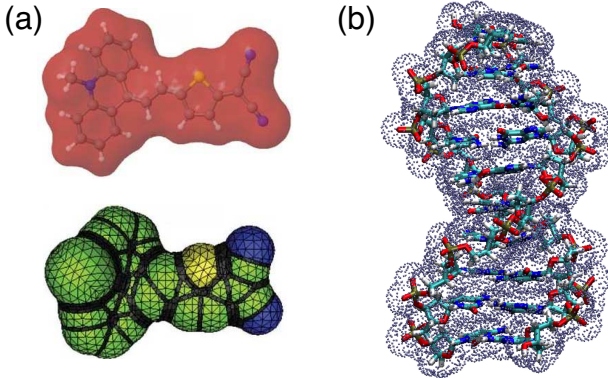


Fig. 4: (a) Example of a molecular surface (top) and its tessellation using the GEPOL algorithm (bottom). (b) Surface discretization grid for a double-stranded segment of DNA. Panel (a) is reprinted from Ref. 15; copyright 2012 John Wiley & Sons.

of discontinuities in molecular surface area algorithms used in biomolecular electrostatics calculations was pointed out long ago,²⁰⁰ and discontinuities are likely the cause of anecdotal complaints about slow convergence of geometry optimizations using PCMs. These discontinuities arise because grid points may disappear into (or emerge from within) the interior of the solute cavity, as displacement of the nuclei modifies the extent of interpenetration amongst the atomic spheres that define the cavity. An example is shown in Fig. 5(a), which plots convergence of the energy during geometry optimization of (adenine)(H₂O)₅₂ in implicit solvent. Two discretization algorithms, the *variable tesserae number* (VTN) method²⁰¹ and the *fixed points with variable areas* (FixPVA) approach,²⁰² are shown to exhibit repeated spikes in the energy.¹⁷ The VTN algorithm uses a fixed surface grid that unceremoniously discards surface elements that are swallowed by the cavity, and it is unsurprising that the corresponding potential surface exhibits discontinuities, although their magnitude (> 20 kcal/mol in one case) is disturbing. The FixPVA algorithm, however, specifically introduces a switching function to attenuate the surface area of each atomic tesserae within the cavity's interior. In fact, the sharp changes in energy along the FixPVA optimization in Fig. 5(a) are not discontinuities *per se* but rather near-singularities induced by the switching function, which allows surface discretization charges to approach one another much more closely as compared to the VTN scheme.^{17,20}

To avoid this, one can use a combination of a switching function with Gaussian blurring of the surface charges, as illustrated in Fig. 5(b), in what has been called the *switching/Gaussian* (SwiG) discretization procedure. This ensures that Coulomb interactions between surface discretization elements remain finite even as the distance between them approaches zero. Such a procedure was originally developed by York and Karplus to obtain a “smooth COSMO”,¹⁹² then later extended by Lange and Herbert to the complete family of PCMs.^{17,18,20,21} This scheme uses Lebedev points to discretize the surface rather than tesserae of finite area. Nevertheless, the solvent-accessible surface area (SASA) for atom B (whose radius is R_B) is easily defined:

$$\text{SASA}(B) = R_B^2 \sum_{i \in B}^{\text{grid}} w_i F_i . \quad (3.6)$$

Here, w_i is the quadrature weight for Lebedev discretization point s_i , and F_i is the switching function associated with that point ($0 \leq F_i \leq 1$), so $a_i = w_i F_i$ is the surface area that is assigned to the point s_i .¹⁷ Equation (3.6) is considerably simpler than geometric algorithms for determining the

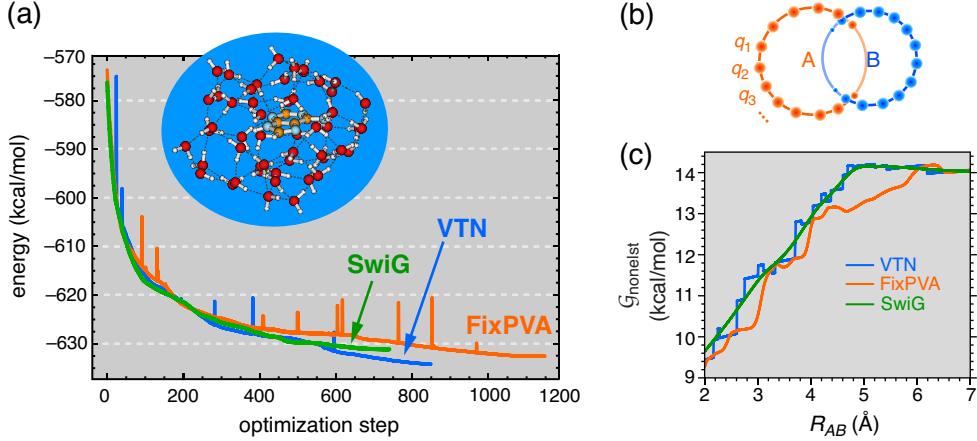


Fig. 5: Demonstration of the SwiG-PCM discretization approach. (a) Geometry optimization trajectories of (adenine)(H₂O)₅₂ in a C-PCM representation of bulk water, using several different algorithms to discretize the vdW cavity surface. (The surface itself is not shown, but the atomistic region appears in the blue inset.) Optimizations are performed in Cartesian coordinates so the total number of steps is large. (b) Schematic of the SwiG discretization algorithm, in which the surface charges $\{q_i\}$ are subject to Gaussian blurring and also to a switching function that attenuates the quadratures weights near the cavity surface. (c) Nonelectrostatic solvation energy ($\mathcal{G}_{\text{nonelst}}$) as spheres A and B are pulled part. The value of $\mathcal{G}_{\text{nonelst}}$ is related to the solvent-exposed surface area and inherits any discontinuities in the surface area function. Panels (a) and (c) are adapted from Ref. 17; copyright 2010 American Chemical Society.

exposed surface areas.¹⁹⁰ As discussed in Section 4.1, models of the nonelectrostatic contributions to the solvation energy usually include terms proportional to the solvent-exposed surface area so continuity of the potential energy surface also demands that the surface area be a continuous function of the nuclear coordinates. For SwiG discretization, it is evident from Fig. 5(c) that this is indeed the case.

Analytic gradients of SwiG-PCMs are greatly simplified relative to those of the corresponding GEPOL-discretized models.¹⁸ SwiG-PCM potential energy surfaces are provably continuous and differentiable,^{18,192} and are free of the unwanted oscillations that plague the FixPVA approach (see Fig. 5).^{18,20} SwiG discretization is well-behaved enough to be used for *ab initio* molecular dynamics simulations involving bond-breaking, as shown in Fig. 6 for intramolecular proton transfer in glycine. SwiG-PCM provides forces that are stable enough to afford good energy conservation despite the significant deformation of the solute cavity as it transforms between two tautomeric forms of glycine. This is demonstrated by the energy profile in Fig. 6(b), which provides a closeup view of ≈ 250 fs of dynamics during which a bond-breaking event occurs. On the other hand, it appears that SwiG discretization exacerbates differences between the $\mathbf{X} = \mathbf{DAS}$ and $\mathbf{X} = \mathbf{SAD}^\dagger$ forms of \mathbf{K}_ϵ [Eq. (3.3)], at least in comparison to GEPOL results where these differences are small.¹⁵³ This is not a major problem insofar as the $\mathbf{X} = \mathbf{DAS}$ form provides correct formal properties and good numerical agreement with Poisson's equation, as demonstrated in Fig. 3.

The SwiG implementation of PCMs first appeared in the Q-CHEM program²⁰³ and related discretization schemes have since been adopted in other software.^{204,205} Other discretization approaches have been described^{206–209} but it is unclear that they have been formulated with gradients in mind. Given the simplicity and success of the SwiG approach, it is also unclear what is to be gained from these formulations.

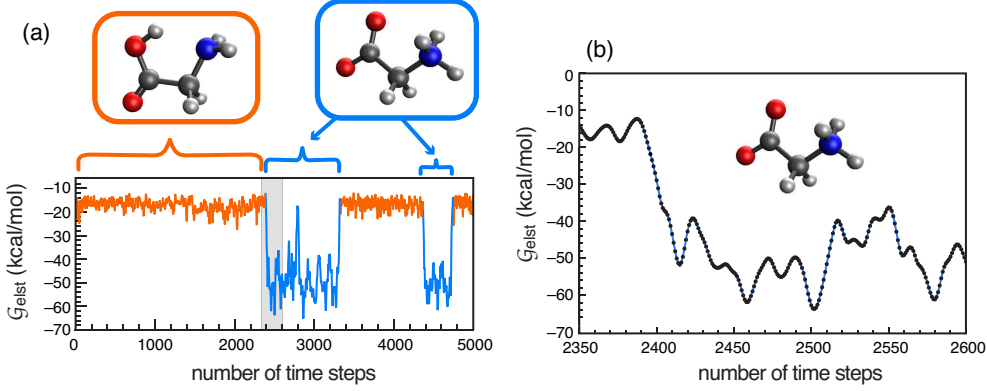


Fig. 6: (a) Electrostatic solvation energy along an *ab initio* molecular dynamics trajectory of glycine (PBE0/6-31+G* level) in implicit water (SwiG/C-PCM). The simulation starts at $t = 0$ from the amino acid tautomer (energy data in orange), which is the most stable form of gas-phase glycine, but this species spontaneously transfers a proton to form the zwitterionic tautomer (energy data in blue), during the time window highlighted in the gray box and shown in detail in (b). The time step is 0.97 fs. (b) Close-up view of G_{elst} in the region where the proton transfer occurs. Energy fluctuations are smooth despite the bond-breaking even that occurs around 2.3 ps. Data are from Ref. 18.

3.3 Isodensity and self-consistent cavity surfaces

Smooth SwiG-PCM discretization schemes been developed for both vdW cavities¹⁸ (including the SAS) and for the “molecular surface” or SES,²¹ thus providing a solution to the practical problem of discontinuities in potential energy surfaces. Unfortunately, these methods do not alter an arguably more fundamental problem, namely, that construction of the solute cavity remains a non-trivial source of arbitrariness in both PCMs and in biomolecular Poisson-Boltzmann electrostatics calculations. Solvation energies¹¹⁹ and other properties²¹⁰ can be quite sensitive to the particular atomic radii that are used, and often the atomic radii that work well for small-molecule solvation energies do not work well for proteins.²¹¹

Both the vdW and SAS cavity constructions consist of atom-centered spheres with radii

$$R_A = \alpha R_{\text{vdW},A} + R_{\text{probe}}. \quad (3.7)$$

The atomic vdW radii $\{R_{\text{vdW},A}\}$ might be taken from crystal structure data (*e.g.*, Bondi’s radii set of radii and its subsequent extensions),^{114–116} or might simply be parameters of the model.¹¹³ For vdW cavities, $R_{\text{probe}} = 0$ and a typical scaling factor is $\alpha = 1.2$,⁹ whereas one generally does not scale the vdW radii for SAS cavities. (As discussed in Ref. 9, the choice $\alpha = 1.2$ does not result from any kind of elaborate fitting procedure and is intended only as a rough guide; common choices range from $\alpha = 1.1$ –1.4.) As an example of just how sensitive G_{elst} is to cavity construction, Table 3 reports calculations for the two tautomers of glycine from Fig. 6, using various cavity definitions. A change from $\alpha = 1.2$ to either $\alpha = 1.1$ or $\alpha = 1.3$ results in changes of anywhere from 3–9 kcal/mol in G_{elst} .

When the solute is described using electronic structure theory, a more satisfying cavity definition uses the solute’s own electron density.^{96,128–130} It is possible to settle on a numerical isocontour value (generally $\rho_0 \sim 0.001$ a.u.) that appears to have some universal validity,^{125,210} and results using $\rho_0 = 0.001$ a.u. are shown in Table 3. It is noteworthy that the standard vdW scaling factor $\alpha = 1.2$ affords the best agreement with the isodensity result for both tautomers of glycine, despite

Table 3: Aqueous solvation energies computed with the SS(V)PE model for two tautomers of glycine using atomic radii in Eq. (3.7). Electronic structure calculations were performed at the B3LYP/6-31+G* level.

Cavity	α	R_{probe} (Å)	$\mathcal{G}_{\text{elst}}$ (kcal/mol)	
			amino acid	zwitterion
vdW ^a	1.0	0.0	-26.1	-68.2
vdW ^a	1.1	0.0	-20.2	-56.0
vdW ^a	1.2	0.0	-16.1	-46.8
vdW ^a	1.3	0.0	-12.9	-39.0
vdW ^a	1.4	0.0	-10.6	-32.6
SAS ^a	1.0	0.2	-18.0	-51.4
SAS ^a	1.0	1.4	-4.3	-13.9
isodensity ^b			-16.4	-48.1

^aUsing $R_{\text{vdW}} = 1.10$ Å (H), 1.70 Å (C), 1.55 Å (N), and 1.52 Å (O), discretized using SwiG with 302 points per atom. ^bUsing an isocontour $\rho_0 = 0.001$ a.u. and 1,202 grid points.

their very different solvation energies. It is also noteworthy that the two SAS cavities in Table 3, using values of R_{probe} that are common in biomolecular Poisson-Boltzmann calculations,¹¹⁹ afford very different solvation energies. The probe radius $R_{\text{probe}} = 1.4$ Å is a realistic measure of the size of a water molecule (based on radial distribution functions for liquid water),¹¹⁸ but affords rather small values of $\mathcal{G}_{\text{elst}}$. In contrast, $R_{\text{probe}} = 0.2$ Å is much too small to represent an actual water molecule but affords solvation energies much closer to values obtained using the isodensity and canonical vdW surface definitions. Values $R_{\text{probe}} = 0.2\text{--}0.3$ Å are consistent with typical solvent probe radii used since the early days of continuum solvation models in quantum chemistry.^{3\text{--}5}

Although the isodensity cavity construction is an appealing choice on physical grounds, existing algorithms to compute this surface are subject to occasional failure for certain molecular geometries.^{129,130} In principle, these difficulties could likely be overcome using an implementation based on the “marching cubes” algorithm that is well known in computer graphics.^{212,213} A more fundamental problem is that for an isodensity cavity the surface normal vector \mathbf{n}_s , which is needed to define the ASC-PCM double-layer operator \hat{D} , depends on the density:^{96,128,129}

$$\mathbf{n}_s = -\frac{\hat{\nabla}\rho(\mathbf{s})}{\|\hat{\nabla}\rho(\mathbf{s})\|} . \quad (3.8)$$

The surface area associated with the discretization point \mathbf{s}_i inherits a density dependence as well, and this significantly complicates the formulation of analytic energy gradients. To date, these have never been published for the combination of PCM (or related models) with an isodensity cavity construction. This limitation could be overcome using an analytically-differentiable pseudo-density, as has sometimes been used in biomolecular electrostatics calculations,^{19,214} perhaps using a superposition of frozen atomic densities. Although this might remove some arbitrariness from the selection of atomic radii, however, it would not represent a self-consistent determination of the cavity surface that could deform to reflect changes in the molecular electronic structure. Conversely, a pseudo-density that is determined in order to reproduce the molecular electrostatic potential $\varphi^\rho(\mathbf{r})$ may afford better solvation energies as compared to vdW radii that do not respond to the electronic structure,²¹⁵ but reintroduces the problem of how to compute the analytic gradient. As such, it is unclear whether such constructions offer advantages over the simplicity of the vdW cavity. As

a simpler workaround, united-atom radii (in which hydrogen atoms are not given atomic spheres) have been parameterized in an effort to reproduce results obtained with an isodensity cavity.¹²⁶

Within the context of solving Poisson's equation in three-dimensional space, this idea has more merit, as one can define "soft" atomic spheres that interpolate the permittivity $\varepsilon(\mathbf{r})$ between limiting values inside ($\varepsilon = 1$) and outside ($\varepsilon = \varepsilon_s$) of the cavity.²¹⁶ Related to this, and offering a more compelling scheme for self-consistent determination of the solute/continuum interface, is a scheme that takes $\varepsilon(\mathbf{r})$ to be a functional of the solute's charge density, $\varepsilon[\rho](\mathbf{r})$, with limiting values $\varepsilon = 1$ near the nuclei and $\varepsilon = \varepsilon_s$ farther away. In practice, "near" and "far" are determined not by distance but by comparison of $\rho(\mathbf{r})$ to a pair of parameters ρ_{\max} and ρ_{\min} , the latter of which establishes what constitutes the "tail" of the density. This idea was originally developed by Fattebert and Gygi^{217–219} then later refined by others;^{220–223} see Ref. 24 for a review. In its modern incarnation,²²¹ it uses a permittivity functional

$$\varepsilon[\rho](\mathbf{r}) = \begin{cases} 1 & \rho(\mathbf{r}) > \rho_{\max} \\ \exp[t(\ln \rho(\mathbf{r}))] & \rho_{\min} < \rho(\mathbf{r}) < \rho_{\max} \\ \varepsilon_s & \rho(\mathbf{r}) < \rho_{\min} \end{cases} \quad (3.9)$$

in which $t(x)$ is a switching function that interpolates smoothly between values $t(\ln \rho_{\min}) = \ln \varepsilon_s$ and $t(\ln \rho_{\max}) = 0$, so that $\varepsilon(\mathbf{r})$ achieves the limits indicated in Eq. (3.9). Inserting this *ansatz* into Poisson's equation [Eq. (2.3)] affords a model in which the dielectric interface is smooth, rather than sharp as it is in PCMs, yet one where the definition of the interface is updated self-consistently as the density $\rho(\mathbf{r})$ is iterated to convergence. For that reason, this approach has been called simply the *self-consistent continuum solvation* (SCCS) model.²⁴ The dependence of $\varepsilon_s(\mathbf{r})$ on the density does mean that the Fock operator $\delta\mathcal{G}/\delta\rho$ acquires an extra term relative to what was discussed in Section 2.1, namely²²¹

$$v_\varepsilon[\rho](\mathbf{r}) = -\frac{1}{8\pi} \|\hat{\nabla}\varphi(\mathbf{r})\|^2 \left(\frac{\delta\varepsilon[\rho]}{\delta\rho(\mathbf{r})} \right). \quad (3.10)$$

The SCCS model is increasingly being used in *ab initio* simulations of materials, *e.g.*, to model the aqueous electrolyte/solid-state interfaces relevant in electrochemistry.^{24,71,223–230} Some of that work points to limitations of the linear dielectric model itself (*i.e.*, the assumption that $\mathbf{P} \propto \mathbf{E}$), because the rotational response of the water molecules saturates at the electrode interface and consequently the susceptibility is smaller than in bulk water.^{227,228} Limitations in the linearized Poisson-Boltzmann description of electrolyte effects have also been demonstrated.^{226–228}

3.4 Linear-scaling algorithms

As noted above, the electrostatic solvation energy obtained from IEF-PCM should be *exactly* equivalent to that obtained by solving Poisson's equation, in the case of a classical solute for which there is no outlying charge. (This equivalence holds only up to discretization errors, but those are controllable and can be driven to zero if systematically-improvable grids are employed.) It is therefore surprising that the PCM formulation of the classical continuum problem has seen very little use in biomolecular electrostatics calculations. Such calculations are almost always performed in water, meaning that the simpler C-PCM should be essentially exact, and modifications have been proposed to treat the linearized Poisson-Boltzmann problem,^{68,155,156,164} including modifications to simulate an ion exclusion layer.⁶⁸ The Poisson-Boltzmann equation in three dimensions [Eq. (2.12)] is typically solved using a finite-difference scheme for the Laplacian operator,^{39,231} and this poses problems for molecular dynamics simulations with implicit solvent, because the forces need not be

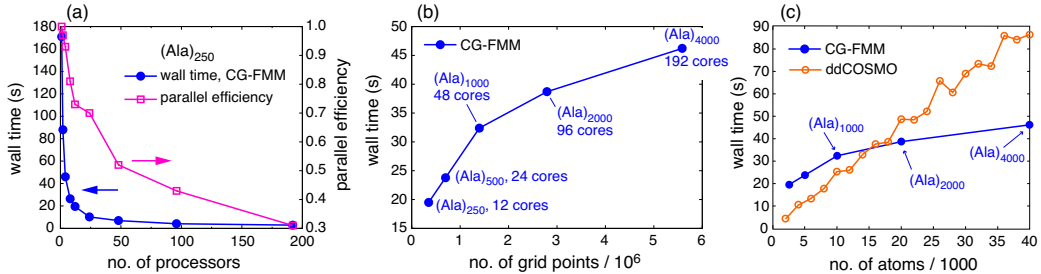


Fig. 7: Timings and parallel scalability data for linear-scaling PCM solvers applied to polyalanine helices, using a classical force field description of the solute. (a) Strong-scaling data for a CG-FMM algorithm applied to (Ala)₂₅₀, running on 12 shared-memory cores per node. (b) Weak-scaling data for (Ala)_n helices of increasing length, versus the number of Lebedev grid points used to discretize the cavity surface. (c) Comparison of timing data for CG-FMM versus ddCOSMO for (Ala)_n. The CG-FMM data in (c) are the same as those in (b), but all ddCOSMO calculations were run on a single 12-core node. Data in (a) and (b) are from Ref. 19 and ddCOSMO data in (c) are from Ref. 165.

continuous when discretized in this way. Although significant effort has gone into obtaining high-quality forces,^{161–163,232–236} from a certain point of view this looks like engineering an elaborate means of escape from the very deep hole created by a numerical framework that admits discontinuities. A better strategy is not to get trapped in that hole in the first place. The SwiG discretization procedure for PCMs (Section 3.2) was designed as a starting point that is free of discontinuities.

All of this suggests that SwiG-PCMs could make very attractive replacements for the finite-difference Poisson-Boltzmann solvers that are commonplace in biomolecular electrostatics calculations. Efforts to do so will quickly run up against the size of the PCM matrix equation, which is equal to the number of discretization grid points, itself proportional to the number of solvent-exposed atoms. This means that a straightforward solution of Eq. (3.2), based on constructing $\mathbf{K}_\varepsilon^{-1}\mathbf{Y}_\varepsilon$ or its equivalent, incurs a CPU cost of $\mathcal{O}(N_{\text{atoms}}^3)$ and a memory footprint of $\mathcal{O}(N_{\text{atoms}}^2)$, albeit with significant prefactors in both cases that reflect the number of discretization points per atom. In QM/MM calculations with continuum boundary conditions, it is the size of the MM region that dictates the matrix dimension and for small QM regions with large MM environments, one can easily encounter scenarios wherein the cost of classical electrostatics (PCM part of the calculation) exceeds the cost of doing the quantum mechanics!¹⁹

A straightforward solution to that problem is to introduce iterative solvers that do not require storage or inversion of the matrix \mathbf{K}_ε ,^{19,237,238} such as conjugate gradient (CG) or biconjugate gradient algorithms.¹⁹ The bottleneck in these methods is computing the Coulomb interactions between surface discretization points, and this can be accelerated using the fast multipole method (FMM),²³⁸ in either its original formulation or using a simpler tree-code approach.^{19,141} Parallelization strategies have also been discussed.¹⁹ Data for polyalanine helices (Fig. 7) show that wall times for iterative solution of the PCM equation (to obtain surface charges) can be reduced to a few seconds, even for (Ala)₄₀₀₀ with 5.6×10^6 surface discretization points. Proof-of-concept MM/PCM molecular dynamics simulations have been reported in which the atomistic MM region consists of a segment of DNA bound to a histone (21,734 classical atoms from a force field), with $\approx 124,000$ point charges used to discretize the surface.¹⁹

An alternative algorithm for fast iterative solution of the PCM equation is based on a domain decomposition procedure.^{165–167,239–241} Here, the solute cavity is divided into overlapping domains,

Table 4: Mean unsigned errors (MUEs) for aqueous hydration energies ($\Delta_{\text{hyd}}\mathcal{G}^\circ$), using continuum solvation models, for small molecules in the Minnesota Solvation Database.^{246–249} Estimated uncertainties in the experimental data are ± 0.2 kcal/mol for neutral solutes^{246,247} and ± 3 kcal/mol for ions.²⁴⁷

Data Set	N_{data}	MUE (kcal/mol)					
		PCM-based			Poisson-based		
		IEF-PCM ^a	SM12 ^b	SMD ^c	CMIRS ^d	SCCS ^e	soft-sphere ^f
neutrals	274	5.7	0.7	0.8	0.8	1.1	1.1
cations	52	12.7	3.5	3.2	1.8	2.3	2.1
anions	60	8.0	3.8	6.2	2.8	5.5	3.0
all ions	112	9.7	3.7	4.7	2.4	4.0	2.6

^aB3LYP/6-31G* level using united-atom radii,¹²⁶ from Ref. 244. ^bB3LYP/6-31G* level using ChElPG charges, from Ref. 248. ^cmPW1PW/6-31G* level, from Ref. 250. ^dB3LYP/6-31G* level using isodensity cavity with $\rho_0 = 0.001$ a.u., from Ref. 251. ^ePBE in a plane-wave basis, from Ref. 252. ^fPBE in a wavelet basis, from Ref. 216.

each consisting of a single atomic sphere, for which the PCM equation can be solved analytically. These single-sphere solutions form the basis for an iterative solution of the PCM equation for the full domain, which can be formulated as sparse matrix equations that can be solved in $\mathcal{O}(N_{\text{atoms}})$ time. This method was originally developed for C-PCM and is thus named “ddCOSMO”,^{165–167,239,240} although it has now been extended to arbitrary PCMs (“ddPCM”).²⁴¹ Timing data on just a single compute node [Fig. 7(c)] show that the method is competitive with a parallel CG-FMM solver. The ddCOSMO algorithm has been implemented for MM/PCM molecular dynamics in the TINKER-HP code,²⁴² using a switching function is used to guarantee smooth forces.²⁴³ Such an approach seems like a practical replacement for finite-difference Poisson-Boltzmann solvers that is inherently free of problems with discontinuous forces.

4 Solvation Energies

Perhaps the single most important property afforded by a solvation model is the free energy of solvation, $\Delta_{\text{solv}}\mathcal{G}$. Using a solvation model to compute $\Delta_{\text{solv}}\mathcal{G}^\circ$ for the reactant and product species in a chemical reaction, combined with a gas-phase calculation of the reaction energy $\Delta_{\text{rxn}}\mathcal{U}$ and free energy

$$\Delta_{\text{rxn}}\mathcal{G}^\circ[\text{gas}] = \Delta_{\text{rxn}}\mathcal{U} - RT \ln \left(\frac{Z_{\text{products}}}{Z_{\text{reactants}}} \right), \quad (4.1)$$

where Z represents the partition function, one may obtain a value for the solution-phase reaction energy, $\Delta_{\text{rxn}}\mathcal{G}^\circ[\text{solv}]$. This procedure is illustrated by the thermodynamic cycle shown in Fig. 8. However, the continuum electrostatics problem discussed heretofore defines only the electrostatic contribution to $\Delta_{\text{solv}}\mathcal{G}^\circ$, and this is generally insufficient to predict accurate solvation energies. This point is demonstrated vividly by statistical errors in IEF-PCM solvation energies,²⁴⁴ summarized for aqueous solutes in Table 4. Errors with respect to experimental solvation energies average about 6 kcal/mol for charge-neutral solutes, 8 kcal/mol for anions, and 13 kcal/mol for cations, despite much smaller errors with respect to exact Poisson electrostatics (see Table 1). In nonaqueous solvents, IEF-PCM errors with respect to experimental values of $\Delta_{\text{solv}}\mathcal{G}^\circ$ are 4.9 kcal/mol for neutral solutes and 12.4 kcal/mol for ions.²⁴⁴ Similarly poor results confirmed using other electrostatics-only PCM approaches including C- and D-PCM.^{220,245}

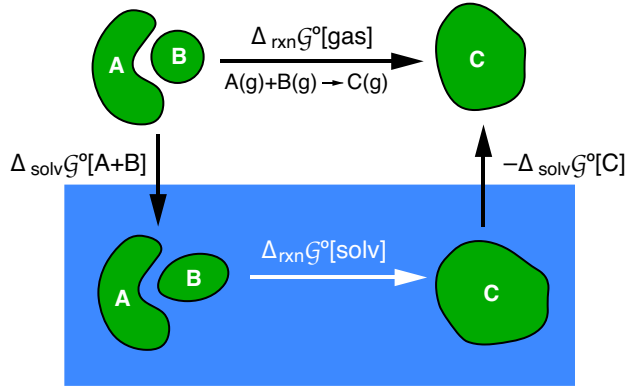
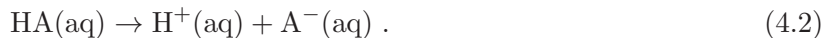


Fig. 8: Thermodynamic cycle connecting gas- and solution-phase reaction energies for $A + B \rightarrow C$. The gas-phase value of $\Delta_{\text{rxn}}G^\circ$ contains the vibrational entropy change in addition to the reaction enthalpy, and a continuum solvation model is used to compute $\Delta_{\text{solv}}G^\circ$ for each reactant and product species. This completes the thermodynamic cycle to compute the solution-phase value of $\Delta_{\text{rxn}}G^\circ$. Changes in shape signify that geometries of A, B, and C may be different in solution than they are in the gas phase, in which case the solvation energies $\Delta_{\text{solv}}G^\circ$ should include a term representing the gas-phase deformation energy.

To do better, these electrostatic solvation models must be augmented to include nonelectrostatic interactions (G_{nonelst}),²⁵³ a catch-all term that includes

- *cavitation*, meaning the energy required to carve out a space in the continuum solvent;
- *Pauli repulsion*, *i.e.*, short-range repulsive interactions with the solvent molecules;
- *dispersion*, which is non-specific but attractive, and finally
- *hydrogen-bonding* between solute and solvent.

Harder-to-define entropic changes to the solvent make a contribution to $\Delta_{\text{solv}}G^\circ$ as well,²⁴⁴ although this effect could be classified as part of the cavitation (free) energy. Indeed, the phenomena on the list above are not wholly independent, *e.g.*, short-range repulsion is also related to cavitation, and hydrogen bonding has contributions from electrostatics, repulsion, and dispersion. In protic solvents, and for solutes where hydrogen bonding is important, one or more explicit solvent molecules could be included as part of the atomistic solute, thereby removing the largest part of the last item on the list. Semicontinuum or “cluster + continuum” approaches of this kind are common, *e.g.*, for calculating hydration energies of ions.^{8,254} An important special case is pK_a calculations,^{8,255–257} corresponding to the ionization reaction



Even with one or more explicit solvent molecules to capture hydrogen bonding, however, the remaining contributions to G_{nonelst} must be added to the electrostatic model in order to obtain accurate reaction energetics. It has occasionally been noted that semicontinuum predictions of hydration energies $\Delta_{\text{hyd}}G^\circ$ may fail to converge as the number of explicit water molecules is increased.^{258–261} In truth, there is no reason why such a calculation *should* converge to $\Delta_{\text{hyd}}G^\circ$, at least in the absence of sampling over the explicit water molecules, because such an approach treats entropic contributions in an unbalanced way.

Nonelectrostatic models appropriate for use with PCMs have been developed over the years on an *ad hoc* basis.^{9,13} These have often appeared under the name of “Miertuš-Scrocco-Tomasi” solvation model,^{98,253,262,263} a term that in practice means a PCM used in conjunction with a SASA-type parameterization of $\mathcal{G}_{\text{nonelectrostatic}}$ along the lines of what is discussed in Section 4.1. These models have retained something of a do-it-yourself aesthetic and have not been packaged into “canned” or “black-box” solvation models, a fact that has occasionally led to hard feelings when errors in IEF-PCM solvation energies (such as those in Table 4) are pointed out.^{253,264} Section 4.1 examines one particular class of black-box solvation model, namely, the SM x models developed by Cramer, Truhlar, and co-workers.^{244,247–250,265,266} An even blacker-box approach is “COSMO-RS”,^{267,268} which is an extension of the COSMO method¹⁶⁸ designed for “real solvents”. The formulation and parameters of COSMO-RS are proprietary, however, so the black box cannot be opened and this method’s performance cannot be independently implemented, verified, or tested. As such, COSMO-RS is not discussed any further.

4.1 SM x and SASA-based models

For computing free energies of solvation, the most successful and popular models within the quantum chemistry community are the “SM x ” models.²⁴⁴ These have version numbers through $x = 12$,²⁴⁸ and later $x = D$ (for “density”).²⁴⁹ Only the most recent versions (SM12 and SMD) are included in Table 4.

To understand how these models work, we first take a step back to discuss implicit solvation in classical biomolecular simulations. Owing in no small part to difficulties in obtaining stable numerical forces for Poisson-Boltzmann electrostatics,^{161–163,236} as discussed in Section 3.4, the most popular implicit solvation models in that context are *not* based directly on solution of the Poisson-Boltzmann equation but instead are methods known as *generalized Born* (GB) models,^{269,270} whose name is a nod to the Born ion formula of Eq. (2.17). GB models use the Born model as a pairwise *ansatz* to compute the total electrostatic solvation energy according to

$$\mathcal{G}_{\text{elst}}^{\text{GB}} = -\frac{1}{2} \left(\frac{1}{\varepsilon_{\text{in}}} - \frac{1}{\varepsilon_{\text{out}}} \right) \sum_{A,B>A}^{\text{atoms}} \frac{Q_A Q_B}{f_{AB}}. \quad (4.3)$$

This expression allows for the possibility of a dielectric constant ε_{in} that is different from unity inside of the solute cavity. The quantity f_{AB}^{-1} in Eq. (4.3) is a parameterized, effective Coulomb potential, the canonical example of which is^{269–271}

$$f_{AB} = [R_{AB}^2 + \bar{R}_A \bar{R}_B \exp(-R_{AB}^2/4\bar{R}_A \bar{R}_B)]^{1/2}. \quad (4.4)$$

Here, $R_{AB} = \|\mathbf{R}_A - \mathbf{R}_B\|$ is the interatomic distance and the quantity Q_A^2/f_{AA} is the Coulomb self-energy in the Born ion model, with an effective cavity radius $f_{AA} \equiv \bar{R}_A$. As such, the quantities $\{\bar{R}_A\}$ are a set of effective radii that measure the “electrostatic size” of each atom in the molecule + continuum environment.^{272–274} For a classical solute, in which $\rho(\mathbf{r})$ is a collection of atom-centered point charges $\{Q_A\}$, these radii can be computed exactly by solving either Poisson’s equation,²⁷³ or else its PCM analogue,²⁷⁵ once per atomic charge Q_A , in a cavity representing the entire molecule. This procedure effectively forces the pairwise GB *ansatz* in Eq. (4.3) to reproduce the exact electrostatic energy defined by the continuum electrostatics problem, and these values of \bar{R}_A have been called the “perfect” Born radii.^{270,273} The procedure just described is not a practical way to determine \bar{R}_A but can be useful to generate data sets that may suggest new analytical forms for GB models.^{19,275–278}

In practice, the radii $\{\bar{R}_K\}$ are typically determined using various surface integration procedures.²⁷⁴ The most popular of these is^{269,270,272,274}

$$\bar{R}_K = \left(\frac{1}{R_{\text{vdW},K}} + \frac{1}{4\pi} \int_{\mathbf{r} \in \Omega} \frac{\theta(\|\mathbf{r} - \mathbf{R}_K\| - R_{\text{vdW},K})}{\|\mathbf{r} - \mathbf{R}_K\|^4} d\mathbf{r} \right)^{-1}. \quad (4.5)$$

Here, θ is a step function with $\theta(x) = 1$ for $x > 0$ and $\theta(x) = 0$ for $x \leq 0$; this limits the integration domain to the region of the solute cavity ($\mathbf{r} \in \Omega$) that lies outside of the vdW sphere for atom K . The expression for \bar{R}_K in Eq. (4.5) comes from the so-called Coulomb-field approximation,^{269,270,272} a charge-in-a-sphere model for the reaction-field potential. This is thought to overestimate electrostatic size, especially for charges close to the cavity surface, and alternatives have been developed,^{270,274} but Eq. (4.5) is the form used in the SM x models that are described below. The requisite integral can be evaluated numerically using concentric atomic radical shells,²⁷⁹ but its gradient with respect to nuclear displacements, which is needed to obtain $dG_{\text{elst}}^{\text{GB}}/dx$, is complicated when defined in terms of the solid geometry of interpenetrating vdW spheres.¹⁹⁰ Both the integral in Eq. (4.5) and its gradient would be straightforward to evaluate using SwiG discretization; see Fig. 5(b).

The GB *ansatz* in Eq. (4.3) specifies only the electrostatic component of the solvation energy. The model is completed by adding a nonelectrostatic term $\mathcal{G}_{\text{nonelectrostatic}}$, for which two forms are common. The simpler of the two consists of a term proportional to the volume of the solute cavity, to model the cavitation energy, and another term proportional to the SASA, which serves to model dispersion:

$$\mathcal{G}_{\text{nonelectrostatic}} = \beta V_{\text{cavity}} + \gamma \times (\text{SASA}). \quad (4.6)$$

The quantities β and γ are empirical parameters. An alternative form that is also widely used is

$$\mathcal{G}_{\text{nonelectrostatic}} = \sum_K^{\text{atoms}} \gamma_K \times \text{SASA}(K), \quad (4.7)$$

where $\text{SASA}(K)$ is the solvent-exposed surface area of atom K and the parameter $\{\gamma_K\}$ have units of surface tension. Note that there is no volumetric term in Eq. (4.7). It has been argued, based on the scaled-particle theory of hard-sphere fluids,²⁸⁰ that for small molecules the cavitation energy ought to be parametrizable in terms of the solvent-exposed surface area,^{98,149,281,282} although the form in Eq. (4.7) has been used for macromolecules as well.²⁸³ Models that combine GB electrostatics [Eq. (4.3)] with force-field charges to represent the solute, using either Eq. (4.6) or Eq. (4.7) for $\mathcal{G}_{\text{nonelectrostatic}}$, are known as “MM/GBSA” methods.^{284–292} There is an analogous set of “MM/PBSA” methods that substitute Poisson-Boltzmann electrostatics in place of the GB model.^{284–293} The MM/GBSA method is the most widely-used implicit solvation model in biomolecular simulation,²⁷⁰ but both approaches are popular in drug-discovery applications, *e.g.*, for calculating ligand–protein binding affinities.^{293–296} In that context, these methods are often used as low-resolution screening tools representing a level of sophistication that is intermediate between “knowledge-based” (but largely physics-free) docking or scoring-function procedures, and much more expensive atomistic free energy simulations in explicit solvent.

In quantum chemistry contexts, it is not uncommon to use different definitions of the cavity surface for the electrostatic and nonelectrostatic interactions. Models for $\mathcal{G}_{\text{nonelectrostatic}}$ introduced above suggest a SAS cavity but numerical results for $\mathcal{G}_{\text{elst}}$ in Table 3 suggest that atomic radii $R = 1.2R_{\text{vdW}}$ correspond more closely to isodensity results as compared to SAS radii ($R = R_{\text{vdW}} + R_{\text{probe}}$), at least when R_{probe} corresponds to a realistic estimate of the size of a solvent molecule. The SM x

models,²⁴⁴ which are the most popular methods for predicting $\Delta_{\text{solv}}\mathcal{G}$ in quantum chemistry calculations, exemplify this distinction. The SM8²⁶⁵ and SM12²⁴⁸ variants, for example, employ GB electrostatics based on radii obtained from Eq. (4.5), along with atom-centered charges derived from the quantum-mechanical charge density by means of certain charge models, CMx.^{247,297–300} The latter are empirically-parameterized improvements upon standard atomic partial charge prescriptions (Mulliken, Hirshfeld, etc.), with additional parameters designed to improve the dipole moments obtained from the partial charges, since Mulliken and Hirshfeld charges known to do a poor job of reproducing the dipole moment corresponding to the SCF charge density from which they were obtained.³⁰¹ CMx charges inherit the basis-set sensitivity of the underlying wave function-derived charges, therefore the SMx models through SM12 are each parameterized for use with particular (small) basis sets, *e.g.* 6-31G*. The SMD model²⁴⁹ was introduced to overcome this limitation, by substituting IEF-PCM electrostatics in place of a GB model, with the result that SMD can be used with arbitrary basis sets whereas other SMx models should only be used in conjunction with the basis sets for which they were parameterized.

The SMx models are completed by adding a nonelectrostatic term of the form in Eq. (4.7). Atomic “surface-tension” parameters $\{\gamma_K\}$ are themselves empirically-fitted functions of certain “solvent descriptors”, which include the surface tension of the solvent itself, its refractive index (which is related to polarizability), and certain Lewis acidity parameters.³⁰² The result is a “universal” model,²⁴⁴ in the sense that once the fitting procedure is completed, parameters $\{\gamma_K\}$ are available for any solvent for which the various solvent descriptors are known. The SM8 model additionally parameterizes $\mathcal{G}_{\text{nonelectrostatic}}$ as a function of temperature.^{303,304}

Error statistics for small-molecule hydration free energies ($\Delta_{\text{hyd}}\mathcal{G}^\circ$), obtained using SM12 and SMD, are listed in Table 4. (The SM8 model has slightly larger errors for ions; see Ref. 244.) The comparison between IEF-PCM and SMD is especially revealing because these two approaches use the same approach for $\mathcal{G}_{\text{elst}}$: IEF-PCM is just SMD without $\mathcal{G}_{\text{nonelectrostatic}}$. Evidently, the nonelectrostatic contribution dramatically reduces errors in $\Delta_{\text{hyd}}\mathcal{G}^\circ$ for both cations and for charge-neutral solutes. Errors for anions are reduced as well although the impact of $\mathcal{G}_{\text{nonelectrostatic}}$ is more muted in that case, which may simply reflect the difficulty of the anion solvation problem. In any case, it is clear that nonelectrostatic interactions must be included to obtain accurate solvation energies. For properties that depend on only a single geometry (*e.g.*, for some spectroscopic applications), the nonelectrostatic contributions may be less important but to compute a reaction profile—reactant, product, and transition state energies in solution—one might worry that changes in geometry along the reaction coordinate could affect the nonelectrostatic contribution differently for the various chemical species involved.

Error statistics for solvents other than water are on par with results for aqueous solutes, *e.g.*, mean unsigned errors (MUEs) of 0.6 kcal/mol for neutral solutes and 4.5 kcal/mol for ions, in the case of SM12,²⁴⁸ versus 0.7 kcal/mol for neutrals and 4.2 kcal/mol for ions using SMD.²⁴⁹ Prediction of $\Delta_{\text{solv}}\mathcal{G}^\circ$ in nonaqueous solvents is necessary in order to predict partition coefficients between different solvents. In particular, the octanol/water partition coefficient (equilibrium constant K_{ow}) is a common measure of lipophilicity (or conversely, hydrophobicity),^{305–307} and is related to solvation energies according to

$$\Delta_{\text{solv}}\mathcal{G}^\circ[\text{octanol}] - \Delta_{\text{solv}}\mathcal{G}^\circ[\text{water}] = -RT \ln K_{\text{ow}}. \quad (4.8)$$

The value of K_{ow} is widely used in drug-discovery applications,^{307–309} and atomic decomposition of terms contributing to $\Delta\Delta\mathcal{G}^\circ$ in Eq. (4.8) has been used to determine similarity indices for predicting quantitative structure–activity relationships.³⁰⁷ For environmental toxicology purposes, K_{ow} is an important physical parameter to determine for any new compound.³¹⁰ The octanol/water partition

coefficient was the subject of a recent blind challenge for theoretical methods,³¹¹ with the SM x models emerging as amongst the best performers with a root-mean-square error of 0.44 in units of $\log_{10} K_{\text{ow}}$.³¹²

Note that by using Eq. (4.7) for $\mathcal{G}_{\text{noneelst}}$, the SM x models do not contain any term proportional to the cavity volume, as is often present in MM/GBSA and MM/PBSA models, and cavitation effects are therefore included by means of *area*-dependent parameters. Although formally justified by appeal to scaled-particle theory,⁹⁸ that argument is probably most convincing for small-molecule solutes. As such, and the success of SM x may partly reflect the fact that it was parameterized using experimental solvation energies of mostly small molecules. (The largest molecules in the training set are *n*-hexadecane and ethyloctadecanoate, at 51 and 63 atoms, respectively, but most of the solutes are much smaller.^{249,250}) Small solutes have limited conformational flexibility and there may not be too much difference in the volumes of different conformers, therefore a term that explicitly accounts for cavitation may be largely redundant and not required to obtain good solvation energies. In contrast, MM/GBSA and MM/PBSA methods are usually parameterized for (or at least tested on) proteins and other macromolecular solutes, where folded and unfolded structures likely have rather different volumes. The benchmarks for MM/GBSA and MM/PBSA are usually solvation energies obtained from molecular dynamics simulations in explicit solvent. Since the SM x models have not been scaled up to macromolecules, it remains unclear how they would perform in that context.

SM x approaches have historically been the go-to models for computing solvation energies in quantum chemistry but two newer approaches based directly on Poisson's equation seem very promising.^{216,252} One of these is the SCCS approach that was described in Section 3.3, which uses a density-dependent permittivity functional $\varepsilon[\rho](\mathbf{r})$ to determine the solute cavity self-consistently alongside the charge density $\rho(\mathbf{r})$, with Poisson's equation solved in three-dimensional space to obtain $\mathcal{G}_{\text{elst}}$. Combined with the simple two-parameter model for $\mathcal{G}_{\text{noneelst}}$ in Eq. (4.6), the SCCS approach achieves a statistical accuracy for aqueous solvation energies that is comparable to SM12 or SMD (see Table 4).²⁵² This is despite using just two empirical parameters in $\mathcal{G}_{\text{noneelst}}$, along with two parameters [and an *ansatz*, Eq. (3.9)] for the cavity determination. The SM x models have a considerably larger number of empirical parameters, although they are designed to be “universal” models for all solvents, whereas the SCCS model is parameterized only for water. Improvement upon SCCS results for anions is obtained using a “soft-sphere” model,²¹⁶ which constructs the cavity from vdW spheres but then interpolates the dielectric function (from $\varepsilon = 1$ to $\varepsilon = 78$) over a narrow switching region centered on the vdW radius.²¹⁶ When combined with the two-parameter model for $\mathcal{G}_{\text{noneelst}}$, the soft-sphere solvation model affords a MUE of 3.0 kcal/mol in $\Delta_{\text{hyd}}\mathcal{G}^\circ$ for anions (Table 4), which is on par with the estimated uncertainty (2–3 kcal/mol) in the experimental data themselves.^{247,313}

4.2 Physics-based models

Occasionally there have been attempts to put the nonelectrostatic contributions to the solvation energy on a more rigorous footing,^{314–324} or at least to develop parameterized models that are more closely connected to the physics of intermolecular interactions as compared to the wholly empirical SASA-type approaches.^{325–329} As a simple example of the latter variety, one might borrow from QM/MM methodology and assume classical interaction potentials, *e.g.*, of Lennard-Jones type that are centered on the solute atoms, with an r^{-6} distance dependence for dispersion. This affords a

model of the form^{326,329}

$$\mathcal{G}_{\text{disp}} = \sum_A^{\text{solvent}} \bar{\rho}_A \sum_B^{\text{solute}} \gamma_{AB} \sum_{i \in B}^{\text{grid}} a_i \left(\frac{\mathbf{r}_{iB} \cdot \mathbf{n}_{\mathbf{s}_i}}{3r_{iB}^6} \right), \quad (4.9)$$

where $\bar{\rho}_A$ is the average number density of solvent atom A , and the parameters γ_{AB} come from a force field. A similar model, depending for example on r_{iB}^{-12} , can be developed to describe the repulsive contribution, \mathcal{G}_{rep} .^{327,329} The quantity $\mathcal{G}_{\text{disp}} + \mathcal{G}_{\text{rep}}$ is usually then combined with a cavitation energy of the form

$$\mathcal{G}_{\text{cav}} = \sum_B^{\text{solute}} \left(\frac{\text{SASA}(B)}{4\pi R_B^2} \right) \Delta G_{\text{HS}}(R_B), \quad (4.10)$$

in which $\Delta G_{\text{HS}}(R_B)$ is the solvation energy for a hard sphere of radius R_B , obtained from scaled-particle theory.²⁸⁰ Typically the atomic radii used in these nonelectrostatic terms are SAS radii, *i.e.*, they include a probe radius representing the assumed size of a solvent atom; see Eq. (3.7). This is the case even if $\mathcal{G}_{\text{elst}}$ is evaluated using a vdW cavity surface.

This is a classical model for the nonelectrostatic interactions but there have also been attempts to derive fully quantum-mechanical dispersion–repulsion models within a continuum framework. One such model, due to Amovilli,^{314,315} starts from the generalized Casimir-Polder expression for the dispersion energy of a supramolecular complex $A \cdots B$,^{330–335}

$$\mathcal{U}_{\text{disp}}^{A \cdots B} = -\frac{\hbar}{2\pi} \left(\frac{e^2}{4\pi\epsilon_0} \right)^2 \int_0^\infty d\omega \int_{\mathbb{R}^3} d\mathbf{r}_1 d\mathbf{r}_2 d\mathbf{r}'_1 d\mathbf{r}'_2 \left(\frac{\chi^A(\mathbf{r}_1, \mathbf{r}'_1 | i\omega) \chi^B(\mathbf{r}_2, \mathbf{r}'_2 | i\omega)}{\|\mathbf{r}_1 - \mathbf{r}'_1\| \|\mathbf{r}_2 - \mathbf{r}'_2\|} \right), \quad (4.11)$$

in which $\chi(\mathbf{r}, \mathbf{r}' | \omega)$ is the frequency-dependent density susceptibility (also known as the polarization propagator),^{334,335} evaluated in Eq. (4.11) at imaginary frequencies. When the monomer separation R_{AB} is large, second-order perturbation theory affords the “uncoupled” approximation,^{331,336–340} which was first derived by London:^{341,342}

$$\mathcal{U}_{\text{disp}}^{A \cdots B}(R_{AB}) = - \left[\frac{3\hbar}{\pi} \int_0^\infty \bar{\alpha}^A(i\omega) \bar{\alpha}^B(i\omega) d\omega \right] \frac{1}{R_{AB}^6}. \quad (4.12)$$

The quantity $\bar{\alpha}(\omega)$ is the frequency-dependent isotropic polarizability. Components of the polarizability tensor, in the spectral representation, are

$$\alpha_{ab}(\omega) = \frac{1}{\hbar} \sum_{n>0} \left[\frac{\langle 0 | \hat{\mu}_a | n \rangle \langle n | \hat{\mu}_b | 0 \rangle}{\omega - \omega_{n0}} + \frac{\langle 0 | \hat{\mu}_b | n \rangle \langle n | \hat{\mu}_a | 0 \rangle}{\omega + \omega_{n0}} \right], \quad (4.13)$$

where $\omega_{n0} = (E_n - E_0)/\hbar$.³⁴³ The term in brackets in Eq. (4.12) provides a microscopic formula for the Lennard-Jones C_6 coefficient.

Returning to the more general expression in Eq. (4.11), a sum-over-states expression (Lehmann representation) can be introduced for the requisite density susceptibilities, writing them in terms of transition densities $\rho_{0n}(\mathbf{r})$:^{333,335}

$$\chi(\mathbf{r}, \mathbf{r}' | i\omega) = -\frac{2}{\hbar} \sum_{n>0} \frac{\omega_{n0} \rho_{0n}(\mathbf{r}) \rho_{0n}(\mathbf{r}')}{\omega_{n0}^2 + \omega^2}, \quad (4.14)$$

Inserting this formula for $\chi^A(\mathbf{r}_1, \mathbf{r}'_1 | i\omega)$ in Eq. (4.11) affords an expression for the dispersion energy of “A-in-B”, *i.e.*, solute A interacting with an implicit representation of B:³¹⁴

$$\mathcal{G}_{\text{disp}}^{\text{A-in-B}} = \frac{1}{\pi} \int_0^\infty d\omega \sum_{n>0} \frac{\omega_{n0}^A}{(\omega_{n0}^A)^2 + \omega^2} \int_{\mathbb{R}^3} d\mathbf{r} \int_{\Gamma} d\mathbf{s} \left(\frac{\rho_{0n}^A(\mathbf{r}) \sigma_B[\varepsilon^B(i\omega), \rho_{0n}^A](\mathbf{s})}{\|\mathbf{r} - \mathbf{s}\|} \right). \quad (4.15)$$

In writing this equation, the susceptibility χ^B in Eq. (4.11) has been eliminated by first introducing a polarization density

$$\rho_{\text{pol}}^B(\mathbf{r}_2) = \int_{\mathbb{R}^3} d\mathbf{r}'_1 d\mathbf{r}'_2 \left(\frac{\chi^B(\mathbf{r}_2, \mathbf{r}'_2 | i\omega) \rho^A(\mathbf{r}'_1)}{\|\mathbf{r}'_1 - \mathbf{r}'_2\|} \right), \quad (4.16)$$

induced on B by the presence of A. This quantity is then replaced with a surface charge $\sigma_B(\mathbf{s})$, in the spirit of the PCM formulation of the continuum electrostatics problem, and which depends on the frequency-dependent dielectric function $\varepsilon(i\omega)$ evaluated at imaginary frequencies. The function $\varepsilon(i\omega)$ is the central quantity in the Lifshitz's general theory of the Casimir force and dispersion energies.^{330,344–346} In a separate approach, Ninham and coworkers^{323,324} use the frequency-dependent dipole- and higher-order (hyper)polarizabilities for the solute, $\bar{\alpha}(i\omega)$ etc., in conjunction with models for $\varepsilon(\omega)$, to model solute–solvent dispersion.

Models for $\mathcal{G}_{\text{disp}}$ can now be constructed based on Eq. (4.15) by modeling the dielectric function $\varepsilon(i\omega)$ and the surface charge density $\sigma_B(\mathbf{s})$ that is induced by various excited states of solute A, via transitions densities $\rho_{0n}^A(\mathbf{r})$. These transition densities, along with the corresponding excitation frequencies ω_{n0}^A that appear in Eq. (4.15), might be computed explicitly (since the solute A is described by quantum chemistry),³¹⁴ or perhaps modeled using SCF eigenvalues.^{315,316} A model suggested for the surface charge is³¹⁵

$$\sigma_B[\rho_{0n}^A](\mathbf{s}) = -\frac{1}{4\pi} \left(\frac{\Omega^2}{\Omega^2 + \omega^2} \right) \left(\frac{\varepsilon_\infty - 1}{\varepsilon_\infty} \right) E_\perp[\rho_{0n}^A](\mathbf{s}), \quad (4.17)$$

where $E_\perp[\rho_{0n}^A](\mathbf{s})$ is the normal electric field generated by the density $\rho_{0n}^A(\mathbf{r})$. Modulo a factor of $\Omega/(\Omega + \omega^2)$, this is precisely the apparent surface charge of the D-PCM approach [Eq. (2.24)], albeit generated by the transition density ρ_{0n}^A rather than the ground-state density and with the “optical” dielectric constant ε_∞ replacing the static dielectric constant ε_s . (As discussed in Section 5, the value ε_∞ is the appropriate one for re-polarization upon sudden or vertical excitation, without orientational contributions from the solvent.) Regarding the factor of $\Omega^2/(\Omega^2 + \omega^2)$, the quantity $\hbar\Omega$ is the characteristic ionization energy of the solvent. [This comes from the approximation of setting every ω_{n0} equal to Ω ;³⁴² In practice, $\hbar\Omega = \varepsilon_\infty \times (\text{IE})_{\text{solvent}}$ has been used.^{315,316}] The integral over ω in Eq. (4.15) remains to be evaluated and this factor interpolates the apparent surface charge between limits of unity for $\omega = 0$, for which the solute sees the full induced polarization response, and zero as $\omega \rightarrow \infty$ because when $\omega \gg \Omega$ the excitation frequency is so large that the response averages to zero. These models have interesting possibilities for the description of solute–environment dispersion in excited states, which are only starting to be explored.^{316,317}

A rather different formulation of the solute–continuum dispersion interaction has been put forward by Pomogaeva and Chipman,³²⁰ who borrow from the nonlocal correlation energy functional developed by Vydrov and Van Voorhis.^{347–350} This functional, usually known as VV10,³⁵¹ represents an attempt to incorporate dispersion interactions into density functional theory in a rigorous way and is itself a simplified form of the nonlocal functional developed by Langreth and Lundqvist.^{352–355} (In a mildly annoying bit of physicist reductionism, the Langreth-Lundqvist functional is often known as “the” van der Waals functional, as if such a designation could possibly be unique.) These nonlocal correlation functionals are already based on a pairwise *ansatz*,³⁵¹ and to use them in conjunction with a continuum representation of the solvent one simply replaces the density of one interacting partner with the bulk solvent density, $\bar{\rho}$. The functional form is then^{251,320}

$$\mathcal{G}_{\text{disp}} = A \int_{\mathbf{r} \in \Omega} \left(\frac{\rho(\mathbf{r}) I(\mathbf{r})}{w[\rho](\mathbf{r})(w[\rho](\mathbf{r}) + \bar{\rho}_{\text{solvent}}^{1/2})} \right) d\mathbf{r} \quad (4.18)$$

where

$$I(\mathbf{r}) = \int_{\mathbf{r}' \notin \Omega} \left(\frac{d\mathbf{r}'}{\|\mathbf{r} - \mathbf{r}'\|^6 + \delta^6} \right) \quad (4.19)$$

and

$$w[\rho](\mathbf{r}) = \left(\rho(\mathbf{r}) + \frac{3C}{4\pi} \frac{\|\hat{\nabla}\rho(\mathbf{r})\|^4}{\rho(\mathbf{r})^4} \right)^{1/2}. \quad (4.20)$$

The parameter C in Eq. (4.20) is taken without modification from VV10,^{348,349} but a parameter δ is introduced in Eq. (4.19) to prevent divergence of the integral. Aside from that, the only additional parameter that has been introduced (beyond those already present in VV10) is an overall scaling factor A in Eq. (4.18). The density $\rho(\mathbf{r})$ is the solute's electron density and the integral in Eq. (4.18) is evaluated over the solute cavity ($\mathbf{r} \in \Omega$). However, the integration domain in Eq. (4.19) is the region $\mathbf{r}' \notin \Omega$ that is *outside* of the solute cavity, which requires integration of three-dimensional space. (In practice the discretization need not extend very far beyond the cavity, since the integrand decays rapidly.) It is worth noting that analytic gradients have not been implemented for the quantum-mechanical dispersion models described in this section, although they have been implemented for the QM/MM-style approach of Eq. (4.9).³²⁹ However, the functional form for $\mathcal{G}_{\text{disp}}$ in Eq. (4.18) may better lend itself to analytic gradients as compared to Eq. (4.5), insofar as the analytic gradient of VV10 has already been reported.³⁴⁹

In contrast to dispersion, a functional form for Pauli repulsion is rather straightforward. This effect arises due to interpenetration of the tails of two non-bonded densities, and one functional form that has been suggested is simply

$$\mathcal{G}_{\text{exch}} = B \int_{\mathbf{r} \notin \Omega} \rho(\mathbf{r}) d\mathbf{r} \quad (4.21)$$

where B is an empirical scaling factor.³¹⁵ (Note also that the integration domain is over the solvent, $\mathbf{r} \notin \Omega$.) An alternative is³²⁰

$$\mathcal{G}_{\text{exch}} = B \int_{\mathbf{r} \notin \Omega} \|\hat{\nabla}\rho(\mathbf{r})\| d\mathbf{r}. \quad (4.22)$$

This latter form is suggested by an exact result for the exchange-repulsion energy of two hydrogen atoms,³⁵⁶ but both models have been used in practice. For example, the model in Eq. (4.21) has been used to develop an “extreme pressure” (XP-) PCM,^{357,358} which is based on the thermodynamic relation $p = -(\partial\mathcal{G}/\partial V)_T$ and calculation of analytic derivatives of $\mathcal{G}_{\text{exch}}$ and $\mathcal{G}_{\text{elst}}$ with respect to the cavity volume. XP-PCM has been used to study how pressures $p > 1$ GPa affect both molecular geometries and the equilibrium positions of chemical reactions.^{359,360} The exchange-repulsion model in Eq. (4.22) has been used as part of a black-box solvation model that is described next.

In an attempt to develop a first-principles implicit solvation model that can compete with SMx, Pomogaeva and Chipman^{318–322} have combined SS(V)PE electrostatics (based on an isodensity cavity construction) with a “minimally parameterized” nonelectrostatic model of the form

$$\mathcal{G}_{\text{nonelst}} = \mathcal{G}_{\text{disp}} + \mathcal{G}_{\text{exch}} + \mathcal{G}_{\text{FESR}}. \quad (4.23)$$

Here, $\mathcal{G}_{\text{disp}}$ and $\mathcal{G}_{\text{exch}}$ are the models in Eq. (4.18) and Eq. (4.22), respectively, and $\mathcal{G}_{\text{FESR}}$ is “field-effect short-range” (FESR) term for hydrogen bonding. The functional form for $\mathcal{G}_{\text{FESR}}$ takes as inputs the maximum and minimum values of the normal electric field at the cavity surface, and has the form³¹⁹

$$\mathcal{G}_{\text{FESR}} = C(\min |E_{\perp}|)^{\xi} + D(\max |E_{\perp}|)^{\xi}. \quad (4.24)$$

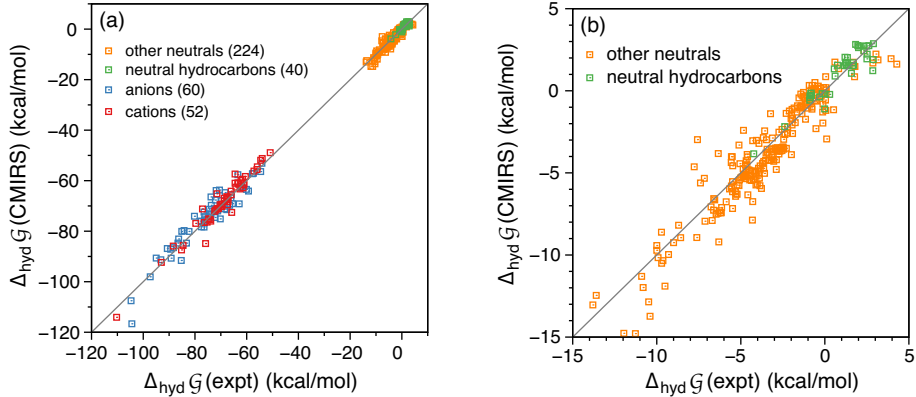


Fig. 9: Comparison of experimental hydration energies in the Minnesota solvation database^{246–249} to predictions from the CMIRS model: (a) all solvation energies, including both neutral molecules as well as ions (with the number of data points indicated in each case), versus (b) results for charge-neutral solutes only. Reprinted from Ref. 251; copyright 2016 American Chemical Society.

(The correlation between hydrogen bond strength and local electric fields in water has been made before.^{361–363}) This *ansatz* is likely only appropriate for small molecules since it would seem to accommodate only a single hydrogen-bond donor site and a single acceptor site.

The combination of SS(V)PE electrostatics with $\mathcal{G}_{\text{nonelst}}$ in Eq. (4.23) has been called the *composite method for implicit representation of solvent* (CMIRS).^{251,320–322} This model contains five empirical parameters for a given solvent: the linear coefficients A , B , C , and D , along with the exponent ξ . (The FESR term is omitted for non-polar solvents.) Pomogaeva and Chipman determined these parameters, by fitting to experimental solvation energies, for benzene,³²⁰ cyclohexane,³²⁰ water,³²¹ dimethyl sulfoxide,³²² and acetonitrile,³²² although all of those parameters were later adjusted to fix an error in the original implementation.²⁵¹ Parameters for methanol have also been reported based on the original implementation.³⁶⁴ For any given solvent, this is considerably fewer parameters than are contained in any of the SM x models, although the latter are designed as “universal” models in which the nonelectrostatic parameters $\{\gamma_K\}$ in Eq. (4.7) are determined only once, and then the model is available for any solvent whose macroscopic descriptors are available.²⁴⁴ For example, the training set for SM12 contains 92 solvents,²⁴⁸ as compared to the six for which CMIRS parameters are currently available.

Of course, water is the solvent to have if you’re only having one, and error statistics versus experimental hydration energies (Table 4) demonstrate that CMIRS is somewhat more accurate (on average) than SM12 or SMD values, especially for ions, despite fewer parameters in the model. The CMIRS error of 2.4 kcal/mol for ions is comparable to the estimated uncertainty (2–3 kcal/mol) in the experimental solvation energies for aqueous ions,^{247,313} and thus represents the practical lower limit for any solvation model trained on these data. Correlation between CMIRS and experimental hydration energies is excellent; see Fig. 9. That said, despite all of the physical considerations that went into the CMIRS model for $\mathcal{G}_{\text{nonelst}}$, and despite the limited number of parameters used per solvent, an error in the original implementation $\mathcal{G}_{\text{disp}}$ went unnoticed despite the fact that it modifies dispersion energies in the training set by up to 8 kcal/mol.²⁵¹ This was able to escape notice because the B parameter in Eq. (4.22) absorbs the discrepancy, making $\mathcal{G}_{\text{exch}}$ more repulsive in order to offset the too-attractive dispersion energy.²⁵¹ A similar cancellation between the repulsive cavitation term and the attractive dispersion term has been noted elsewhere,³²⁴ and in fact $\mathcal{G}_{\text{disp}} + \mathcal{G}_{\text{exch}}$ is often parameterized together as a single entity in empirical models, including SM x and others that use

the atomic surface tension *ansatz* of Eq. (4.7). This may hide certain subtleties, such as the fact that cavitation effects are more important than dispersion to explain binding affinities of rare-gas guest atoms to cucurbituril host molecules,³⁶⁵ or that the unfavorable hydration energies of small nonpolar polymers are well approximated by the cavitation energy ($\Delta_{\text{hyd}}\mathcal{G} \approx \mathcal{G}_{\text{cav}}$),³⁶⁶ suggesting near-cancellation of other effects.

5 Nonequilibrium Solvation

5.1 Conceptual overview

How does a continuum solvent respond to a sudden change in the solute's charge distribution? This question must be considered for electronic spectroscopies, including absorption to (or emission from) an excited electronic state, or photoelectron spectroscopy that removes an electron from the solute. The general theory of time-dependent processes in dielectric materials introduces a frequency-dependent dielectric function $\varepsilon(\omega)$, such that the induction field \mathbf{D} responds to a frequency-dependent electric field \mathbf{E} according to $\mathbf{D}(\mathbf{r}, \omega) = \varepsilon(\omega) \mathbf{E}(\mathbf{r}, \omega)$.^{367–370} In the presence of a time-dependent field, the permittivity $\varepsilon(\mathbf{r}, \omega)$ is complex-valued, in order to describe the phase lag between \mathbf{E} and \mathbf{D} .^{367,370} Often, the complex-valued permittivity is denoted as $\hat{\varepsilon}$ or ε^* but we will not do so here. Where needed, we will simply indicate the frequency dependence explicitly.

The permittivity is real-valued in two important limits, namely, $\varepsilon_s \equiv \varepsilon(0)$, which is the static (zero-frequency) limit, and also in the high-frequency limit. The limiting value $\varepsilon_\infty = \lim_{\omega \rightarrow \infty} \varepsilon(\omega)$ is known as the *optical dielectric constant*, for reasons that are described below, and describes the fact that there is always some part of the polarization that is able to remain in phase with the applied field. Switching to the time domain and labeling that part of the medium's response as “fast” polarization,

$$\mathbf{P}_{\text{fast}}(t) = \left(\frac{\varepsilon_\infty - 1}{4\pi} \right) \mathbf{E}(t) , \quad (5.1)$$

the remaining (“slow”) component is then defined by the time-dependent analogue of Eq. (2.1):³⁶⁷

$$\mathbf{D}(t) = \varepsilon_\infty \mathbf{E}(t) + 4\pi \mathbf{P}_{\text{slow}}(t) , \quad (5.2)$$

The frequency components of $\mathbf{P}_{\text{slow}}(t)$ depend on $\varepsilon(\omega)$, but generally speaking the slow polarization response consists of vibrational contributions with timescales of 10^{-12} – 10^{-14} s, along with orientational components having timescales slower than 10^{-12} s. For example, the primary relaxation timescale for liquid water is 8–10 ps under ambient conditions.^{77,371–373}

It is possible to model the frequency dependence of $\varepsilon(\omega)$ directly.^{374–378} A phenomenological model is

$$\varepsilon(\omega) = \varepsilon_\infty + (\varepsilon_s - \varepsilon_\infty) \sum_k \frac{c_k}{1 + i\omega\tau_k} , \quad (5.3)$$

where the τ_k are a set of characteristic time constants, representing microscopic relaxation processes, and $\sum_k c_k = 1$.³⁶⁷ (The version with only a single timescale was originally introduced by Debye.^{77,370,379}) When such a model is used in the context of continuum solvation theory, the polarization charge becomes explicitly time-dependent and the permittivity for “fast” polarization is the real part of $\varepsilon(\omega)$ for frequencies larger than the perturbation of interest. Such models have been used to simulate the time-dependent Stokes shift in the fluorescence energy,^{374–376} and to simulate the combined response of the molecule and the medium to an external field that is resonant with an excited state of the solute.³⁷⁸ The latter application makes the most sense when combined

Table 5: Static dielectric constants^a (ε_s) and optical dielectric constants^b (ε_∞) for some common solvents. (These are given as dimensionless values relative to vacuum permittivity.)

Solvent	ε_s	ε_∞	Solvent	ε_s	ε_∞
<i>n</i> -hexane	1.9	1.89	ethanol	24.3	1.85
cyclohexane	2.0	2.03	ethylene glycol	30.9	2.05
benzene	2.3	2.25	methanol	33.0	1.77
toluene	2.4	2.24	nitrobenzene	34.7	2.41
diethyl ether	4.2	1.83 ^c	acetonitrile	36.0	1.81
chloroform	4.7	2.08	dimethyl acetamide	39.6	2.07
dichloromethane	8.9	2.03	dimethyl sulfoxide	46.6	2.18
2-propanol	18.2	1.92	water	78.4	1.78 ^d
acetone	20.8	1.85	formamide	109.6	2.10

^a At 25°C, from Ref. 395. ^b At 20°C except where noted, based on refractive indices $n(\lambda)$ measured at $\lambda = 589$ nm, from Ref. 383. ^c At 16.5°C. ^d From Ref. 396, valid for 20–25°C.

with electronic structure methods that simulate time-dependent electron dynamics,^{380,381} but these explicitly time-dependent approaches are not considered in this work.

Instead, this work is focused on the nonequilibrium response to a sudden (vertical or Franck-Condon) change in the solute density. For a vertical absorption, emission, or ionization process, the nuclei are fixed and the continuum solvent “molecules” cannot vibrate or reorient. This limits the continuum solvation response to the fast component of the polarization, which is electronic in nature and remains in equilibrium with the sudden change in $\rho(\mathbf{r})$. The slow component is dictated by the solute’s initial electronic state and cannot respond on the timescale of a vertical excitation or ionization process, and is therefore out of equilibrium with the final electronic state. Phenomenologically, this is accomplished by reducing $\varepsilon(\omega)$ to its limiting values, ε_s and ε_∞ .

The value of ε_∞ can be related to the polarizability of the solvent molecules (Lorenz-Lorentz equation),³⁶⁷ but in the present context is simple a measured property of the solvent, determined from the solvent’s refractivity $n(\omega) = \sqrt{\varepsilon(\omega)}$.^{367,382} Formally this should be done in the limit $\omega \rightarrow \infty$ but also needs to be measured away from any resonances and therefore optical wavelengths are often used, hence the “optical” dielectric constant. Values are often measured at the sodium D-line, $\lambda = 589$ nm,³⁸³ and for water the value obtained is $\varepsilon_\infty(\lambda) = 1.78$ at $\lambda = 589$ nm, as compared to $\varepsilon_\infty(\lambda) = 1.95$ at $\lambda = 200$ nm.³⁸⁴ In older literature (and sometimes repeated more recently),^{385,386} values of $\varepsilon_\infty = 4.0$ –5.5 are occasionally reported for water,^{77,387} the larger value originally being thought to agree better with predictions from Onsager’s reaction-field theory.³⁸⁷ In fact, the larger value of ε_∞ is based on a false extrapolation using Debye’s model of a single relaxation timescale ($\tau_1 = 8$ –10 ps), whereas permittivity data that extend to terahertz frequencies reveal at least two distinct relaxation timescales,^{373,388–391} including a faster process $\tau_2 < 1$ ps.^{373,388,389} (The microscopic explanation for these timescales remains a topic of current debate.^{392,393}) The data therefore appear to approach a limiting value $\varepsilon_\infty \approx 5$ in the microwave regime,^{77,394} but further decay to $\varepsilon_\infty \approx 2$ at terahertz frequencies,^{389,391} the latter value being consistent with $n^2(\lambda)$ measured at optical wavelengths.³⁸⁴

Looking at a modern tabulation of the data for common solvents (Table 5),³⁸³ one finds little variation in refractive indices at visible wavelengths, which generally range from $n \approx 1.3$ –1.5. Despite having static dielectric constants ranging from $\varepsilon_s = 2$ –78, there is considerable uniformity in ε_∞ , which ranges from $\varepsilon_\infty = 1.7$ –2.3. This reflects the the fact that typical solvents are closed-shell, small-molecule insulators with band gaps in the vacuum ultraviolet, and therefore

roughly similar molecular polarizabilities. Inorganic solids may have considerably larger indices of refraction,³⁹⁷ *e.g.*, $n = 2.43$ at 589 nm (and therefore $\varepsilon_\infty = 5.90$) for BaTiO₃(s),³⁹⁸ a material used in nonlinear optical applications. These larger values are attributable to low-lying excited states that facilitate more substantial electronic polarization and therefore significant dispersion of light, but this behavior is simply not found in common solvents.

Before introducing a modern computational formalism for nonequilibrium polarization, we first consider two historical examples. The first is a well-known result in electronic spectroscopy that relates the Stokes shift ($\Delta\nu = \nu_{\text{abs}} - \nu_{\text{fluor}}$) to the change in the solute's dipole moment upon excitation ($\Delta\mu$), and which is known as the *Lippert-Mataga equation*,^{41,399–401}

$$hc\Delta\nu = \text{constant} + \frac{2(\Delta\mu)^2}{\bar{R}^3} \underbrace{\left[\frac{\varepsilon_s - 1}{\varepsilon_s + 1} - \frac{\varepsilon_\infty - 1}{2\varepsilon_\infty + 1} \right]}_{F(\varepsilon_s, \varepsilon_\infty)}. \quad (5.4)$$

In practice this equation is used to determine excited-state dipole moments (assuming that the ground-state dipole moment is known) by measuring the Stokes shift in solvents of differing polarity. In fact, a variety of alternative formulas for this purpose have been suggested,^{402–410} along the lines of Eq. (5.4) but differing somewhat in their treatment of excited-state polarization, which leads to differences in the form of the “solvent polarity function” $F(\varepsilon_s, \varepsilon_\infty)$. These models (including the Lippert-Mataga one) are so crude that often experimental data can be fit equally well to any one of them.^{411–417} More important is the basic molecular physics that underlies this approach. Comparison to the model of a dipole in a spherical cavity [Eq. (2.18)] shows that the physical content of Eq. (5.4) is to take the difference dipole moment $\Delta\mu$ and solvate it using permittivity ε_∞ rather than ε_s .

The solvent parameter ε_∞ also makes an appearance in Marcus' theory of electron transfer,^{418–423} in which the “outer-sphere” reorganization energy is given by

$$\lambda_{\text{outer}} = (\Delta Q)^2 \left(\frac{1}{\varepsilon_\infty} - \frac{1}{\varepsilon_s} \right) \left(\frac{1}{2R_D} + \frac{1}{2R_A} - \frac{1}{\|\mathbf{r}_D - \mathbf{r}_A\|} \right). \quad (5.5)$$

This formula is derived from what is essentially a nonequilibrium formulation of the Born ion model [Eq. (2.17)], combined with a Coulomb interaction between charges centered in a donor sphere (radius R_D centered at \mathbf{r}_D) and an acceptor sphere (radius R_A centered at \mathbf{r}_A). The electron transfer is assumed to occur instantaneously—before the orientational degrees of freedom of the solvent molecules can respond—hence the change in $\mathcal{G}_{\text{elst}}$ involves ε_∞ in addition to ε_s . The prefactor of $(\varepsilon_\infty^{-1} - \varepsilon_s^{-1})$ in Eq. (5.5) is sometimes called the *Pekar factor*,^{386,424} and replaces the prefactor of $(1 - \varepsilon_s^{-1})$ in the equilibrium version of the Born model. For water, ε_s is large due to the sizable H₂O dipole moment, leading to a large orientational component to the dielectric screening effect, but for non-polar solvents most or all of the solvent response is electronic since $\varepsilon_\infty \approx \varepsilon_s$ (see Table 5). The electronic contribution comes from the intrinsic polarizability of the solvent molecules, and for this reason ε_∞ has sometimes been called the “dielectric constant for induced polarization”.³⁶⁷

5.2 State-specific approach

The phenomenology introduced above can be generalized to a rigorous description of electrostatics beyond the Born or models,^{425,426} affording a continuum theory of nonequilibrium solvation.^{385,422,424–428} Several variations and implementations have been formulated for PCMs,^{185,429–433} as well as for continuum solvation based on Poisson's equation.^{39,434} Operationally, a charge density $\rho_0(\mathbf{r})$ corresponding to the initial electronic state of the solute is first equilibrated with a continuum

whose dielectric constant is ε_s . The following excitation (or ionization) from state $|0\rangle$ to state $|k\rangle$, the difference density $\Delta\rho_k(\mathbf{r}) = \rho_k(\mathbf{r}) - \rho_0(\mathbf{r})$ is allowed to polarize a continuum whose dielectric constant is ε_∞ . We now consider this in detail.

Consistent with the appearance of the zero- and infinite-frequency dielectric constants in Eqs. (5.4) and (5.5), a general nonequilibrium theory of continuum electrostatics is based upon a partition $\mathbf{P} = \mathbf{P}_{\text{fast}} + \mathbf{P}_{\text{slow}}$ in which the fast component of the polarization remains in equilibrium with the solute even when the latter experiences a sudden change in its charge density. The slow polarization is frozen on this timescale, fixed at the value determined by equilibrium solvation of the initial state. This is accomplished via a partition of the (linear) electric susceptibility, $\chi(\omega) = [\varepsilon(\omega) - 1]/4\pi$. Separating the susceptibility $\chi = \chi_f + \chi_s$ into fast and slow contributions, the form of χ_f is suggested by Eq. (5.1), namely^{185,410,426,435,436}

$$\chi_f = (\varepsilon_\infty - 1)/4\pi \quad (5.6a)$$

$$\chi_s = (\varepsilon_s - \varepsilon_\infty)/4\pi, \quad (5.6b)$$

This has been called the “Marcus partition” of the polarization response,¹⁸⁵ although it was actually formalized by Brady and Carr.⁴¹⁰ It embodies the phenomenological concepts introduced above, *e.g.*, that \mathbf{P}_{fast} originates with molecular polarizability while \mathbf{P}_{slow} is orientational.

An alternative to Eq. (5.6) is the so-called “Pekar partition”,^{185,436} which was originally introduced to describe self-trapped polarons,^{437,438} then subsequently adapted for optical spectroscopy,^{400,404,439} and still later adopted for use in ASC-type continuum solvation models.^{5,13,440–442} Its use is prevalent in older literature so the distinction with respect to Eq. (5.6) is worth pointing out. Within the Pekar approach, the induced surface charge is partitioned into “inertial” and “dynamic” components ($\mathbf{P} = \mathbf{P}_{\text{in}} + \mathbf{P}_{\text{dyn}}$). The total surface charge $\sigma(\mathbf{s})$ is given by Eq. (2.24) and the dynamical part by the analogous expression⁵

$$\sigma_{\text{dyn}}(\mathbf{s}) = \frac{1}{4\pi} \left(\frac{\varepsilon_\infty - 1}{\varepsilon_\infty} \right) \left(\frac{\partial\varphi}{\partial\mathbf{n}_s} \right)_{s=s^-} \quad (5.7)$$

that is obtained with ε_∞ replacing ε_s . The inertial charge represents the difference, $\sigma_{\text{in}}(\mathbf{s}) = \sigma(\mathbf{s}) - \sigma_{\text{dyn}}(\mathbf{s})$.

The difference between these two partitions can readily be understood using the reaction-field for a ground-state dipole μ_0 in a spherical cavity. The slow contribution to the reaction field is⁴³⁶

$$\mathbf{E}_{\text{rxn}}^s = \begin{cases} g_1(\varepsilon_s, \bar{R}) \left(\frac{\varepsilon_s - \varepsilon_\infty}{\varepsilon_s - 1} \right) \mu_0 & (\text{Marcus-Brady-Carr}) \\ [g_1(\varepsilon_s, \bar{R}) - g_1(\varepsilon_\infty, \bar{R})] \mu_0 & (\text{Pekar}) \end{cases}, \quad (5.8)$$

where $g_1(\varepsilon, \bar{R})$ is the “Onsager factor” defined in Eq. (2.19). The Marcus-Brady-Carr result follows from the fact that the slow polarization constitutes a fraction $\chi_s/\chi = (\varepsilon_s - \varepsilon_\infty)/(\varepsilon_s - 1)$ of the total polarization, according to Eq. (5.6), whereas the Pekar result is set by fiat. Both partitions afford the *same* total reaction field,⁴³⁶ $\mathbf{E}_{\text{rxn}}^s + \mathbf{E}_{\text{rxn}}^f$, and therefore the same nonequilibrium free energy,^{185,436,443} up to some minor issues involving discretization along the lines of what was discussed in Section 3.1.¹⁸⁵ However, the partition into fast and slow components is different. Noting that $g_1(\varepsilon_s, \bar{R}) \approx \bar{R}^{-3}$ for high-dielectric solvents, Brady and Carr⁴¹⁰ noted that the Pekar result for $\mathbf{E}_{\text{rxn}}^s$ seems oddly small (and also decoupled from the value of ε_s) in this limit. Indeed, for water one obtains $\mathbf{E}_{\text{rxn}}^s = 0.97\mu_0/\bar{R}^3$ for the Marcus-Brady-Carr case and $\mathbf{E}_{\text{rxn}}^s = 0.63\mu_0/\bar{R}^3$ for the Pekar partition. For that reason, the Marcus-Brady-Carr partition is the more common choice in modern literature although the Pekar partition has not vanished.⁴⁴³ (The Marcus partition has also been

criticized recently, and some alternatives have been suggested.³⁸⁶) Side-by-side expressions for the free energy $\mathcal{G}_{\text{elst}}$ in the Marcus-Brady-Carr and the Pekar partitions are provided by Tomasi *et al.*¹³ As those authors note, there is some confusion in the literature regarding the names, *e.g.*, Eq. (5.6) is called Pekar partition by Chipman.⁴³¹ As such, Tomasi *et al.* designate these schemes as “partition I”, meaning Eq. (5.6), and “partition II”, meaning Eq. (5.7). Although this notation has been adopted in a few places,^{427,443} the names “Marcus” (for partition I) and “Pekar” (for partition II) remain common.

Having settled on the partition given in Eq. (5.6), the basic idea of nonequilibrium polarization is that the susceptibility χ_s should be used to induce polarization for the initial state (“0”), whose solute charge density is $\rho_0(\mathbf{r})$, and then χ_f should be used in conjunction with the difference density $\Delta\rho(\mathbf{r})$ in order to adjust the polarization to reflect the final state. To realize this in practice, one first computes the surface charge $\sigma_0(\mathbf{s})$ that is induced by $\rho_0(\mathbf{r})$ in a medium whose dielectric constant is ε_s , according to a normal equilibrium solvation calculation. Next, $\sigma_0(\mathbf{s})$ is partitioned into fast and slow contributions,^{385,426,432}

$$\sigma_0^f(\mathbf{s}) = \left(\frac{\varepsilon_\infty - 1}{\varepsilon_s - 1} \right) \sigma_0(\mathbf{s}) \quad (5.9a)$$

$$\sigma_0^s(\mathbf{s}) = \left(\frac{\varepsilon_s - \varepsilon_\infty}{\varepsilon_s - 1} \right) \sigma_0(\mathbf{s}) . \quad (5.9b)$$

The quantity $\sigma_0^s(\mathbf{s})$ is retained, whereas $\sigma_0^f(\mathbf{s})$ is replaced by a surface charge induced by the excited-state charge distribution, in a medium whose dielectric constant is ε_∞ .

In order to derive rigorous formulas for the electrostatic free energy of an excited state, introduce a Schrödinger equation of the form

$$\underbrace{\left(\hat{\mathcal{H}}_{\text{vac}} + \hat{\mathcal{R}}_0^s + \hat{\mathcal{R}}_k^f \right)}_{\hat{\mathcal{H}}_k^{\text{SS}}} |\Psi_k\rangle = \mathcal{E}_k^{\text{SS}} |\Psi_k\rangle \quad (5.10)$$

with $k = 0$ for the ground state. The quantity $\hat{\mathcal{H}}_{\text{vac}}$ is the vacuum Hamiltonian and the reaction-field contribution $\hat{\mathcal{R}}_k = \hat{\mathcal{R}}_0^s + \hat{\mathcal{R}}_k^f$ consists of a slow component $\hat{\mathcal{R}}_0^s$ that originates with the ground-state density ρ_0 and susceptibility χ_s , along with a fast component $\hat{\mathcal{R}}_k^f$ based on the final-state density $\rho_k(\mathbf{r})$ and susceptibility χ_f . Because $\hat{\mathcal{R}}_k^f$ depends on the wave function $|\Psi_k\rangle$ that is used to compute the excited state’s electrostatic potential, the Hamiltonian $\hat{\mathcal{H}}_k^{\text{SS}} = \hat{\mathcal{H}}_{\text{vac}} + \hat{\mathcal{R}}_k$ that is introduced in Eq. (5.10) is “state-specific” (SS), and straightforward attempts to solve this equation encounter significant complications including convergence difficulties and ambiguous formulas for transition moments.⁴⁴⁴ These problems can be circumvented by treating $\hat{\mathcal{R}}_k^f$ as a perturbation on top of zeroth-order states that are eigenfunctions of $\hat{\mathcal{H}}_0^{\text{SS}}$, as discussed below.

First, let us consider an expression for the free energy in an excited state. Note that Eq. (2.8) for the ground-state free energy \mathcal{G}_0 is implicitly based on a Hamiltonian

$$\hat{\mathcal{H}}_0 \equiv \hat{\mathcal{H}}_0^{\text{SS}} = \hat{\mathcal{H}}_{\text{vac}} + \hat{\mathcal{R}}_0^{s+f} , \quad (5.11)$$

however \mathcal{G}_0 differs from $\langle \Psi_0 | \hat{\mathcal{H}}_0 | \Psi_0 \rangle$ by an amount equal to the work $\mathcal{W}_0 = \frac{1}{2} \langle \Psi_0 | \hat{\mathcal{R}}_0 | \Psi_0 \rangle$ that is required to polarize the continuum. This expression for the work can be generalized to an arbitrary state $|\Psi_k\rangle$:

$$\mathcal{W}_k = \frac{1}{2} \langle \Psi_k | \hat{\mathcal{R}}_k | \Psi_k \rangle = \frac{1}{2} \int_{\Gamma} \sigma_k(\mathbf{s}) \varphi^{\rho_k}(\mathbf{s}) . \quad (5.12)$$

Superscripts “s” or “f” will be added to $\sigma_k(\mathbf{s})$, and thus to $\hat{\mathcal{R}}_k$ and \mathcal{W}_k , signifying the partition into slow or fast charge according to Eq. (5.9). With this notation, the excited-state generalization of \mathcal{G}_0 is¹⁸⁵

$$\mathcal{G}_k^{\text{SS}} = \mathcal{E}_k^{\text{SS}} - \mathcal{W}_0^{\text{s}} - \mathcal{W}_k^{\text{f}} + \mathcal{W}_{0,k} . \quad (5.13)$$

where

$$\mathcal{E}_k^{\text{SS}} = \langle \Psi_k | \hat{\mathcal{H}}_k^{\text{SS}} | \Psi_k \rangle = \langle \Psi_k | \hat{\mathcal{H}}_{\text{vac}} + \hat{\mathcal{R}}_0^{\text{s}} + \hat{\mathcal{R}}_k^{\text{f}} | \Psi_k \rangle \quad (5.14)$$

and

$$\mathcal{W}_{0,k} = \frac{1}{2} \int_{\Gamma} \varphi^{\sigma_0^{\text{s}}}(\mathbf{s}) \left[\sigma_k^{\text{f}}(\mathbf{s}) - \sigma_0^{\text{f}}(\mathbf{s}) \right] d\mathbf{s} . \quad (5.15)$$

Equation (5.13) has a straightforward interpretation. To obtain the *free* energy $\mathcal{G}_k^{\text{SS}}$ for state k , which includes the effects of averaging over implicit solvent degrees of freedom, the energy $\mathcal{E}_k^{\text{SS}}$ that is obtained from the Schrödinger equation must be reduced by the work $\mathcal{W}_0^{\text{s}} + \mathcal{W}_k^{\text{f}}$ that is required for the ground- and excited-state polarization processes. The final term, $\mathcal{W}_{0,k}$, accounts for the Coulomb interaction between initial- and final-state surface charge. This term has sometimes been omitted from similar treatments that start from a nonequilibrium free energy expression that is otherwise analogous to Eq. (5.13),^{376,445} however its presence is necessary when the Marcus partition of the polarization is used.^{13,185,426,435,436,443} The nonequilibrium expression for excitation energies is $\hbar\omega_k = \mathcal{G}_k^{\text{SS}} - \mathcal{G}_0$, which is¹⁸⁵

$$\mathcal{G}_k^{\text{SS}} - \mathcal{G}_0 = \Delta\mathcal{E}_k^{\text{SS}} - \mathcal{W}_k^{\text{f}} + \mathcal{W}_0^{\text{f}} + \mathcal{W}_{0,k} , \quad (5.16)$$

where $\Delta\mathcal{E}_k^{\text{SS}} = \mathcal{E}_k^{\text{SS}} - \mathcal{E}_0$. Equation (5.16) also has a straightforward interpretation. The quantity $\Delta\mathcal{E}_k^{\text{SS}}$ is the difference between ground- and excited-state eigenvalues of the SS Hamiltonian [Eq. (5.10)], but must be corrected by the difference in the work required to polarize either state, which is restricted to the fast part of the response ($\mathcal{W}_k^{\text{f}} - \mathcal{W}_0^{\text{f}}$) since that is all that changes upon vertical excitation.

As a simple example of the nonequilibrium formalism, we consider calculations of vertical ionization energies (VIEs) in aqueous solution. These can be measured using liquid microjet photoelectron spectroscopy,^{446–448} and may be quite different from gas-phase values,⁴⁴⁶ especially for singly-charged anions X^- (aq) where the initial state is solvated much more strongly than the final state, and while equilibrium solvation models might be appropriate for computing *adiabatic* ionization energies, in which solvent has the opportunity to re-equilibrate following ionization, these models do a poor job of predicting VIEs.^{446,449} From a computational perspective, the change in charge upon photoionization means that long-range polarization effects are significant, requiring hundreds of explicit solvent molecules (with concomitant sampling) to obtain a converged result.^{450–454} Convergence is significantly accelerated by continuum boundary conditions, using an atomistic solute $X^-(H_2O)_n$ that contains one or two solvation shells of explicit water molecules.^{39,434} The limited size of the atomistic region not only reduces the cost of the quantum chemistry calculation for any one structure, but also reduces the sampling that is required in order to obtain converged averages. (A similar cluster + continuum strategy is often used in pK_a calculations, for essentially the same reasons.^{8,255–257}) PCM boundary conditions have also been shown to accelerate convergence of absorption spectra with respect to inclusion of explicit water molecules,⁴⁵⁵ although the effects (in absolute energy shifts) are not as dramatic as they are for ionization.

Table 6 shows aqueous VIEs computed for several small solutes using a cluster + continuum approach with an atomistic region extending to a radius of 5.5 Å around the solute, containing ≈ 30 explicit water molecules. Shown side-by-side in Table 6 are VIEs computed using “gas phase” (vacuum) boundary conditions that include the explicit water molecules but lack any continuum

Table 6: Vertical ionization energies (VIEs) for aqueous ions, comparing experimental results to calculations using nonequilibrium MP2 + PCM calculations.⁴⁵⁶ Each calculation contains ≈ 30 explicit water molecules and each calculated VIE represents an average over ≈ 100 snapshots from a simulation.

Solute	Exptl. VIE (eV)	Computed VIE (eV)				
		Noneq. PCM		Equil. PCM		No PCM
		spherical ^a	SAS ^b	spherical ^a	SAS ^b	
Li ⁺	60.4 ^c	61.8	61.6	61.3	61.0	64.2
Na ⁺	35.4 ^c	36.5	36.3	36.0	35.8	38.9
H ₂ O	11.7 ^d	11.6	11.6	11.1	10.9	13.8
e ⁻	3.7 ^e	3.2	3.2	2.6	2.6	1.8
F ⁻	11.6 ^f	11.4	11.5	10.8	10.9	10.0
Cl ⁻	9.6 ^c	9.4	9.4	8.8	8.8	7.9

^aSingle spherical cavity for the entire atomistic region, $R = 7.525$ Å. ^bEq. (3.7) with $\alpha = 1.0$, $R_{\text{probe}} = 1.4$ Å, and atomic radii $\{R_{\text{vdW},A}\}$ from Ref. 115. ^cRef. 449. ^dRef. 457. ^eRef. 458.

^fRef. 448.

model, versus results using equilibrium and nonequilibrium PCMs. In the latter case, results are shown both using a SAS cavity but also using a cavity consisting of a single sphere around atomistic region, which affords VIEs that are essentially identical to the SAS values. The nonequilibrium PCM results are ≈ 1 eV too large for Li⁺(aq) and Na⁺(aq) but significantly more accurate for the aqueous halide ions. For the halides, these calculations are also significantly more accurate than previous QM/MM or equilibrium PCM calculations.⁴⁴⁹ For neat liquid water, these calculations represent the most accurate VIE to date, in line with new experiments,⁴⁵⁷ and are also one of the most accurate VIE calculations to date for the challenging e⁻(aq) system.⁴⁵⁹

More germane to the present discussion is the comparison of various boundary conditions. The “gas phase” results, meaning X⁻(H₂O)₃₀ and M⁺(H₂O)₃₀, are in serious error relative to experiment, with VIEs that are too small for the anions and too large for the cations. This is consistent in both cases with understabilization of the state with larger charge. Addition of equilibrium PCM boundary conditions modifies VIEs for these systems by up to 3 eV for the cations, which is perhaps unsurprising given that the divalent ion M²⁺ incurs very long-range polarization effects in the final state, but more surprisingly even neutral H₂O as the solute sees a shift of 3 eV when continuum boundary conditions are activated. While the application of an equilibrium PCM pushes the VIE substantially in the right direction with respect to experiment, results remain far from quantitative until the nonequilibrium correction is added. The latter ranges in magnitude up to ≈ 0.6 eV. Other calculations for aqueous nucleobases find nonequilibrium corrections to VIEs of ≈ 1 eV,⁴⁶⁰ and the latter results suggest that for those particular systems at least, the solvent response upon ionization is the most important difference between vertical and adiabatic ionization energies, more so than geometric relaxation of the ionized solute.⁴⁶⁰

The nonequilibrium formalism is relatively straightforward for ionization, assuming that the final state is the ground state of the ionized species, but is more complicated for excited states. For one, the state-specific nature of the Hamiltonian in Eq. (5.10) may cause convergence problems in the presence of (near-)degeneracies.^{444,461} Even when the states are well-separated, properties such as oscillator strengths are ill-defined because the various final-state wave functions are not eigenfunctions of a common Hamiltonian, and therefore are not mutually orthogonal.⁴⁴⁴ These problems are not unique to continuum solvation methods and arise for any kind of polarizable model of the environment, *e.g.*, for QM/MM methods that employ polarizable force fields.^{444,462}

A solution to this conundrum is to treat $\hat{\mathcal{R}}_k^f$ in Eq. (5.10) as a perturbation.^{185,376,432,433,445,463} To do so, first introduce a set of zeroth-order states

$$\hat{\mathcal{H}}_0 \left| \Psi_k^{(0)} \right\rangle = \mathcal{E}_k^{(0)} \left| \Psi_k^{(0)} \right\rangle , \quad (5.17)$$

such that the eigenvalue $\mathcal{E}_k^{(0)}$ includes the effects of the ground-state reaction field, $\hat{\mathcal{R}}_0$. Eigenfunctions in Eq. (5.17) are orthonormal, thus a convenient approximation for $\mathcal{G}_k^{\text{SS}}$ in Eq. (5.13) uses $\mathcal{E}_k^{(0)}$ in place of $\mathcal{E}_k^{\text{SS}}$ and furthermore uses $|\Psi_k^{(0)}\rangle$ to evaluate the electrostatic potential for state k . This avoids the complexities of the SS approach, and is equivalent to first-order perturbation theory with respect to a perturbation $\hat{W} = \hat{\mathcal{R}}_k^f - \hat{\mathcal{R}}_0^f$, obtained from a partition

$$\hat{\mathcal{H}}_k^{\text{SS}} = \underbrace{\hat{\mathcal{H}}_{\text{vac}} + \hat{\mathcal{R}}_0^{\text{s+f}}}_{\hat{\mathcal{H}}_0} + \underbrace{\hat{\mathcal{R}}_k^f - \hat{\mathcal{R}}_0^f}_{\hat{W}} \quad (5.18)$$

of the SS Hamiltonian. This has been called the *perturbation theory state-specific* (ptSS) approach to nonequilibrium solvation.^{185,432,433} (In principle, it could be extended to higher-order perturbation theory but it is not clear that is warranted.) Note that a widely-used “corrected linear response” (cLR) procedure,³⁷⁶ introduced for excited-state PCM calculations at the level of time-dependent (TD-)DFT is really a ptSS approach; the “linear response” refers to TDDFT, not to the linear-response PCM formalism that is discussed in Section 5.3. In the context of the ptSS or cLR approach, it is best to view TDDFT as a form of configuration interaction with single substitutions (CIS), which provides an eigenvalue equation of the form in Eq. (5.17). This is consistent with the idea that the SS version of TDDFT, as implemented by Imrota *et al.*,^{464,465} is a fully iterative version of Eq. (5.10) within a CIS-style *ansatz*. Both the ptSS and the fully SS approaches to TDDFT do require construction of the “relaxed” density^{466–468} for the TDDFT excited state in question, in order to compute its electrostatic potential.

To obtain practical formulas, *e.g.*, for ASC-PCMs, let us introduce a vector notation for surface integrals. As an example, we rewrite Eq. (2.36) for $\mathcal{G}_{\text{elst}}$ in the form

$$\mathcal{G}_{\text{elst}} = \frac{1}{2} \int_{\Gamma} \sigma(\mathbf{s}) \varphi^{\rho}(\mathbf{s}) d\mathbf{s} = \frac{1}{2} \mathbf{q} \cdot \mathbf{v}^{\rho} . \quad (5.19)$$

The quantities \mathbf{q} and \mathbf{v}^{ρ} were introduced in Eq. (3.2) and the dot-product notation represents how ASC-PCM surface integrals are evaluated in practice, upon discretization of the cavity surface. Using this notation, an expression for the nonequilibrium free energy for excited state k can be manipulated into the form³⁷⁶

$$\mathcal{G}_k^{\text{neq}} = \mathcal{E}_k^{(0)} + \frac{1}{2} \mathbf{v}_0 \cdot \mathbf{q}_0 + \frac{1}{2} (\mathbf{v}_k - \mathbf{v}_0) \cdot (\Delta \mathbf{q}_k^f) + \mathcal{W}_{0,k} , \quad (5.20)$$

where \mathbf{v}_0 and \mathbf{v}_k represent the electrostatic potentials for states $|\Psi_0^{(0)}\rangle$ and $|\Psi_k^{(0)}\rangle$, and $\Delta \mathbf{q}_k^f = \mathbf{q}_k^f - \mathbf{q}_0^f$ is the difference in the fast polarization charges in the two states. The latter is computed according to

$$\Delta \mathbf{q}_k^f = \mathbf{Q}_{\varepsilon_{\infty}} (\mathbf{v}_k - \mathbf{v}_0) = \mathbf{Q}_{\varepsilon_{\infty}} \mathbf{v}^{\Delta \rho} \quad (5.21)$$

for a reaction-field operator ($\mathbf{Q}_{\varepsilon} = \mathbf{K}_{\varepsilon}^{-1} \mathbf{Y}_{\varepsilon}$) involving the optical dielectric constant. The second equality in Eq. (5.21) recognizes that $\mathbf{v}^{\Delta \rho} = \mathbf{v}_k - \mathbf{v}_0$ is the electrostatic potential corresponding to the difference density $\Delta \rho_k(\mathbf{r}) = \rho_k(\mathbf{r}) - \rho_0(\mathbf{r})$. Somewhat similar expressions to Eq. (5.20) can be found elsewhere,^{430,464,465} but the connection to the actual free energy of the excited state is most explicit in the work of Caricato *et al.*³⁷⁶ For cases where the solvent polarization has

had time to fully equilibrate with respect to the excited-state density, an analogous expression for the *equilibrium* free energy $\mathcal{G}_k^{\text{eq}}$ is obtained from Eq. (5.20) by replacing $\Delta\mathbf{q}_k^{\text{f}}$ with $\mathbf{q}_k - \mathbf{q}_0$, where both ground- and excited-state charges are equilibrium ones, so that in the equilibrium case $\mathbf{q}_k = \mathbf{Q}_{\varepsilon_s} \mathbf{v}_k$.³⁷⁶

The solvent-corrected excitation energy is simply the difference between ground- and excited-state free energies,^{376,469}

$$\hbar\omega_{0k}^{\text{neq}} = \mathcal{G}_k^{\text{neq}} - \mathcal{G}_0 = \Delta\mathcal{E}_k^{(0)} + \frac{1}{2}(\mathbf{v}_k - \mathbf{v}_0) \cdot (\Delta\mathbf{q}_k^{\text{f}}) + \mathcal{W}_{0,k} . \quad (5.22)$$

The quantity $\Delta\mathcal{E}_k^{(0)} = \mathcal{E}_k^{(0)} - \mathcal{E}_0$ is the excitation energy computed in the presence of the ground-state reaction field, which is then corrected in Eq. (5.22) for the change in the fast polarization. These equations remain valid for the Pekar partition if $\mathcal{W}_{0,k}$ is omitted from Eqs. (5.20) and (5.22). As noted by Cammi *et al.*,⁴⁶³ Eq. (5.22) is the detailed analogue of the heuristic theories of excited-state solvation developed much earlier, *e.g.*, by McRae,^{404,439,470} Lippert,⁴⁰⁰ and Mataga.^{399,401} This becomes clear upon considering the special case of a polarizable dipole in a spherical cavity.^{463,464}

Although presented here in the notation of ASC-PCMs, an analogous theory of nonequilibrium solvation can be developed based directly on Poisson's equation.^{39,434} In that context, the total charge density $\rho_{\text{tot}}(\mathbf{r}) = \rho(\mathbf{r}) + \rho_{\text{pol}}(\mathbf{r})$ includes an induced polarization $\rho_{\text{pol}}(\mathbf{r})$ [as in Eq. (2.6)], in addition to the charge density $\rho(\mathbf{r})$ due to the atomistic solute. The reaction-field potential is the electrostatic potential arising from $\rho_{\text{pol}}(\mathbf{r})$ and surface integrals such as the ones in Eqs. (5.12) and (5.15) are replaced by volumetric integration. Conveniently, the dot product notation introduced in Eq. (5.19) is ambivalent to this distinction and a formula analogous to Eq. (5.20) can be derived,³⁹ where the dot product signifies volumetric integration.

In the interest of brevity, the notation introduced above omits a subscript “elst” on both $\mathcal{G}_k^{\text{SS}}$ [Eq. (5.13)] and $\mathcal{G}_k^{\text{neq}}$ [Eq. (5.20)], and for that matter on \mathcal{G}_0 in Eq. (2.8) as well. In each case, these quantities represent only the electrostatic contribution to the free energy. Some of the earliest theoretical work on solvatochromatic shifts was concerned not just with changes in the chromophore's dipole moment, as in the Onsager-style treatment leading to the Lippert-Mataga equation, but also with the role of dispersion effects.^{470–473} In modern formulations of continuum theory, however, there have been only preliminary efforts to incorporate nonelectrostatic interactions (as described in Section 4) into excited-state calculations.^{316,317,474,475} This is an interesting problem insofar as solute–solvent dispersion is likely more attractive in an excited state, as the excited-state wave function is probably more polarizable than the ground state, but at the same time Pauli repulsion probably increases in the excited state due to its larger size. To a significant extent, the favorable results for solvatochromic shifts that are obtained with electrostatic-only models^{432,443,461,476} likely rely on some error cancellation along these lines. Models that introduce state-specific nonelectrostatic interactions also do well for solvatochromic shifts.⁴⁷⁵

There is one remaining source of complexity when the nonequilibrium theory is applied to excited states, in that the Schrödinger equation in Eq. (5.10) leaves open the question of what level of self-consistency should be sought in obtaining the excited-state reaction-field operator, $\hat{\mathcal{R}}_k^{\text{f}}$, which depends on $|\Psi_k\rangle$. The multiple-choice answer to this question leads to several categories of methods that are mapped out in Fig. 10, and which are called “perturbation to energy” (PTE), “perturbation to density” (PTD), and “perturbation with self-consistent energy and density” (PTED). This nomenclature derives from efforts to use perturbation theory to include correlation in the ground-state calculation (*e.g.*, MP2 + SCRF),^{477–480} and the question of whether (and how) electron correlation should be included in the density that is used to polarize the continuum. The same notation has been adopted for PCM calculations using non-perturbative models such as coupled-cluster theory,^{481,482} and is used here in a discussion that is formulated specifically with excited-state

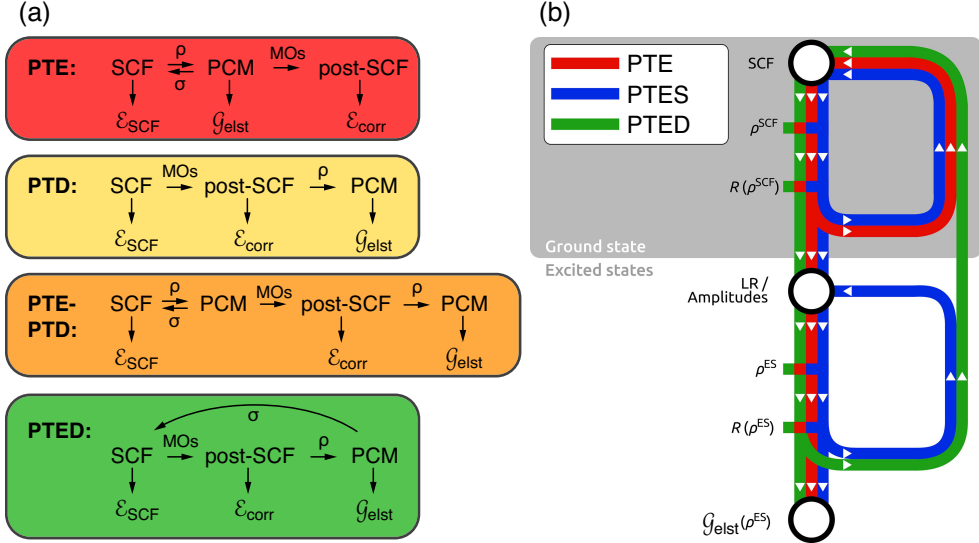


Fig. 10: Flowcharts of various state-specific pathways for combining a PCM or other SCRF procedure with a quantum chemistry method requiring a post-SCF step. (a) Illustration of the PTE and PTD schemes and two combinations thereof. Forward-backward arrows (\rightleftharpoons) indicate where solute density (ρ) and polarization charge (σ) are iterated to self-consistency, and downward arrows indicate the point at which various contributions to the energy are extracted. (b) Schematic representation of the PTE and PTED procedures for an excited-state (ES) calculation, along with the PTES procedure designed as a lower-cost approximation to PTED. Panel (a) is adapted from Ref. 433; copyright 2017 The PCCP Owner Societies. Panel (b) is adapted from Ref. 428; copyright 2019 John Wiley & Sons.

calculations in mind. As illustrated in Fig. 10(a), the PTE scheme involves self-consistent solution of the SCF + SCRF problem followed by a single-shot post-SCF calculation using solvent-polarized molecular orbitals (MOs). This represents a kind of “zeroth-order” inclusion of solvation effects in the correlated calculation,⁴³² and has obvious advantages in terms of cost: assuming that the post-SCF step dominates the cost of the gas-phase calculation, then then addition of SCRF boundary conditions adds little to the overall cost of the calculation. Alternatively, in the PTD scheme the correlated calculation is performed in the gas phase and then the correlated density (rather than the SCF density) is used to polarize the solvent. This introduces solvation effects beyond zeroth order in perturbation theory,⁴⁷⁹ at marginally increased cost: it is still a single-shot correlation calculation, however the relaxed density is required, which entails computational effort along the lines of a gradient calculation at the correlated level of theory. A slightly better-performing variant of the traditional PTD approach is the PTE-PTD scheme,⁴³³ in which the SCF + SCRF calculation is solved self-consistently and those MOs are used in the post-SCF calculation, but then the correlated density is used in a final, single-shot PCM calculation to compute the solvation energy $\mathcal{G}_{\text{elst}}$. None of the aforementioned approaches constitutes a fully self-consistent treatment of post-SCF correlation effects, but this can be accomplished using the PTED scheme that is mapped out in Fig. 10(a). Here, the correlated density is used to obtain the PCM surface charge and this procedure is iterated to self-consistency. This approach is significantly more expensive because the correlated calculation is performed at each SCRF iteration.

These ideas have since been extended beyond their perturbation theory origins and represent the various possible levels of self-consistency in any calculation that combines an SCRF approach

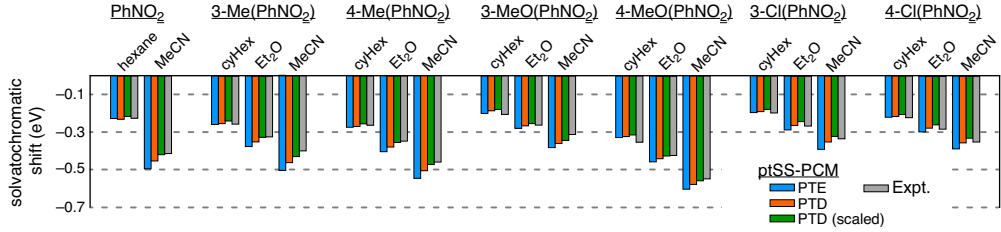


Fig. 11: Solvatochromic shifts in lowest ${}^1\pi\pi$ state for derivatives of nitrobenzene (PhNO_2) in different solvents, comparing experimental values to ADC(2) + C-PCM calculations. Solvent effects are described using PTE and PTD variants of the ptSS approach. Also shown are results for an empirically-scaled version of the nonequilibrium PTD correction. Adapted from Ref. 432; copyright 2015 American Chemical Society.

with a quantum chemistry method requiring a post-SCF calculation,^{428,432,433,461,483–485} including TDDFT. An alternative pictorial representation of the simplest method (PTE) and most complete scheme (PTED) is provided in Fig. 10(b), which provides a flowchart for an excited-state calculation, indicating which densities are used to construct the various reaction-field operators $\hat{\mathcal{R}}$. Because of the expense associated with the fully self-consistent PTED approach, approximations have been developed in which both the ground- and excited-state calculations are iterative, but those two iterative sequences are uncoupled to one another.^{480,483–486} This scheme, which Caricato calls “PTES” and has implemented at the coupled-cluster level of theory,^{483–485} is analogous to a “vertical excitation model” introduced for TDDFT.⁴⁷⁴ At the DFT level, the PTED scheme in Fig. 10 is essentially equivalent to the SS-TDDFT + PCM method introduced by Imrota *et al.*^{464,465}

Figure 11 presents solvatochromic shifts for a set of nitrobenzene derivatives,⁴³² with excitation energies computed at the level of second-order algebraic diagrammatic construction [ADC(2)],⁴⁸⁷ which is something of an excited-state analogue of MP2. Solvent contributions in Fig. 11 are incorporated using either the PTE or PTD variant of the ptSS approach. Differences between the two variants are negligible, and both approaches show good agreement with experimental shifts, without the need to invoke the more expensive PTED scheme. For many of these molecules, the first-order ptSS contribution to the solvatochromic shift (representing fast polarization) is 0.10–0.15 eV, in shifts ranging up to 0.6 eV. The remaining part comes from the zeroth-order contribution of simply inserting solvent-polarized MOs into the correlated part of the calculation.⁴³² Tests on a more diverse set of systems do reveal a small systematic error in the PTE approach,⁴⁶¹ but the mean error with respect to experiment remains < 0.1 eV and the systematic error can be eliminated by intermediate approaches that do not require the full self-consistency of the PTED approach.⁴⁶¹ In particular, the PTE-PTD scheme [see Fig. 10(a)] works well in this regard.⁴³³ This approach requires the correlated density but is not iterative at the correlated level of theory. Other benchmark studies comparing continuum approaches to large QM calculations with explicit solvent have suggested that QM/PCM excitation energies may agree better with full-QM result as compared to QM/MM calculations, but explicit water molecules in the QM/PCM calculation are required to obtain good agreement for oscillator strengths.⁴⁸⁸ Simulation of band shapes requires thermal sampling, which cannot be accomplished without at least some explicit solvent molecules.

5.3 Linear response approach

Despite its computational complexities, the SS approach to excited-state solvation is conceptually straightforward. An alternative to the state-by-state approach, which has fewer moving parts at the computational level, is based on linear-response (LR) quantum chemistry methods in which excitation energies are computed from the poles of the frequency-dependent response to a perturbation, rather than from the Schrödinger equation. Given that the PCM electrostatic contribution to the energy is

$$\mathcal{G}_{\text{elst}} = \frac{1}{2} \int_{\Gamma} \int_{\Gamma} \varphi(\mathbf{s}) Q_{\varepsilon}(\mathbf{s}, \mathbf{s}') \varphi(\mathbf{s}') d\mathbf{s} d\mathbf{s}' , \quad (5.23)$$

where $Q_{\varepsilon}(\mathbf{s}, \mathbf{s}')$ is the kernel of the solvent response operator $\hat{Q}_{\varepsilon} = \hat{K}_{\varepsilon}^{-1} \hat{Y}_{\varepsilon}$, the solvent model contributes only a one-electron potential, $v^{\text{PCM}}(\mathbf{r}) = \delta \mathcal{G}_{\text{elst}} / \delta \rho(\mathbf{r})$. The matrix elements of $v^{\text{PCM}}(\mathbf{r})$ are⁴⁸⁹

$$v_{\mu\nu}^{\text{PCM}} = \int_{\Gamma} \int_{\Gamma} \varphi(\mathbf{s}) Q_{\varepsilon}(\mathbf{s}, \mathbf{s}') \varphi_{\mu\nu}(\mathbf{s}') d\mathbf{s} d\mathbf{s}' = (\mathbf{v}^{\rho})^{\dagger} \mathbf{Q}_{\varepsilon} \mathbf{v}^{\mu\nu} , \quad (5.24)$$

where $\varphi_{\mu\nu}(\mathbf{s}')$ is the electrostatic potential generated by the function pair $\mu\nu$ at the point \mathbf{s}' . The second equality in Eq. (5.24) demonstrates how the Fock matrix contribution from $v^{\text{PCM}}(\mathbf{r})$ is evaluated in practice, and analogous expressions exist for three-dimensional Poisson approaches.³⁹ The quantities \mathbf{v}^{ρ} and $\mathbf{v}^{\mu\nu}$ involve only one-electron integrals, so incorporating the PCM contribution into a LR calculation incurs negligible overhead with respect to the cost of the gas-phase calculation, and meanwhile this approach is free of the iterative complexities of the SS method. A general LR-PCM formulation has been given by Cammi *et al.*,^{463,490} and specific formulations for different excited state methods are available as well, *e.g.*, for TDDFT and other single-excitation theories,^{489–493} following on earlier implementations of the coupled-perturbed SCF + PCM procedure for response properties;^{180,494} for multiconfigurational SCF wave functions;⁸⁸ for ADC;^{445,486} for the *GW*/Bethe-Salpeter equation formalism.⁴⁹⁵ Finally, it has been implemented for coupled-cluster theory,^{496–500} based on the coupled-cluster response formalism.⁴⁸²

For isolated-molecule quantum chemistry, the LR formalism for excitation energies is generally equivalent to solving the corresponding Schrödinger equation,⁵⁰¹ but the LR- and SS-PCM formalisms are *not* equivalent.^{463,502} The general form of the LR-PCM result is⁴⁶³

$$\hbar\omega_{0k}^{\text{neq,LR}} = \hbar\omega_k^{(0)} + \underbrace{\langle \Psi_k | \hat{\mathcal{V}} | \Psi_0 \rangle \langle \Psi_0 | \hat{\mathcal{Q}}^{\text{f}} | \Psi_k \rangle}_{\Delta \mathcal{R}^{\text{f}}(\mu_{0k})} , \quad (5.25)$$

where $\langle \Psi_k | \hat{\mathcal{V}} | \Psi_0 \rangle$ is the electrostatic potential generated by the *transition* density, $\rho_{k0}(\mathbf{r})$, and $\langle \Psi_0 | \hat{\mathcal{Q}}^{\text{f}} | \Psi_k \rangle$ is the apparent surface charge induced by $\rho_{k0}(\mathbf{r})$. For comparison, the SS-PCM result in Eq. (5.22) can be rewritten in similar notation:

$$\hbar\omega_{0k}^{\text{neq,SS}} = \hbar\omega_k^{(0)} + \underbrace{\frac{1}{2} \left[\langle \Psi_k | \hat{\mathcal{V}} | \Psi_k \rangle - \langle \Psi_0 | \hat{\mathcal{V}} | \Psi_0 \rangle \right] \cdot \left[\langle \Psi_k | \hat{\mathcal{Q}}^{\text{f}} | \Psi_k \rangle - \langle \Psi_0 | \hat{\mathcal{Q}}^{\text{f}} | \Psi_0 \rangle \right]}_{\Delta \mathcal{R}^{\text{f}}(\Delta \rho_k)} . \quad (5.26)$$

In both cases, the quantity $\hbar\omega_{0k}^{(0)} \equiv \Delta \mathcal{E}_k^{(0)}$ is the zeroth-order approximation to the solution phase excitation energy, calculated in the static reaction field of the ground state. The quantity $\Delta \mathcal{R}^{\text{f}}$ represents the change in the dynamical part of the reaction field, which is a function of the transition dipole moment $\mu_{0k} = \langle \Psi_0 | \hat{\mu} | \Psi_k \rangle$ in the LR case but a function of the difference density $\Delta \rho_k(\mathbf{r})$ in the SS case. A detailed analysis of the two formalisms suggests that their differences arise from the nonlinear nature of the SS Hamiltonian combined with the lack of entanglement between the atomistic wave function and its continuum environment.⁵⁰²

Whatever the origin of the discrepancy, the form of the LR-PCM correction in Eq. (5.25) is problematic because the correction vanishes for optically-forbidden transitions, as is readily seen from a model of a dipole in a spherical cavity, for which $\Delta\mathcal{R}^f = -g_1(\varepsilon_\infty, \bar{R})\mu_{0k}$.⁴⁶⁴ For the same reason, the LR-PCM correction $\Delta\mathcal{R}^f(\mu_{0k})$ will be rather small for any excitation involving significant displacement of charge, whereas intuitively (and in the SS formalism) one expects a significant solvent effect for a charge-transfer excitation in a polar solvent. Indeed, SS-PCM results are consistently superior to LR-PCM calculations for excited states with charge-transfer character.^{503–508} (As discussed in Section 5.2, the cLR formalism encountered in some of these studies is really a ptSS-PCM approach.) Even for states not dominated by charge transfer, the SS-PCM approach generally affords smaller errors for solvatochromatic shifts in the absorption spectrum as compared to LR-PCM calculations,^{432,443,476} although it is worth bearing in mind that the experimental λ_{\max} need not correspond to the origin (0–0) transition, due to vibrational structure.^{509–511} The ptSS-PCM approach also affords more accurate results for emission energies,⁵¹² although LR-PCM calculations can be used to optimize the excited-state geometries, which simplifies the procedure. It has also been argued that the LR correction $\Delta\mathcal{R}^f(\mu_{0k})$ constitutes a solute–continuum dispersion interaction,^{428,502,513} insofar as it has the form of the solute charge distribution oscillating at the Bohr frequency $\omega_{0k}^{(0)}$ and coupling to the dynamical response of the environment. As such, some studies have opted to include both the LR- and ptSS-PCM corrections to $\omega_{0k}^{(0)}$.⁴³²

6 Anisotropic Solvation

Up to this point we have assumed that the continuum environment is isotropic, which is usually the case for a bulk liquid although there are certain exceptions (notably, liquid crystals) where polarization of the medium depends upon the orientation of the electric field vector. This can be described by allowing ε to take the form of a 3×3 matrix, with orientation-dependent permittivities ε_{xx} , ε_{yy} , and ε_{zz} . The ASC-PCM formalism, and in particular IEF-PCM, has been formulated to handle a permittivity tensor.^{155–157,514}

A more general class of anisotropic solvation problems are interfacial phenomena. An example is shown in Fig. 12(a), in which an atomistic solute consisting for a ClO_3^- ion with approximately two solvation shells of explicit water molecules is situated at a dielectric representation of the air/water interface. Here, the atomistic region is subject to a dielectric environment characterized by $\varepsilon = 78$ on one side but $\varepsilon = 1$ on the other. The basic PCM formalism is not equipped to handle such a situation, as it is predicted on a sharp dielectric interface between $\varepsilon_{\text{in}} = 1$ inside the cavity and a bulk solvent value (ε_{out}) outside, although it can be accomplished piecewise if the medium is divided into separate domains, each with its own value of ε .⁵¹⁵ Alternatively, to describe the liquid/vapor interface the PCM equations have been to interpolate matrix elements between different values of ε .^{516–523} Treatment of nonelectrostatic effects proves to be crucial. It has been suggested that continuum models cannot describe specific-ion (“Hofmeister”) effects,^{524,525} in part because the Born model [Eq. (2.17)] cannot distinguish between cations and anions, although that particular shortcoming is better ascribed to an overly-simplified cavity shape.⁵²⁶ Another commonly held view is that continuum models are incapable of describing the interfacial affinity exhibited by soft ions,^{524,525} because (so the logic goes) the ion in a continuum solvent ought to be repelled from the interface by its own image charge.^{525,527} Despite this conventional wisdom, continuum models that include nonelectrostatic interactions have been shown to predict interfacial free energy minima for dragging a soft ion through the air/water interface.^{516,518,528,529}

Fundamentally, however, the interfacial solvation problem seems to cry out for a permittivity function $\varepsilon(\mathbf{r})$ that can take different values in different regions of space, *i.e.*, a method that

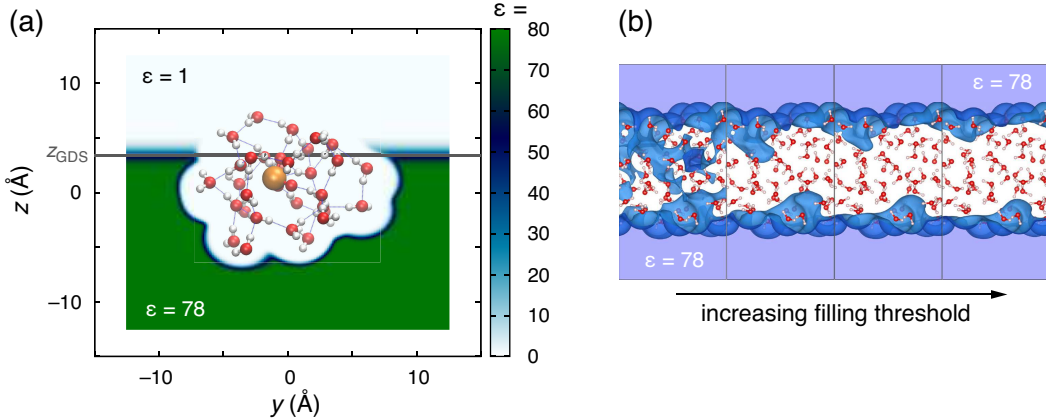


Fig. 12: Illustrations of anisotropic permittivity functions $\epsilon(\mathbf{r})$ for use in Poisson's equation. (a) Cluster + continuum description of chlorate ion at the air/water interface, in which the atomistic solute is ClO_3^- (H_2O)₃₀. The background color shows the function $\epsilon(\mathbf{r})$, interpolating between $\epsilon_{\text{out}} = 1$ above the Gibbs dividing surface (GDS) and $\epsilon_{\text{out}} = 78$ below it, with $\epsilon_{\text{in}} = 1$ inside of the solute cavity. The horizontal line indicates the position of the dividing surface, $z_{\text{GDS}} = 3.5 \text{ \AA}$. (b) Periodic water slab bounded on either side by continuum water ($\epsilon = 78$, shown in purple), with regions characterized by $\epsilon > 15$ shown in blue. From left to right, the interpolating function is modified (using a “filling threshold” parameter) in order to exclude pockets of high permittivity that encroach into the interstices between the atomistic water molecules. Panel (b) is adapted from Ref. 225; copyright 2019 American Chemical Society.

solves the generalized Poisson equation with an anisotropic permittivity function $\epsilon(\mathbf{r})$. Such a strategy has been pursued to describe the interface between a solid-state electrode and an aqueous electrolyte,^{24,71,223–230} as well as host/guest systems where the guest experiences a low-dielectric environment despite the fact that the host is dissolved in water.⁵³⁰ Finally, anisotropic models have been used to compute VIEs of solutes at the air/water interface,^{39,434} in order to connect with liquid microjet photoelectron spectroscopy.

The setup for an interfacial calculation of this type is illustrated in Fig. 12(a), which depicts an atomistic model of ClO_3^- (aq) at the air/water interface and shows how the function $\epsilon(\mathbf{r})$ is defined. In this particular example, two solvation shells of explicit water molecules are included in the atomistic region in order to account for hydrogen-bonding effects; the continuum model takes care of long-range polarization upon ionization of ClO_3^- . VIE calculations based on a nonequilibrium formulation of Poisson's equation suggest that the VIEs of common inorganic anions are very nearly the same at the air/water interface as they are in bulk water.³⁹ Even for an exotic anion like e^- (aq),^{459,531} it appears that the interfacial VIE that is no more than 0.2–0.4 eV different from its bulk value.^{39,434}

In continuum solvation calculations where the atomistic region contains explicit solvent molecules, one must be careful to parameterize the function $\epsilon(\mathbf{r})$ to avoid artificial penetration of high-dielectric regions into the interstices between molecules. This includes not just methods that are directly based on Poisson's equation but also PCMs, where explicit solvent molecules might be also be added, for the purpose of describing solute–solvent hydrogen bonds, as in the aforementioned pK_a calculations. Oddly, the dielectric penetration problem in semicontinuum calculations has received scant attention in the quantum chemistry literature,^{39,225} although there is an analogous problem in classical Poisson-Boltzmann electrostatics calculations for biomolecules that is widely discussed.

In that context, the problem is that standard cavity construction algorithms (based on intersecting atomic spheres) may leave pockets of high-dielectric “solvent” in the hydrophobic interior of a protein.^{52,119,211,532–535} This can be mitigated in Poisson-based continuum methods by appropriate adjustment of the interpolating function that defines the dielectric boundary. A spatially-varying permittivity function has been suggested as a solution to the problem that there is no single optimal value for the dielectric “constant” inside of a protein.⁵²

Figure 12(b) presents an example in which the SCCS model of Section 3.3, which is based on a functional $\varepsilon[\rho](\mathbf{r})$, is used to remove artificial high-dielectric regions. In these simulations, the goal is to perform *ab initio* molecular dynamics simulations of explicit water but to use continuum boundary conditions in order to limit the size of the atomistic QM simulation cell that is required. The parameters that define $\varepsilon[\rho](\mathbf{r})$ must be chosen carefully, lest high-dielectric regions penetrate between the explicit water molecules, as they do on the left side of Fig. 12(b). This situation is physically incorrect because the QM calculation is based on Coulomb operators that assume vacuum permittivity. This undesirable situation has been rectified by introducing “solvent awareness” into the definition of the permittivity function, so that $\varepsilon(\mathbf{r})$ depends on the coordinates in the atomistic region *directly*, and not just implicitly through the functional $\varepsilon[\rho]$.²²⁵ Moving from left to right in Fig. 12(b), this solvent awareness is activated and removes the spurious high-dielectric regions.

7 Closing remarks

With the contents of this review serving as a lengthy introduction to what continuum solvation models can do, in closing it feels *a propos* to comment briefly on their limitations. These are very crude models. That is not inconsistent with being *useful* models, but one should not demand too much of something so simple. It is perhaps best to think of continuum solvation as improved boundary conditions (as compared to vacuum boundary conditions) for condensed-phase electronic structure calculations. The primary way in which most users will encounter the crudeness of these models is in the fact that there is considerable arbitrariness in construction of the solute cavity, for which there is no “right” choice, although there are certainly plenty of wrong ones. In particular, there is no “magical” cavity construction or scaling factor for the van der Waals radii that will make these quantities universal. Small tweaks that might provide better answers in one system may very well degrade the accuracy in other cases. Isodensity cavity constructions, and smooth interfaces or “soft” cavities, based on permittivity functionals $\varepsilon[\rho(\mathbf{r})]$, seem like the least arbitrary choices.

With that in mind, differences between how $\mathcal{G}_{\text{elst}}$ is computed amongst different PCMs seem quite minor in comparison to the overall quality of these models, to the point where these differences can likely be parameterized away, or are simply washed out, by minor changes in cavity construction. The COSMO method, for example, performs well in comparison to more exact formulations of the continuum electrostatics problem, even in low-dielectric solvents.¹⁷⁰ For the SS(V)PE approach, discretization of $\hat{D}^\dagger \sigma(\mathbf{s})$ proves to be challenging,^{20,185} leading to a wrong conductor limit in some cases,²⁰ nevertheless this model has successfully been used as the basis of a composite model of solvation.²⁵¹ Errors in the implementation of certain nonelectrostatic are completely absorbed in the parameterization of other terms.²⁵¹

In view of all this, there would seem to be little room to further improve upon the electrostatic part of continuum solvation models. A corollary is that efforts to make the solvation model fully consistent with correlated wave function electronic structure methods, either in the ground or excited states, seem misguided. The “zeroth-order” model, in which solvent-polarized MOs are inserted into a post-SCF correlation calculation, recovers the most important effects, and a ptSS-

style correction for the fast polarization response affords a simple-to-use model for what remains. Differences with respect to a fully self-consistent model are likely considerably smaller than errors introduced by continuum representation of the solvent itself. Keeping those caveats in mind, the continuum solvation approach can be highly effective in situations where vacuum boundary conditions are dubious, *e.g.*, due to significant charge rearrangement in a polar solvent (including redox chemistry), or to modulate the energy levels of the frontier, solvent-exposed orbitals at play in electronic spectroscopy.

Regarding calculation of solvation energies, which is arguably the primary application of continuum solvation models in chemistry, the nonelectrostatic contributions that are needed for favorable agreement with experiment can now be modeled (in a variety of ways) with an accuracy of < 1 kcal/mol for charge-neutral solutes. For ions, the best methods approach the accuracy (± 3 kcal/mol)²⁴⁷ of the experimental data themselves.^{216,248,251} That said, these models are trained on relatively small solutes (for which experimental values of $\Delta_{\text{solv}}\mathcal{G}$ are available); it remains unclear whether the aforementioned level of statistical accuracy is transferrable to significantly larger solutes.

Regarding macromolecular solutes, it is clear that PCMs with linear-scaling solvers ought to be seriously considered as replacements for biomolecular electrostatics calculations based on finite-difference solution of the Poisson-Boltzmann equation. The former approaches provide an *exact* solution to the classical electrostatics problem,^{19,20} up to controllable discretization errors, and can be formulated in such a way that potential energy surfaces are inherently continuous and smooth.^{17,18} Indeed, it is this author's opinion that theorists should not accept as their starting point any approach that does not intrinsically provide a smooth potential energy surface, as the finite-difference approach clearly fails to do. The ability to explore the potential energy surface, and thus to have a well-defined "model chemistry",⁵³⁶ is too important to sacrifice.

Acknowledgements

This work was supported by National Science Foundation, grant nos. CHE-1665322 and CHE-1955282. It is a pleasure to acknowledge current and former group members who have worked on these projects: Dr. Adrian Lange, Benjamin Albrecht, Dr. Zhi-Qiang You, Dr. Marc Coons, and Suranjan Paul. Collaborations with Dr. Jan-Michael Mewes (from the group of Prof. Andreas Dreuw) and Dr. Christopher Stein (from the group of Prof. Martin Head-Gordon) are also happily acknowledged.

Conflict of Interest

J.M.H. serves on the board of directors of Q-Chem Inc.

References

- [1] D. Rinaldi and J.-L. Rivail, "Polarisabilités moléculaires et effet diélectrique de milieu à l'état liquide. Étude théorique de la molécule d'eau et de ses dimères", *Theor. Chem. Acc.*, **32**, 57–70 (1973).
- [2] J.-L. Rivail and D. Rinaldi, "A quantum chemical approach to dielectric solvent effects in molecular liquids", *J. Chem. Phys.*, **65**, 233–242 (1976).

- [3] S. Miertuš, E. Scrocco, and J. Tomasi, “Electrostatic interaction of a solute with a continuum. A direct utilization of ab initio molecular potentials for the prevision of solvent effects”, *Chem. Phys.*, **55**, 117–129 (1981).
- [4] S. Miertuš and J. Tomasi, “Approximate evaluations of the electrostatic free energy and internal energy changes in solution processes”, *Chem. Phys.*, **65**, 239–245 (1982).
- [5] R. Bonaccorsi, R. Cimiraglia, and J. Tomasi, “*Ab initio* evaluation of absorption and emission transitions for molecular solutes, including separate consideration of orientational and inductive solvent effects”, *J. Comput. Chem.*, **4**, 567–577 (1983).
- [6] J. Tomasi, “Thirty years of continuum solvation chemistry: A review, and prospects for the near future”, *Theor. Chem. Acc.*, **112**, 184–203 (2004).
- [7] P. Grochowski and J. Trylska, “Continuum molecular electrostatics, salt effects, and counterion binding—A review of the Poisson–Boltzmann theory and its modifications”, *Biopolymers*, **89**, 93–113 (2008).
- [8] J. R. Pliego Jr. and J. M. Riveros, “Hybrid discrete-continuum solvation methods”, *WIREs Comput. Mol. Sci.*, **10**, e1440:1–25 (2020).
- [9] J. Tomasi and M. Persico, “Molecular interactions in solution: An overview of methods based on continuous distributions of the solvent”, *Chem. Rev.*, **94**, 2027–2094 (1994).
- [10] C. Amovilli, V. Barone, R. Cammi, E. Cancès, M. Cossi, B. Mennucci, C. S. Pomelli, and J. Tomasi, “Recent advances in the description of solvent effects with the polarizable continuum model”, *Adv. Quantum Chem.*, **32**, 227–261 (1999).
- [11] J. Tomasi, B. Mennucci, R. Cammi, and M. Cossi, “Quantum mechanical models for reactions in solution”, in *Computational Approaches to Biochemical Reactivity*, G. Nâaray-Szabâo and A. Warshel, Eds., Vol. 19 of *Understanding Chemical Reactivity*; Springer: New York, 2002; chapter 1, pages 1–102.
- [12] R. Cammi, B. Mennucci, and J. Tomasi, “Computational modelling of the solvent effects on molecular properties: An overview of the polarizable continuum model (PCM) approach”, in *Computational Chemistry: Reviews of Current Trends*, J. Leszczynski, Ed., Vol. 8; World Scientific: Singapore, 2003; chapter 1, pages 1–79.
- [13] J. Tomasi, B. Mennucci, and R. Cammi, “Quantum mechanical continuum solvation models”, *Chem. Rev.*, **105**, 2999–3093 (2005).
- [14] J. Tomasi, “Selected features of the polarizable continuum model for the representation of solvation”, *WIREs Comput. Mol. Sci.*, **1**, 855–867 (2011).
- [15] B. Mennucci, “Polarizable continuum model”, *WIREs Comput. Mol. Sci.*, **2**, 386–404 (2012).
- [16] F. Lipparini and B. Mennucci, “Perspective: Polarizable continuum models for quantum-mechanical descriptions”, *J. Chem. Phys.*, **144**, 160901:1–9 (2016).
- [17] A. W. Lange and J. M. Herbert, “Polarizable continuum reaction-field solvation models affording smooth potential energy surfaces”, *J. Phys. Chem. Lett.*, **1**, 556–561 (2010).

- [18] A. W. Lange and J. M. Herbert, “A smooth, nonsingular, and faithful discretization scheme for polarizable continuum models: The switching/Gaussian approach”, *J. Chem. Phys.*, **133**, 244111:1–18 (2010).
- [19] J. M. Herbert and A. W. Lange, “Polarizable continuum models for (bio)molecular electrostatics: Basic theory and recent developments for macromolecules and simulations”, in *Many-Body Effects and Electrostatics in Biomolecules*, Q. Cui, P. Ren, and M. Meuwly, Eds.; CRC Press: Boca Raton, 2016; chapter 11, pages 363–416.
- [20] A. W. Lange and J. M. Herbert, “Symmetric versus asymmetric discretization of the integral equations in polarizable continuum solvation models”, *Chem. Phys. Lett.*, **509**, 77–87 (2011).
- [21] A. W. Lange, J. M. Herbert, B. J. Albrecht, and Z.-Q. You, “Intrinsically smooth discretization of Connolly’s solvent-excluded molecular surface”, *Mol. Phys.*, **118**, e1644384:1–18 (2020).
- [22] C. Cappelli, “Integrated QM/polarizable MM/continuum approaches to model chiroptical properties of strongly interacting solute–solvent systems”, *Int. J. Quantum Chem.*, **116**, 1532–1542 (2016).
- [23] M. Caricato, “Coupled cluster theory with the polarizable continuum model of solvation”, *Int. J. Quantum Chem.*, **119**, e25674:1–19 (2019).
- [24] O. Andreussi and G. Fisicaro, “Continuum embeddings in condensed-matter simulations”, *Int. J. Quantum Chem.*, **119**, e25725:1–17 (2019).
- [25] J. Sadlej and M. Pecul, “Computational modelling of the solvent–solute effect on NMR parameters by a polarizable continuum model”, in *Continuum Solvation Models in Chemical Physics*, B. Mennucci and R. Cammi, Eds.; Wiley: Chichester, UK, 2007; pages 125–144.
- [26] V. Barone, P. Cimino, and M. Pavone, “EPR spectra of organic free radicals in solution from an integrated computational approach”, in *Continuum Solvation Models in Chemical Physics*, B. Mennucci and R. Cammi, Eds.; Wiley: Chichester, UK, 2007; pages 145–166.
- [27] C. Cappelli, “Continuum solvation approach to vibrational properties”, in *Continuum Solvation Models in Chemical Physics*, B. Mennucci and R. Cammi, Eds.; Wiley: Chichester, UK, 2007; pages 167–179.
- [28] M. Pecul and K. Ruud, “Solvent effects on natural optical activity”, in *Continuum Solvation Models in Chemical Physics*, B. Mennucci and R. Cammi, Eds.; Wiley: Chichester, UK, 2007; pages 180–205.
- [29] R. Cammi and B. Mennucci, “Macroscopic nonlinear optical properties from cavity models”, in *Continuum Solvation Models in Chemical Physics*, B. Mennucci and R. Cammi, Eds.; Wiley: Chichester, UK, 2007; pages 238–251.
- [30] H. Ågren and K. V. Mikkelsen, “Homogeneous and heterogeneous solvent models for nonlinear optical properties”, in *Continuum Solvation Models in Chemical Physics*, B. Mennucci and R. Cammi, Eds.; Wiley: Chichester, UK, 2007; pages 282–299.
- [31] R. Improta, “UV–visible absorption and emission energies in condensed phase by PCM/TD-DFT methods”, in *Computational Strategies for Spectroscopy: From Small Molecules to Nano*

Systems, V. Barone, Ed.; John Wiley & Sons: Hoboken, NJ, 1st ed., 2012; chapter 1, pages 39–76.

- [32] M. V. Basilevsky and D. F. Parsons, “An advanced continuum medium model for treating solvation effects: Nonlocal electrostatics with a cavity”, *J. Chem. Phys.*, **105**, 3734–3746 (1996).
- [33] O. S. Jenkins and K. L. C. Hunt, “Nonlocal dielectric functions on the nanoscale: Screened forces from unscreened potentials”, *J. Chem. Phys.*, **119**, 8250–8256 (2003).
- [34] M. V. Basilevsky and G. N. Chuev, “Nonlocal solvation theories”, in *Continuum Solvation Models in Chemical Physics*, B. Mennucci and R. Cammi, Eds.; Wiley: Chichester, UK, 2007; pages 94–109.
- [35] D. H. Whiffen, “Manual of symbols and terminology for physicochemical quantities and units”, *Pure Appl. Chem.*, **51**, 1–41 (1979).
- [36] A. Rizzo, “Birefringences in liquids”, in *Continuum Solvation Models in Chemical Physics*, B. Mennucci and R. Cammi, Eds.; Wiley: Chichester, UK, 2007; pages 252–264.
- [37] A. Ferrarini, “Anisotropic fluids”, in *Continuum Solvation Models in Chemical Physics*, B. Mennucci and R. Cammi, Eds.; Wiley: Chichester, UK, 2007; pages 265–281.
- [38] R. K. Wangsness, *Electromagnetic Fields*, John Wiley & Sons: Hoboken, 2nd ed., 1986.
- [39] M. P. Coons and J. M. Herbert, “Quantum chemistry in arbitrary dielectric environments: Theory and implementation of nonequilibrium Poisson boundary conditions and application to compute vertical ionization energies at the air/water interface”, *J. Chem. Phys.*, **148**, 222834:1–21 (2018). Erratum: *J. Chem. Phys.*, **151**, 189901:1–2 (2019).
- [40] K. Patkowski, “Recent developments in symmetry-adapted perturbation theory”, *WIREs Comput. Mol. Sci.*, **10**, e1452:1–47 (2020).
- [41] C. J. F. Böttcher, *Theory of Electric Polarization*, Vol. 1, Elsevier: Amsterdam, 2nd ed., 1976.
- [42] L. D. Jacobson, C. F. Williams, and J. M. Herbert, “The static-exchange electron-water pseudopotential, in conjunction with a polarizable water model: A new Hamiltonian for hydrated-electron simulations”, *J. Chem. Phys.*, **130**, 124115:1–18 (2009).
- [43] M. Caricato, G. Scalmani, and M. J. Frisch, “A Lagrangian formulation for continuum models”, in *Continuum Solvation Models in Chemical Physics*, B. Mennucci and R. Cammi, Eds.; Wiley: Chichester, UK, 2007; pages 64–81.
- [44] H. Nakamura, “Roles of electrostatic interaction in proteins”, *Q. Rev. Biophys.*, **29**, 1–90 (1996).
- [45] E. Alexov, E. L. Mehler, N. Baker, A. M. Baptista, Y. Huang, F. Milletti, J. E. Nielsen, D. Farrell, T. Carstensen, M. H. M. Olsson, J. K. Shen, J. Warwicker, S. Williams, and J. M. Word, “Progress in the prediction of pK_a values in proteins”, *Proteins*, **79**, 3260–3275 (2011).
- [46] J. Antosiewicz, J. A. McCammon, and M. K. Gilson, “Prediction of pH-dependent properties of proteins”, *J. Mol. Biol.*, **238**, 415–436 (1994).

- [47] E. Demchuk and R. C. Wade, “Improving the continuum dielectric approach to calculating pK_{as} of ionizable groups in proteins”, *J. Phys. Chem.*, **100**, 17373–17387 (1996).
- [48] T. Grycuk, “Revision of the model system concept for the prediction of pK_a ’s in proteins”, *J. Phys. Chem. B*, **106**, 1434–1445 (2002).
- [49] A. Warshel and S. T. Russell, “Calculations of electrostatic interactions in biological systems and in solutions”, *Q. Rev. Biophys.*, **17**, 283–422 (1984).
- [50] C. N. Schutz and A. Warshel, “What are the dielectric “constants” of proteins and how to validate electrostatic models?”, *Proteins*, **44**, 400–417 (2001).
- [51] A. Warshel, P. K. Sharma, M. Kato, and W. W. Parson, “Modeling electrostatic effects in proteins”, *Biochim. Biophys. Acta*, **1764**, 1647–1676 (2006).
- [52] L. Li, C. Li, Z. Zhang, and E. Alexov, “On the dielectric “constant” of proteins: Smooth dielectric function for macromolecular modeling and its implementation in DelPhi”, *J. Chem. Theory Comput.*, **9**, 2126–2136 (2013).
- [53] K. A. Sharp and B. Honig, “Electrostatic interactions in macromolecules”, *Annu. Rev. Biophys. Biophys. Chem.*, **19**, 301–332 (1990).
- [54] F. Fogolari, A. Brigo, and H. Molinari, “The Poisson–Boltzmann equation for biomolecular electrostatics: A tool for structural biology”, *J. Mol. Recognit.*, **15**, 377–392 (2002).
- [55] N. A. Baker, “Biomolecular applications of Poisson-Boltzmann methods”, in *Reviews in Computational Chemistry*, K. Lipkowitz, R. Larter, and T. R. Cundari, Eds., Vol. 21; John Wiley & Sons: Hoboken, 2005; pages 349–379.
- [56] W. M. Botello-Smith, Q. Cai, and R. Luo, “Biological applications of classical electrostatics methods”, *J. Theor. Comput. Chem.*, **13**, 1440008:1–25 (2014).
- [57] M. J. Schnieders and J. W. Ponder, “Polarizable atomic multipole solutes in a generalized Kirkwood continuum”, *J. Chem. Theory Comput.*, pages 2083–2097 (2007).
- [58] M. J. Schnieders, N. A. Baker, P. Ren, and J. W. Ponder, “Polarizable atomic multipole solutes in a Poisson-Boltzmann continuum”, *J. Chem. Phys.*, **126**, 124114:1–21 (2007).
- [59] K. A. Sharp and B. Honig, “Calculating total electrostatic energies with the nonlinear Poisson–Boltzmann equation”, *J. Phys. Chem.*, **94**, 7684–7692 (1990).
- [60] M. Deserno and C. Holm, “Cell model and Poisson-Boltzmann theory: A brief introduction”, in *Electrostatic Effects in Soft Matter and Biophysics*, C. Holm, P. Kékicheff, and R. Podgornik, Eds., Vol. 46 of *NATO Science Series*; Springer Science+Business Media: Dordrecht, 2001; pages 27–52.
- [61] G. Lamm, “The Poisson-Boltzmann equation”, in *Reviews in Computational Chemistry*, K. B. Lipkowitz, R. Larter, T. R. Cundari, and D. B. Boyd, Eds., Vol. 19; Wiley-VCH: New York, 2003; chapter 4, pages 147–366.
- [62] N. A. Baker, “Poisson–Boltzmann methods for biomolecular electrostatics”, *Method. Enzymol.*, **383**, 94–118 (2004).

- [63] A. G. Moreira and R. R. Netz, “Field-theoretic approaches to classical charged systems”, in *Electrostatic Effects in Soft Matter and Biophysics*, C. Holm, P. Kékicheff, and R. Podgornik, Eds., Vol. 46 of *NATO Science Series*; Springer Science+Business Media: Dordrecht, 2001; pages 367–408.
- [64] C. J. Stein, J. M. Herbert, and M. Head-Gordon, “The Poisson–Boltzmann model for implicit solvation of electrolyte solutions: Quantum chemical implementation and assessment via Sechenov coefficients”, *J. Chem. Phys.*, **151**, 224111:1–14 (2019).
- [65] H.-X. Zhou, “Macromolecular electrostatic energy within the nonlinear Poisson–Boltzmann equation”, *J. Chem. Phys.*, **100**, 3152–3162 (1993).
- [66] F. Fogolari, P. Zuccato, G. Esposito, and P. Viglino, “Biomolecular electrostatics with the linearized Poisson-Boltzmann equation”, *Biophys. J.*, **76**, 1–16 (1999).
- [67] P. Debye and E. Hückel, “On the theory of electrolytes. I. Freezing point depression and related phenomena”, in *Collected Papers of Peter J. W. Debye*; Interscience: New York, 1954; pages 217–263.
- [68] A. W. Lange and J. M. Herbert, “A simple polarizable continuum solvation model for electrolyte solutions”, *J. Chem. Phys.*, **134**, 204110:1–15 (2011).
- [69] C. Wang, P. Ren, and R. Luo, “Ionic solution: What goes right and wrong with continuum solvation modeling”, *J. Phys. Chem. B*, **121**, 11159–11179 (2017).
- [70] V. Vlachy, “Ionic effects beyond Poisson-Boltzmann theory”, *Annu. Rev. Phys. Chem.*, **50**, 145–165 (1999).
- [71] J. Dziedzic, A. Bhandari, L. Anton, C. Peng, J. Womack, M. Famili, D. Kramer, and C.-K. Skylaris, “Practical approach to large-scale electronic structure calculations in electrolyte solutions via continuum-embedded linear-scaling density functional theory”, *J. Phys. Chem. C*, **124**, 7860–7872 (2020).
- [72] M. Born, “Volumen und Hydratationswärme der Ionen”, *Z. Phys.*, **1**, 45–48 (1920).
- [73] A. A. Rashin and B. Honig, “Reevaluation of the Born model of ion hydration”, *J. Phys. Chem.*, **89**, 5588–5593 (1985).
- [74] L. Onsager, “Electric moments of molecules in liquids”, *J. Am. Chem. Soc.*, **58**, 1486–1493 (1936).
- [75] R. P. Bell, “The electrostatic energy of dipole molecules in different media”, *Trans. Faraday Soc.*, **27**, 797–802 (1931).
- [76] C. J. F. Böttcher, “The dielectric constant of dipole liquids”, *Physica*, **5**, 635–639 (1938).
- [77] J. B. Hasted, “Liquid water: Dielectric properties”, in *Water: A Comprehensive Treatise*, F. Franks, Ed., Vol. 1; Plenum Press: New York, 1972; pages 255–309.
- [78] J. S. Høye and G. Stell, “Statistical mechanics of polar systems. II”, *J. Chem. Phys.*, **64**, 1952–1966 (1976).
- [79] J. H. Hannay, “The Clausius–Mossotti equation: An alternative derivation”, *Eur. J. Phys.*, **4**, 141–143 (1983).

- [80] J. G. Kirkwood, “Theory of solutions of molecules containing widely separated charges with special application to zwitterions”, *J. Chem. Phys.*, **2**, 351–361 (1934).
- [81] J. G. Kirkwood and F. H. Westheimer, “The electrostatic influence of substituents on the dissociation constants of organic acids. I.”, *J. Chem. Phys.*, **6**, 506–512 (1938).
- [82] F. H. Westheimer and J. G. Kirkwood, “The electrostatic influence of substituents on the dissociation constants of organic acids. II.”, *J. Chem. Phys.*, **6**, 513–517 (1938).
- [83] W. B. Bonner, “The electrostatic energy of molecules in solution”, *Trans. Faraday Soc.*, **47**, 1143–1152 (1951).
- [84] D. Rinaldi, M. F. Ruiz-Lopez, and J.-L. Rivail, “*Ab initio* SCF calculations on electrostatically solvated molecules using a deformable three axes ellipsoidal cavity”, *J. Chem. Phys.*, **78**, 834–838 (1983).
- [85] K. V. Mikkelsen, E. Dalgaard, and P. Swanstrøm, “Electron-transfer reactions in solution. An ab initio approach”, *J. Phys. Chem.*, **91**, 3081–3092 (1987).
- [86] K. V. Mikkelsen, H. Ågren, H. J. A. Jensen, and T. Helgaker, “A multiconfigurational self-consistent reaction-field method”, *J. Chem. Phys.*, **89**, 3086–3095 (1988).
- [87] Y. Kong and J. W. Ponder, “Calculation of the reaction field due to off-center point multipoles”, *J. Chem. Phys.*, **107**, 481–492 (1997).
- [88] K. V. Mikkelsen, P. Jørgensen, and H. J. A. Jensen, “A multiconfigurational self-consistent reaction field response method”, *J. Chem. Phys.*, **100**, 6597–6607 (1994).
- [89] M. Medved’, Š. Budzák, W. Bartkowiak, and H. Reis, “Solvent effects on molecular electric properties”, in *Handbook of Computational Chemistry*, J. Leszczynski, A. Kaczmarek-Kedziera, T. Puzyn, M. G. Papadopoulos, H. Reis, and M. K. Shukla, Eds.; Springer International Publishing: Switzerland, 2nd ed., 2017; chapter 17, pages 741–794.
- [90] I. Lotan and T. Head-Gordon, “An analytical electrostatic model for salt screened interactions between multiple proteins”, *J. Chem. Theory Comput.*, **2**, 541–555 (2006).
- [91] C.-G. Zhan, J. Bentley, and D. M. Chipman, “Volume polarization in reaction field theory”, *J. Chem. Phys.*, **108**, 177–192 (1998).
- [92] D. M. Chipman, “Charge penetration in dielectric models of solvation”, *J. Chem. Phys.*, **106**, 10194–10206 (1997).
- [93] D. M. Chipman, “Simulation of volume polarization in reaction field theory”, *J. Chem. Phys.*, **110**, 8012–8018 (1999).
- [94] D. M. Chipman, “Reaction field treatment of charge penetration”, *J. Chem. Phys.*, **112**, 5558–5565 (2000).
- [95] D. M. Chipman, “Comparison of solvent reaction field representations”, *Theor. Chem. Acc.*, **107**, 80–89 (2002).
- [96] D. M. Chipman, “New formulation and implementation for volume polarization in dielectric continuum theory”, *J. Chem. Phys.*, **124**, 224111:1–10 (2006).

- [97] D. M. Chipman, “Energy correction to simulation of volume polarization in reaction field theory”, *J. Chem. Phys.*, **116**, 10129–10138 (2002).
- [98] F. J. Luque, C. Curutchet, J. Muñoz-Muriedas, A. Bidon-Chanal, I. Soteras, A. Morreale, J. L. Gelpi, and M. Orozco, “Continuum solvation models: Dissecting the free energy of solvation”, *Phys. Chem. Chem. Phys.*, **5**, 3827–3836 (2003).
- [99] D. Beglov and B. Roux, “Finite representation of an infinite bulk system: Solvent boundary potential for computer simulations”, *J. Chem. Phys.*, **100**, 9050–9063 (1994).
- [100] I. G. Tironi, R. Sperb, P. E. Smith, and W. F. van Gunsteren, “A generalized reaction field method for molecular dynamics simulations”, *J. Chem. Phys.*, **102**, 5451–5459 (1995).
- [101] W. Im, S. Bernèche, and B. Roux, “Generalized solvent boundary potential for computer simulations”, *J. Chem. Phys.*, **114**, 2924–2937 (2001).
- [102] P. Schaefer, D. Riccardi, and Q. Cui, “Reliable treatment of electrostatics in combined QM/MM simulation of macromolecules”, *J. Chem. Phys.*, **123**, 014905:1–14 (2005).
- [103] T. Benighaus and W. Thiel, “Efficiency and accuracy of the generalized solvent boundary potential for hybrid QM/MM simulations: Implementation for semiempirical Hamiltonians”, *J. Chem. Theory Comput.*, **4**, 1600–1609 (2008).
- [104] T. Benighaus and W. Thiel, “A general boundary potential for hybrid QM/MM simulations of solvated biomolecular systems”, *J. Chem. Theory Comput.*, **5**, 3114–3128 (2009).
- [105] T. Benighaus and W. Thiel, “Long-range electrostatic effects in QM/MM studies of enzymatic reactions: Application of the solvated macromolecule boundary potential”, *J. Chem. Theory Comput.*, **7**, 238–249 (2011).
- [106] A. Aleksandrov and M. Field, “Efficient solvent boundary potential for hybrid potential simulations”, *Phys. Chem. Chem. Phys.*, **13**, 10503–10509 (2011).
- [107] J. Zienau and Q. Cui, “Implementation of the solvent macromolecular boundary potential and application to model and realistic enzyme systems”, *J. Phys. Chem. B*, **116**, 12522–12534 (2012).
- [108] X. Lu and Q. Cui, “Charging free energy calculations using the generalized solvent boundary potential (GSBP) and periodic boundary condition: A comparative analysis using ion solvation and oxidation free energy in proteins”, *J. Phys. Chem. B*, **117**, 2005–2018 (2013).
- [109] N. Rega, G. Brancato, and V. Barone, “Non-periodic boundary conditions for ab initio molecular dynamics in condensed phase using localized basis functions”, *Chem. Phys. Lett.*, **422**, 367–371 (2006).
- [110] G. Brancato, N. Rega, and V. Barone, “Reliable molecular simulations of solute-solvent systems with a minimum number of solvent shells”, *J. Chem. Phys.*, **124**, 214505:1–9 (2006).
- [111] G. Brancato, N. Rega, and V. Barone, “A hybrid explicit/implicit solvation method for first-principle molecular dynamics simulations”, *J. Chem. Phys.*, **128**, 144501:1–10 (2008).
- [112] G. Brancato, N. Rega, and V. Barone, “Molecular dynamics simulations in a *NpT* ensemble using non-periodic boundary conditions”, *Chem. Phys. Lett.*, **483**, 177–181 (2009).

- [113] J. M. J. Swanson, S. A. Adcock, and J. A. McCammon, “Optimized radii for Poisson–Boltzmann calculations with the AMBER force field”, *J. Chem. Theory Comput.*, **1**, 484–493 (2005).
- [114] A. Bondi, “Van der Waals volumes and radii”, *J. Phys. Chem.*, **68**, 441–451 (1964).
- [115] R. S. Rowland and R. Taylor, “Intermolecular nonbonded contact distances in organic crystal structures: Comparison with distances expected from van der Waals radii”, *J. Phys. Chem.*, **100**, 7384–7391 (1996).
- [116] M. Manjeera, A. C. Chamberlin, R. Valero, C. J. Cramer, and D. G. Truhlar, “Consistent van der Waals radii for the whole main group”, *J. Phys. Chem. A*, **113**, 5806–5812 (2009).
- [117] R. Bonaccorsi, P. Palla, and J. Tomasi, “Conformational energy of glycine in aqueous solutions and relative stability of the zwitterionic and neutral forms. An ab initio study”, *J. Am. Chem. Soc.*, **106**, 1945–1950 (1984).
- [118] D. H. Brookes and T. Head-Gordon, “Family of oxygen–oxygen radial distribution functions for water”, *J. Phys. Chem. Lett.*, **6**, 2938–2943 (2015).
- [119] A. V. Onufriev and B. Aguilar, “Accuracy of continuum electrostatic calculations based on three common dielectric boundary definitions”, *J. Theor. Comput. Chem.*, **13**, 1440006:1–25 (2014).
- [120] M. L. Connolly, “Solvent-accessible surfaces of proteins and nucleic acids”, *Science*, **221**, 709–713 (1983).
- [121] F. M. Richards, “Areas, volumes, packing, and protein structure”, *Annu. Rev. Biophys. Bio.*, **6**, 151–176 (1977).
- [122] B. Lee and F. M. Richards, “The interpretation of protein structures: Estimation of static accessibility”, *J. Mol. Biol.*, **55**, 379–400 (1971).
- [123] D.-S. Kim, C.-I. Won, and J. Bhak, “A proposal for the revision of molecular boundary typology”, *J. Biomol. Struct. Dyn.*, **28**, 277–287 (2010).
- [124] C. S. Pomelli, “Cavity surfaces and their discretization”, in *Continuum Solvation Models in Chemical Physics*, B. Mennucci and R. Cammi, Eds.; Wiley: Chichester, UK, 2007; pages 49–63.
- [125] C.-G. Zhan and D. M. Chipman, “Cavity size in reaction field theory”, *J. Chem. Phys.*, **109**, 10543–10558 (1998).
- [126] V. Barone, M. Cossi, and J. Tomasi, “A new definition of cavities for the computation of solvation free energies by the polarizable continuum model”, *J. Chem. Phys.*, **107**, 3210–3221 (1997).
- [127] B. Ginovska, D. M. Camaioni, M. Dupuis, C. A. Schwerdtfeger, and Q. Gil, “Charge-dependent cavity radii for an accurate dielectric continuum model of solvation with emphasis on ions: Aqueous solutes with oxo, hydroxo, amino, methyl, chloro, bromo, and fluoro functionalities”, *J. Phys. Chem. A*, **112**, 10604–10613 (2008).

- [128] J. B. Foresman, T. A. Keith, K. B. Wiberg, J. Snoonian, and M. J. Frisch, “Solvent effects. 5. Influence of cavity shape, truncation of electrostatics, and electron correlation on ab initio reaction field calculations”, *J. Phys. Chem.*, **100**, 16098–16104 (1996).
- [129] D. M. Chipman and M. Dupuis, “Implementation of solvent reaction fields for electronic structure”, *Theor. Chem. Acc.*, **107**, 90–102 (2002).
- [130] F. Chen and D. M. Chipman, “Boundary element methods for dielectric cavity construction and integration”, *J. Chem. Phys.*, **119**, 10289–10297 (2003).
- [131] P. C. do Couto and D. M. Chipman, “How does dielectric solvation affect the size of an ion?”, *J. Phys. Chem. A*, **114**, 12788–12793 (2010).
- [132] M. Holst and F. Saied, “Multigrid solution of the Poisson–Boltzmann equation”, *J. Comput. Chem.*, **14**, 105–113 (1993).
- [133] M. J. Holst and F. Saied, “Numerical solution of the nonlinear Poisson–Boltzmann equation: Developing more robust and efficient methods”, *J. Comput. Chem.*, **16**, 337–364 (1995).
- [134] M. Holst, N. Baker, and F. Wang, “Adaptive multilevel finite element solution of the Poisson–Boltzmann equation I. Algorithms and examples”, *J. Comput. Chem.*, **21**, 1319–1342 (2000). Erratum: *J. Comput. Chem.*, **22**, 45 (2001).
- [135] B. Z. Lu, Y. C. Zhou, M. J. Holst, and J. A. McCammon, “Recent progress in numerical methods for the Poisson–Boltzmann equation in biophysical applications”, *Commun. Comput. Phys.*, **3**, 973–1009 (2008).
- [136] J. Wang and R. Luo, “Assessment of linear finite-difference Poisson–Boltzmann solvers”, *J. Comput. Chem.*, **31**, 1689–1698 (2010).
- [137] E.-H. Yap and T. Head-Gordon, “New and efficient Poisson–Boltzmann solver for interaction of multiple proteins”, *J. Chem. Theory Comput.*, **6**, 2214–2224 (2010).
- [138] A. H. Boschitsch and M. O. Fenley, “A fast and robust Poisson–Boltzmann solver based on adaptive Cartesian grids”, *J. Chem. Theory Comput.*, **7**, 1524–1540 (2011).
- [139] M. Holst, J. A. McCammon, Z. Yu, and Y. C. Zhou, “Adaptive finite element modeling techniques for the Poisson–Boltzmann equation”, *Commun. Comput. Phys.*, **11**, 179–214 (2012).
- [140] C. Li, L. Li, M. Petukh, and E. Alexov, “Progress in developing Poisson–Boltzmann equation solvers”, *Mol.-Based Math. Biol.*, **1**, 42–62 (2013).
- [141] W. Geng and R. Krasny, “A treecode-accelerated boundary integral Poisson–Boltzmann solver for electrostatics of solvated biomolecules”, *J. Comput. Phys.*, **247**, 62–78 (2013).
- [142] I. Sakalli, J. Schöberl, and E. W. Knapp, “mFES: A robust molecular finite element solver for electrostatic energy computations”, *J. Chem. Theory Comput.*, **10**, 5095–5112 (2014).
- [143] G. Fisicaro, L. Genovese, O. Andreussi, N. Marzari, and S. Goedecker, “A generalized Poisson and Poisson–Boltzmann solver for electrostatic environments”, *J. Chem. Phys.*, **144**, 014103:1–12 (2016).

- [144] S. Ringe, H. Oberhofer, C. Hille, S. Matera, and K. Reuter, “Function-space-based solution scheme for the size-modified Poisson–Boltzmann equation in full-potential DFT”, *J. Chem. Theory Comput.*, **12**, 4052–4066 (2016).
- [145] J. C. Womack, L. Anton, J. Dziedzic, P. J. Hasnip, M. I. J. Probert, and C.-K. Skylaris, “DL_MG: A parallel multigrid Poisson and Poisson–Boltzmann solver for electronic structure calculations in vacuum and solution”, *J. Chem. Theory Comput.*, **14**, 1412–1432 (2018).
- [146] V. Luzhkov and A. Warshel, “Microscopic models for quantum mechanical calculations of chemical processes in solutions: LD/AMPAC and SCAAS/AMPAC calculations of solvation energies”, *J. Comput. Chem.*, **13**, 199–213 (1992).
- [147] J. Florián and A. Warshel, “Langevin dipoles model for ab initio calculations of chemical processes in solution: Parameterization and application to hydration free energies of neutral and ionic solutes and conformational analysis in aqueous solution”, *J. Phys. Chem. B*, **101**, 5583–5595 (1997).
- [148] A. Papazyan and A. Warshel, “Continuum and dipole-lattice models of solvation”, *J. Phys. Chem. B*, **101**, 11254–11264 (1997).
- [149] J. Langlet, P. Claverie, J. Caillet, and A. Pullman, “Improvements of the continuum model. 1. Application to the calculation of the vaporization of thermodynamic quantities of nonassociated liquids”, *J. Phys. Chem.*, **92**, 1617–1631 (1988).
- [150] M. Orozco and F. J. Luque, “Theoretical methods for the description of the solvent effect in biomolecular systems”, *Chem. Rev.*, **100**, 4187–4225 (2000). Erratum: *Chem. Rev.*, **101**, 203 (2001).
- [151] R. Constanciel, “Theoretical basis of the empirical reaction field approximations through continuum model”, *Theor. Chem. Acc.*, **69**, 505–523 (1986).
- [152] E. Cancès, “Integral equation approaches for continuum models”, in *Continuum Solvation Models in Chemical Physics*, B. Mennucci and R. Cammi, Eds.; Wiley: Chichester, UK, 2007; pages 29–48.
- [153] M. Cossi, G. Scalmani, N. Rega, and V. Barone, “New developments in the polarizable continuum model for quantum mechanical and classical calculations on molecules in solution”, *J. Chem. Phys.*, **117**, 43–54 (2002).
- [154] J. Tomasi, B. Mennucci, and E. Cancès, “The IEF version of the PCM solvation method: An overview of a new method addressed to study molecular solutes at the QM ab initio level”, *J. Mol. Struct. (Theochem)*, **464**, 211–226 (1999).
- [155] E. Cancés, B. Mennucci, and J. Tomasi, “A new integral equation formalism for the polarizable continuum model: Theoretical background and applications to isotropic and anisotropic dielectrics”, *J. Chem. Phys.*, **107**, 3032–3041 (1997).
- [156] B. Mennucci, E. Cancés, and J. Tomasi, “Evaluation of solvent effects in isotropic and anisotropic dielectrics and in ionic solutions with a unified integral equation method: Theoretical bases, computational implementation, and numerical applications”, *J. Phys. Chem. B*, **101**, 10506–10517 (1997).

- [157] E. Cancès and B. Mennucci, “New applications of integral equations methods for solvation continuum models: Ionic solutions and liquid crystals”, *J. Math. Chem.*, **23**, 309–326 (1998).
- [158] E. Cancès and B. Mennucci, “Comment on “Reaction field treatment of charge penetration””, *J. Chem. Phys.*, **114**, 4744–4745 (2001).
- [159] M. E. Davis and J. A. McCammon, “Solving the finite difference linearized Poisson–Boltzmann equation: A comparison of relaxation and conjugate gradient methods”, *J. Comput. Chem.*, **10**, 386–391 (1989).
- [160] B. A. Luty, M. E. Davis, and J. A. McCammon, “Solving the finite-difference non-linear Poisson–Boltzmann equation”, *J. Comput. Chem.*, **13**, 1114–1118 (1992).
- [161] J. Wang, Q. Cai, Y. Xiang, and R. Luo, “Reducing grid dependence in finite-difference Poisson–Boltzmann calculations”, *J. Chem. Theory Comput.*, **8**, 2741–2751 (2012).
- [162] L. Xiao, Q. Cai, X. Ye, J. Wang, and R. Luo, “Electrostatic forces in the Poisson–Boltzmann systems”, *J. Chem. Phys.*, **139**, 094106:1–12 (2013).
- [163] L. Xiao, C. Wang, and R. Luo, “Recent progress in adapting Poisson–Boltzmann methods to molecular simulations”, *J. Theor. Comput. Chem.*, **13**, 1430001:1–19 (2014).
- [164] D. M. Chipman, “Solution of the linearized Poisson–Boltzmann equation”, *J. Chem. Phys.*, **120**, 5566–5575 (2004).
- [165] F. Lippalini, B. Stamm, E. Cancès, Y. Maday, and B. Mennucci, “Fast domain decomposition algorithm for continuum solvation models: Energy and first derivatives”, *J. Chem. Theory Comput.*, **9**, 3637–3648 (2013).
- [166] F. Lippalini, L. Lagardère, G. Scalmani, B. Stamm, E. Cancès, Y. Maday, J.-P. Piquemal, M. J. Frisch, and B. Mennucci, “Quantum calculations in solution for large to very large molecules: A new linear scaling QM/continuum approach”, *J. Phys. Chem. Lett.*, **5**, 953–958 (2014).
- [167] S. Caprasecca, S. Jurinovich, L. Lagardère, B. Stamm, and F. Lippalini, “Achieving linear scaling in computational cost for a fully polarizable MM/continuum embedding”, *J. Chem. Theory Comput.*, **11**, 694–704 (2015).
- [168] A. Klamt and G. Schüürmann, “COSMO: A new approach to dielectric screening in solvents with explicit expressions for the screening energy and its gradient”, *J. Chem. Soc., Perkin Trans. 2*, pages 799–805 (1993).
- [169] E. Cancès and B. Mennucci, “The escaped charge problem in solvation continuum models”, *J. Chem. Phys.*, **115**, 6130–6135 (2001).
- [170] A. Klamt, C. Moya, and J. Palomar, “A comprehensive comparison of the IEFPCM and SS(V)PE continuum solvation methods with the COSMO approach”, *J. Chem. Theory Comput.*, **11**, 4220–4225 (2015).
- [171] E. V. Stefanovich and T. N. Truong, “Optimized atomic radii for quantum dielectric continuum solvation models”, *Chem. Phys. Lett.*, **244**, 65–74 (1995).

- [172] T. N. Truong and E. V. Stefanovich, “A new method for incorporating solvent effects into the classical, ab initio molecular orbital and density functional theory frameworks for arbitrary cavity shape”, *Chem. Phys. Lett.*, **240**, 253–260 (1995).
- [173] T. N. Truong and E. V. Stefanovich, “Analytical first and second energy derivatives of the generalized conductorlike screening model for free energy of solvation”, *J. Chem. Phys.*, **103**, 3709–3717 (1995).
- [174] T. N. Truong, U. N. Nguyen, and E. V. Stefanovich, “Generalized conductor-like screening model (GCOSMO) for solvation: An assessment of its accuracy and applicability”, *Int. J. Quantum Chem. Symp.*, **60**, 1615–1622 (1996).
- [175] V. Barone and M. Cossi, “Quantum calculation of molecular energies and energy gradients in solution by a conductor solvent model”, *J. Phys. Chem. A*, **102**, 1995–2001 (1998).
- [176] M. Cossi, N. Rega, G. Scalmani, and V. Barone, “Energies, structures, and electronic properties of molecules in solution with the C-PCM solvation model”, *J. Comput. Chem.*, **24**, 669–681 (2003).
- [177] R. Cammi and J. Tomasi, “Analytical derivatives for molecular solutes. I. Hartree–Fock energy first derivatives with respect to external parameters in the polarizable continuum model”, *J. Chem. Phys.*, **100**, 7495–7502 (1994).
- [178] A. Klamt and V. Jonas, “Treatment of the outlying charge in continuum solvation models”, *J. Chem. Phys.*, **105**, 9972–9981 (1996).
- [179] B. Mennucci and J. Tomasi, “Continuum solvation models: A new approach to the problem of solute’s charge distribution and cavity boundaries”, *J. Chem. Phys.*, **106**, 5151–5158 (1997).
- [180] R. Cammi, M. Cossi, and J. Tomasi, “Analytical derivatives for molecular solutes. III. Hartree–Fock static polarizabilities in the polarizable continuum model”, *J. Chem. Phys.*, **104**, 4611–4620 (1996).
- [181] J. Gauss, “Molecular properties”, in *Modern Methods and Algorithms of Quantum Chemistry*, J. Grotendorst, Ed., Vol. 3 of *NIC Series*; John von Neumann Institute for Computing: Jülich, 2nd ed., 2000; pages 541–592.
- [182] A. Rizzo, S. Coriani, and K. Ruud, “Response function theory computational approaches to linear and nonlinear optical spectroscopy”, in *Computational Strategies for Spectroscopy: From Small Molecules to Nano Systems*, V. Barone, Ed.; John Wiley & Sons: Hoboken, NJ, 1st ed., 2012; chapter 2, pages 77–136.
- [183] T. Helgaker, S. Coriani, P. Jørgensen, K. Kristensen, J. Olsen, and K. Ruud, “Recent advances in wave function-based methods of molecular-property calculations”, *Chem. Rev.*, **112**, 543–631 (2012).
- [184] E. Jurrus, D. Engel, K. Star, K. Monson, J. Brandi, L. E. Felberg, D. H. Brookes, L. Wilson, J. Chen, K. Liles, M. Chun, P. Li, D. W. Gohara, T. Dolinsky, R. K. D. R. Koes, J. E. Nielsen, T. Head-Gordon, W. Geng, R. Krasny, G.-W. Wei, M. J. Holst, J. A. McCammon, and N. A. Baker, “Improvements to the APBS biomolecular solvation software suite”, *Protein Sci.*, **27**, 112–128 (2018).

- [185] Z.-Q. You, J.-M. Mewes, A. Dreuw, and J. M. Herbert, “Comparison of the Marcus and Pekar partitions in the context of non-equilibrium, polarizable-continuum reaction-field solvation models”, *J. Chem. Phys.*, **143**, 204107:1–14 (2015).
- [186] E. Silla, F. Villar, O. Nilsson, J. L. Pascual-Ahuir, and O. Tapia, “Molecular volumes and surfaces of biomacromolecules via GEOPOL: A fast and efficient algorithm”, *J. Mol. Graphics*, **8**, 168–172 (1990).
- [187] J. L. Pascual-Ahuir and E. Silla, “GEOPOL: An improved description of molecular surfaces. I. Building the spherical surface set”, *J. Comput. Chem.*, **11**, 1047–1060 (1990).
- [188] E. Silla, I. Tuñon, and J. L. Pascual-Ahuir, “GEOPOL: An improved description of molecular surfaces. II. Computing the molecular area and volume”, *J. Comput. Chem.*, **12**, 1077–1088 (1991).
- [189] J. L. Pascual-Ahuir, E. Silla, and I. Tuñon, “GEOPOL: An improved description of molecular surfaces. III. A new algorithm for the computation of a solvent-excluding surface”, *J. Comput. Chem.*, **15**, 1127–1138 (1994).
- [190] D. A. Liotard, G. D. Hawkins, G. C. Lynch, C. J. Cramer, and D. G. Truhlar, “Improved methods for semiempirical solvation models”, *J. Comput. Chem.*, **16**, 422–440 (1995).
- [191] M. Cossi, B. Mennucci, and R. Cammi, “Analytical first derivatives of molecular surfaces with respect to nuclear coordinates”, *J. Comput. Chem.*, **17**, 57–73 (1996).
- [192] D. M. York and M. Karplus, “Smooth solvation potential based on the conductor-like screening model”, *J. Phys. Chem. A*, **103**, 11060–11079 (1999).
- [193] B. A. Gregersen and D. M. York, “High-order discretization schemes for biochemical applications of boundary element solvation and variational electrostatic projection methods”, *J. Chem. Phys.*, **122**, 194110:1–4 (2005).
- [194] J. Khandogin, B. A. Gregersen, W. Thiel, and D. M. York, “Smooth solvation method for d-orbital semiempirical calculations of biological reactions. 1. Implementation”, *J. Phys. Chem. B*, **109**, 9799–9809 (2005).
- [195] C. W. Murray, N. C. Handy, and G. J. Laming, “Quadrature schemes for integrals of density functional theory”, *Mol. Phys.*, **78**, 997–1014 (1993).
- [196] P. M. W. Gill, B. G. Johnson, and J. A. Pople, “A standard grid for density-functional calculations”, *Chem. Phys. Lett.*, **209**, 506–512 (1993).
- [197] S.-H. Chien and P. M. W. Gill, “SG-0: A small standard grid for DFT quadrature on large systems”, *J. Comput. Chem.*, **27**, 730–739 (2006).
- [198] S. Dasgupta and J. M. Herbert, “Standard grids for high-precision integration of modern density functionals: SG-2 and SG-3”, *J. Comput. Chem.*, **38**, 869–882 (2017).
- [199] J. Liu and W. Liang, “Analytical second derivatives of excited-state energy within the time-dependent density functional theory coupled with a conductor-like polarizable continuum model”, *J. Chem. Phys.*, **138**, 024101:1–10 (2013).
- [200] R. J. Wawak, K. D. Gibson, and H. A. Scheraga, “Gradient discontinuities in calculations involving molecular surface area”, *J. Math. Chem.*, **15**, 207–232 (1994).

- [201] H. Li and J. H. Jensen, “Improving the efficiency and convergence of geometry optimization with the polarizable continuum model: New energy gradients and molecular surface tessellation”, *J. Comput. Chem.*, **25**, 1449–1462 (2004).
- [202] P. Su and H. Li, “Continuous and smooth potential energy surface for conductor-like screening solvation model using fixed points with variable areas”, *J. Chem. Phys.*, **130**, 074109:1–13 (2009).
- [203] A. I. Krylov and P. M. W. Gill, “Q-Chem: An engine for innovation”, *WIREs Comput. Mol. Sci.*, **3**, 317–326 (2013).
- [204] G. Scalmani and M. J. Frisch, “Continuous surface charge polarizable continuum models of solvation. I. General formalism”, *J. Chem. Phys.*, **132**, 114110:1–15 (2010).
- [205] M. Garcia-Ratès and F. Neese, “Effect of the solute cavity on the solvation energy and its derivatives within the framework of the Gaussian charge scheme”, *J. Comput. Chem.*, **41**, 922–939 (2020).
- [206] H. Harbrecht and M. Randrianarivony, “Wavelet BEM on molecular surfaces: Parameterization and implementation”, *Computing*, **86**, 1–22 (2009).
- [207] V. Weijo, M. Randrianarivony, H. Harbrecht, and L. Frediani, “Wavelet formulation of the polarizable continuum model”, *J. Comput. Chem.*, **31**, 1469–1477 (2010).
- [208] M. Bugeanu, R. Di Remigio, K. Mozgawa, S. S. Reine, H. Harbrecht, and L. Frediani, “Wavelet formulation of the polarizable continuum model. II. Use of piecewise bilinear boundary elements”, *Phys. Chem. Chem. Phys.*, **17**, 31566–31581 (2015).
- [209] M. Bugeanu and H. Harbrecht, “Parametric representation of molecular surfaces”, *Int. J. Quantum Chem.*, **119**, e25695:1–12 (2019).
- [210] C.-G. Zhan and D. M. Chipman, “Reaction field effects on nitrogen shielding”, *J. Chem. Phys.*, **110**, 1611–1622 (1999).
- [211] H. Tjong and H.-X. Zhou, “On the dielectric boundary in Poisson–Boltzmann calculations”, *J. Chem. Theory Comput.*, **4**, 507–514 (2008).
- [212] W. E. Lorensen and H. E. Cline, “Marching cubes: A high resolution 3D surface construction algorithm”, *Comp. Graph.*, **21**, 163–169 (1987).
- [213] D. A. Rajon and W. E. Bolch, “Marching cubes algorithm: Review and trilinear interpolation adaptation for image-based dosimetric models”, *Comput. Med. Imag. Grap.*, **27**, 411–435 (2003).
- [214] Z. Yu, M. P. Jacobson, and R. Friesner, “What role do surfaces play in GB models? A new-generation of surface-generalized Born model based on a novel Gaussian surface for biomolecules”, *J. Comput. Chem.*, **27**, 72–89 (2005).
- [215] B. Zhou, M. Agarwal, and C. F. Wong, “Variable atomic radii for continuum-solvent electrostatics calculation”, *J. Chem. Phys.*, **129**, 014509:1–9 (2008).
- [216] G. Fisicaro, L. Genovese, O. Andreussi, S. Mandai, N. N. Nair, N. Marzari, and S. Goedecker, “Soft-sphere continuum solvation in electronic-structure calculations”, *J. Chem. Theory Comput.*, **13**, 3829–3845 (2017).

- [217] J.-L. Fattebert and F. Gygi, “Density functional theory for efficieint *ab initio* molecular dynamics simulations in solution”, *J. Comput. Chem.*, **23**, 662–666 (2002).
- [218] J.-L. Fattebert and F. Gygi, “First-principles molecular dynamics simulations in a continuum solvent”, *Int. J. Quantum Chem.*, **93**, 139–147 (2003).
- [219] D. A. Scherlis, J.-L. Fattebert, F. Gygi, M. Cococcioni, and N. Marzari, “A unified electrostatic and cavitation model for first-principles molecular dynamics in solution”, *J. Chem. Phys.*, **124**, 074103:1–12 (2006).
- [220] J. Dziedzic, H. H. Helal, C.-K. Skylaris, A. A. Mostofi, and M. C. Payne, “Minimal parameter implicit solvent model for ab initio electronic-structure calculations”, *Europhys. Lett.*, **95**, 43001:1–6 (2011).
- [221] O. Andreussi, I. Dabo, and N. Marzari, “Revised self-consistent continuum solvation in electronic-structure calculations”, *J. Chem. Phys.*, **136**, 064102:1–20 (2012).
- [222] K. Mathew, R. Sundararaman, K. Letchworth-Weaver, T. A. Arias, and R. G. Hennig, “Implicit solvation model for density-functional study of nanocrystal surfaces and reaction pathways”, *J. Chem. Phys.*, **140**, 084106:1–8 (2014).
- [223] V. M. Sánchez, M. Sued, and D. A. Scherlis, “First-principles molecular dynamics simulations at solid-liquid interfaces with a continuum solvent”, *J. Chem. Phys.*, **131**, 174108:1–9 (2009).
- [224] F. Nattino, M. Truscott, N. Marzari, and O. Andreussi, “Continuum models of the electrochemical diffuse layer in electronic-structure calculations”, *J. Chem. Phys.*, **150**, 041722:1–17 (2019).
- [225] O. Andreussi, N. G. Hörmann, F. Nattino, G. Fisicaro, S. Goedecker, and N. Marzari, “Solvent-aware interfaces in continuum solvation”, *J. Chem. Theory Comput.*, **15**, 1996–2009 (2019).
- [226] R. Sundararaman and K. Schwarz, “Evaluating continuum solvation models for the electrode-electrolyte interface: Challenges and strategies for improvement”, *J. Chem. Phys.*, **146**, 084111:1–5 (2017).
- [227] R. Sundararaman, K. Letchworth-Weaver, and K. A. Schwarz, “Improving accuracy of electrochemical capacitance and solvation energetics in first-principles calculations”, *J. Chem. Phys.*, **148**, 144105:1–7 (2018).
- [228] K. Schwarz and R. Sundararaman, “The electrochemical interface in first-principles calculations”, *Surf. Sci. Rep.*, **75**, 100492:1–22 (2020).
- [229] G. Bramley, M.-T. Nguyen, V.-A. Glezakou, R. Rousseau, and C.-K. Sylaris, “Reconciling work functions and adsorption enthalpies for implicit solvent models: A Pt(111)/water interface case study”, *J. Chem. Theory Comput.*, **16**, 2703–2715 (2020).
- [230] A. Bhandari, L. Anton, J. Dziedzic, C. Peng, D. Kramer, and C.-K. Skylaris, “Electronic structure calculations in electrolyte solutions: Methods for neutralization of extended charged interfaces”, *J. Chem. Phys.*, **153**, 124101:1–12 (2020).
- [231] M. E. Davis and J. A. McCammon, “Dielectric boundary smoothing in finite difference solutions of the Poisson equation: An approach to improve accuracy and convergence”, *J. Comput. Chem.*, **12**, 909–912 (1991).

- [232] M. K. Gilson, M. E. Davis, B. A. Luty, and J. A. McCammon, “Computation of electrostatic forces on solvated molecules using the Poisson-Boltzmann equation”, *J. Phys. Chem.*, **97**, 3591–3600 (1993).
- [233] W. Im, D. Beglov, and B. Roux, “Continuum solvation model: Computation of electrostatic forces from numerical solutions to the Poisson–Boltzmann equation”, *Comput. Phys. Commun.*, **111**, 59–75 (1998).
- [234] B. Lu, D. Zhang, and J. A. McCammon, “Computation of electrostatic forces between solvated molecules determined by the Poisson–Boltzmann equation using a boundary element method”, *J. Chem. Phys.*, **122**, 214102:1–7 (2005).
- [235] J. Wang, C. Tan, E. Chanco, and R. Luo, “Quantitative analysis of Poisson–Boltzmann implicit solvent in molecular dynamics”, *Phys. Chem. Chem. Phys.*, **12**, 1194–1202 (2010).
- [236] Q. Cai, X. Ye, J. Wang, and R. Luo, “Dielectric boundary force in numerical Poisson–Boltzmann methods: Theory and numerical strategies”, *Chem. Phys. Lett.*, **514**, 368–373 (2011).
- [237] N. Rega, M. Cossi, and V. Barone, “Towards linear scaling in continuum solvent models. A new iterative procedure for energies and geometry optimizations”, *Chem. Phys. Lett.*, **293**, 221–229 (1998).
- [238] G. Scalmani, V. Barone, K. N. Kudin, C. S. Pomelli, G. E. Scuseria, and M. J. Frisch, “Achieving linear-scaling computational cost for the polarizable continuum model of solvation”, *Theor. Chem. Acc.*, **111**, 90–100 (2004).
- [239] P. Gatto, F. Lipparini, and B. Stamm, “Computation of forces arising from the polarizable continuum model within the domain-decomposition paradigm”, *J. Chem. Phys.*, **147**, 224108:1–11 (2017).
- [240] B. Stamm, L. Lagardère, G. Scalmani, P. Gatto, E. Cancès, J.-P. Piquemal, Y. Maday, B. Mennucci, and F. Lipparini, “How to make continuum solvation incredibly fast in a few simple steps: A practical guide to the domain decomposition paradigm for the conductor-like screening model”, *Int. J. Quantum Chem.*, **119**, e25669:1–15 (2019).
- [241] M. Nottoli, B. Stamm, G. Scalmani, and F. Lipparini, “Quantum calculations in solution of energies, structures, and properties with a domain decomposition polarizable continuum model”, *J. Chem. Theory Comput.*, **15**, 6061–6073 (2019).
- [242] L. Lagardère, L.-H. Jolly, F. Lipparini, F. Aviat, B. Stamm, Z. F. Jing, M. Harger, H. Tora-bifard, G. A. Cisneros, M. J. Schneiders, N. Gresh, Y. Maday, P. Y. Ren, J. W. Ponder, and J.-P. Piquemal, “Tinker-HP: A massively parallel molecular dynamics package for multiscale simulations of large complex systems with advanced point dipole polarizable force fields”, *Chem. Sci.*, **9**, 956–972 (2018).
- [243] F. Lipparini, L. Lagardère, C. Raynaud, B. Stamm, E. Cancès, B. Mennucci, M. Schnieders, P. Ren, Y. Maday, and J.-P. Piquemal, “Polarizable molecular dynamics in a polarizable continuum solvent”, *J. Chem. Theory Comput.*, **11**, 623–634 (2014).
- [244] C. J. Cramer and D. G. Truhlar, “A universal approach to solvation modeling”, *Acc. Chem. Res.*, **41**, 760–768 (2008).

- [245] C. J. Cramer and D. G. Truhlar, “SM x continuum models for condensed phases”, in *Trends and Perspectives in Modern Computational Science*, G. Maroulis and T. E. Simos, Eds., Vol. 6 of *Lecture Series on Computer and Computational Sciences*; Brill/VSP: Leiden, 2006; pages 112–140.
- [246] J. D. Thompson, C. J. Cramer, and D. G. Truhlar, “New universal solvation model and comparison of the accuracy of the SM5.42R, SM5.43R, C-PCM, D-PCM, and IEF-PCM continuum solvation models for aqueous and organic solvation free energies and for vapor pressures”, *J. Phys. Chem. A*, **108**, 6532–6542 (2004).
- [247] C. P. Kelly, C. J. Cramer, and D. G. Truhlar, “SM6: A density functional theory continuum solvation model for calculating aqueous solvation free energies of neutrals, ions, and solute–water clusters”, *J. Chem. Theory Comput.*, **1**, 1133–1152 (2005).
- [248] A. V. Marenich, C. J. Cramer, and D. G. Truhlar, “Generalized Born solvation model SM12”, *J. Chem. Theory Comput.*, **9**, 609–620 (2013).
- [249] A. V. Marenich, C. J. Cramer, and D. G. Truhlar, “Universal solvation model based on solute electron density and on a continuum model of the solvent defined by the bulk dielectric constant and atomic surface tensions”, *J. Phys. Chem. B*, **113**, 6378–6396 (2009).
- [250] A. V. Marenich, C. J. Cramer, and D. G. Truhlar, “Performance of SM6, SM8, and SMD on the SAMPL1 test set for the prediction of small-molecule solvation free energies”, *J. Phys. Chem. B*, **113**, 4538–4543 (2009).
- [251] Z.-Q. You and J. M. Herbert, “Reparameterization of an accurate, few-parameter implicit solvation model for quantum chemistry: Composite method for implicit representation of solvent, CMIRS v. 1.1”, *J. Chem. Theory Comput.*, **12**, 4338–4346 (2016).
- [252] C. Dupont, O. Andreussi, and N. Marzari, “Self-consistent continuum solvation (SCCS): The case of charged systems”, *J. Chem. Phys.*, **139**, 214110:1–8 (2013).
- [253] A. Klamt, B. Mennucci, J. Tomasi, V. Barone, C. Curutchet, M. Orozco, and F. J. Luque, “On the performance of continuum solvation methods. A comment on “Universal approaches to solvation modeling””, *Acc. Chem. Res.*, **42**, 489–492 (2009).
- [254] L. Tomaník, E. Muchová, and P. Slavíček, “Solvation energies of ions with ensemble cluster-continuum approach”, *Phys. Chem. Chem. Phys.*, **22**, 22357–22368 (2020).
- [255] R. Casasnovas, J. Ortega-Castro, J. Frau, J. Donoso, and F. Muñoz, “Theoretical p K_a calculations with continuum model solvents, alternative protocols to thermodynamic cycles”, *Int. J. Quantum Chem.*, **114**, 1350–1363 (2014).
- [256] B. Thapa and H. B. Schlegel, “Calculations of p K_a ’s and redox potentials of nucleobases with explicit waters and polarizable continuum solvation”, *J. Phys. Chem. A*, **119**, 5134–5144 (2015).
- [257] B. Thapa and H. B. Schlegel, “Density functional theory calculation of p K_a ’s of thiols in aqueous solution using explicit water molecules and the polarizable continuum model”, *J. Phys. Chem. A*, **120**, 5726–5735 (2016).

- [258] V. S. Bryantsev, M. S. Diallo, and W. A. Goddard III, “Calculation of solvation free energies of charged solutes using mixed cluster/continuum models”, *J. Phys. Chem. B*, **112**, 9709–9719 (2008).
- [259] D. Riccardi, H.-B. Guo, J. M. Parks, B. Gu, L. Liang, and J. C. Smith, “Cluster-continuum calculations of hydration free energies of anions and group 12 divalent cations”, *J. Chem. Theory Comput.*, **9**, 555–569 (2013).
- [260] S. Dhillon and A. L. East, “Challenges in predicting $\Delta_{\text{rxn}}G$ in solution: Hydronium, hydroxide, and water autoionization”, *Int. J. Quantum Chem.*, **118**, e25703:1–7 (2018).
- [261] D. H. Patel and A. L. L. East, “Semicontinuum (cluster-continuum) modeling of acid-catalyzed aqueous reactions: Alkene hydration”, *J. Phys. Chem. A*, **124**, 9088–9104 (2020).
- [262] I. Soteras, C. Curutchet, A. Bidon-Chanal, M. Orozco, and F. J. Luque, “Extension of the MST model to the IEF formalism: HF and B3LYP parameterizations”, *J. Mol. Struct. (Theochem)*, **727**, 29–40 (2005).
- [263] C. Curutchet, M. Orozco, F. J. Luque, B. Mennucci, and J. Tomasi, “Dispersion and repulsion contributions to the solvation free energy: Comparison of quantum mechanical and classical approaches in the polarizable continuum model”, *J. Comput. Chem.*, **27**, 1769–1780 (2006).
- [264] C. J. Cramer and D. G. Truhlar, “Reply to comment on “A universal approach to solvation modeling””, *Acc. Chem. Res.*, **42**, 493–497 (2009).
- [265] A. V. Marenich, R. M. Olson, C. P. Kelly, C. J. Cramer, and D. G. Truhlar, “Self-consistent reaction field model for aqueous and nonaqueous solutions based on accurate polarized partial charges”, *J. Chem. Theory Comput.*, **3**, 2011–2033 (2007).
- [266] A. C. Chamberlin, C. J. Cramer, and D. G. Truhlar, “Performance of SM8 on a test to predict small-molecule solvation free energies”, *J. Phys. Chem. B*, **112**, 8651–8655 (2008).
- [267] A. Klamt, “The COSMO and COSMO-RS solvation models”, *WIREs Comput. Mol. Sci.*, **1**, 699–709 (2011).
- [268] A. Klamt, “The COSMO and COSMO-RS solvation models”, *WIREs Comput. Mol. Sci.*, **8**, e1338:1–11 (2018).
- [269] D. Bashford and D. A. Case, “Generalized Born models of macromolecular solvation effects”, *Annu. Rev. Phys. Chem.*, **51**, 129–152 (2000).
- [270] A. V. Onufriev and D. A. Case, “Generalized Born implicit solvent models for biomolecules”, *Annu. Rev. Biophys.*, **48**, 275–296 (2019).
- [271] W. C. Still, A. Tempczyk, R. C. Hawley, and T. Hendrickson, “Semianalytical treatment of solvation for molecular mechanics and dynamics”, *J. Am. Chem. Soc.*, **112**, 6127–6129 (1990).
- [272] A. Onufriev, D. Bashford, and D. A. Case, “Modification of the generalized Born models suitable for macromolecules”, *J. Phys. Chem. B*, **104**, 3712–3720 (2000).
- [273] A. Onufriev, D. A. Case, and D. Bashford, “Effective Born radii in the generalized Born model approximation: The importance of being perfect”, *J. Comput. Chem.*, **23**, 1297–1304 (2002).

- [274] J. Mongan, W. A. Svrcek-Seiler, and A. Onufriev, “Analysis of integral expressions for effective Born radii”, *J. Chem. Phys.*, **127**, 185101:1–10 (2007).
- [275] A. W. Lange and J. M. Herbert, “Improving generalized Born models by exploiting connections to polarizable continuum models. I. An improved effective Coulomb operator”, *J. Chem. Theory Comput.*, **8**, 1999–2011 (2012).
- [276] M. S. Lee, F. R. Salsbury, Jr., and C. L. Brooks III, “Novel generalized Born methods”, *J. Chem. Phys.*, **116**, 10606–10614 (2002).
- [277] F. R. Salsbury, Jr., “Analysis of errors in Still’s equation for macromolecular electrostatic solvation energies”, *Mol. Phys.*, **104**, 1299–1309 (2006).
- [278] A. W. Lange and J. M. Herbert, “Improving generalized Born models by exploiting connections to polarizable continuum models. II. Corrections for salt effects”, *J. Chem. Theory Comput.*, **8**, 4381–4392 (2012).
- [279] M. Scarsi, J. Apostolakis, and A. Caflisch, “Continuum electrostatics energies of macromolecules in aqueous solutions”, *J. Phys. Chem. A*, **101**, 8098–8106 (1997).
- [280] R. A. Pierotti, “A scaled particle theory of aqueous and nonaqueous solutions”, *Chem. Rev.*, **76**, 717–726 (1976).
- [281] F. M. Floris, M. Selmi, A. Tani, and J. Tomasi, “Free energy and entropy for inserting cavities in water: Comparison of Monte Carlo simulation and scaled particle theory results”, *J. Chem. Phys.*, **107**, 6353–6365 (1997).
- [282] M. Cossi and N. Rega, “First and second derivatives of the free energy in solution”, in *Continuum Solvation Models in Chemical Physics*, B. Mennucci and R. Cammi, Eds.; Wiley: Chichester, UK, 2007; pages 313–322.
- [283] E. Gallicchio and R. M. Levy, “AGBNP: An analytic implicit solvent model suitable for molecular dynamics simulations and high-resolution modeling”, *J. Comput. Chem.*, **25**, 479–499 (2004).
- [284] T. Hou, J. Wang, Y. Li, and W. Wang, “Assessing the performance of the MM/PBSA and MM/GBSA methods. 1. The accuracy of binding free energy calculations based on molecular dynamics simulations”, *J. Chem. Inf. Model.*, **51**, 69–82 (2011).
- [285] T. Hou, J. Wang, Y. Li, and W. Wang, “Assessing the performance of the molecular mechanics/Poisson Boltzmann surface area and molecular mechanics/generalized Born surface area methods. II. The accuracy of ranking poses generated from docking”, *J. Comput. Chem.*, **32**, 866–877 (2011).
- [286] L. Xu, H. Sun, Y. Li, J. Wang, and T. Hou, “Assessing the performance of MM/PBSA and MM/GBSA methods. 3. The impact of force fields and ligand charge models”, *J. Phys. Chem. B*, **117**, 8408–8421 (2013).
- [287] H. Sun, Y. Li, M. Shen, S. Tian, L. Xu, P. Pan, Y. Guan, and T. Hou, “Assessing the performance of MM/PBSA and MM/GBSA methods. 5. Improved docking performance using high solute dielectric constant MM/GBSA and MM/PBSA rescoring”, *Phys. Chem. Chem. Phys.*, **16**, 22035–22045 (2014).

- [288] H. Sun, Y. Li, S. Tian, L. Xu, and T. Hou, “Assessing the performance of MM/PBSA and MM/GBSA methods. 4. Accuracies of MM/PBSA and MM/GBSA methodologies evaluated by various simulation protocols using PDBbind data set”, *Phys. Chem. Chem. Phys.*, **16**, 15719–16729 (2014).
- [289] F. Chen, H. Liu, H. Sun, P. Pan, Y. Li, D. Li, and T. Hou, “Assessing the performance of the MM/PBSA and MM/GBSA methods. 6. Capability to predict protein–protein binding free energies and re-rank binding poses generated by protein–protein docking”, *Phys. Chem. Chem. Phys.*, **18**, 22129–22139 (2016).
- [290] H. Sun, L. Duan, F. Chen, H. Liu, Z. Wang, P. Pan, F. Zhu, J. Z. H. Zhang, and T. Hou, “Assessing the performance of MM/PBSA and MM/GBSA methods. 7. Entropy effects on the performance of end-point binding free energy calculation approaches”, *Phys. Chem. Chem. Phys.*, **20**, 14450–14460 (2018).
- [291] G. Weng, E. Wang, F. Chen, H. Sun, Z. Wang, and T. Hou, “Assessing the performance of MM/PBSA and MM/GBSA methods. 9. Prediction of reliability of binding affinities and binding poses for protein–peptide complexes”, *Phys. Chem. Chem. Phys.*, **21**, 10135–10145 (2019).
- [292] E. Wang, G. Weng, H. Sun, H. Du, F. Zhu, F. Chen, Z. Wang, and T. Hou, “Assessing the performance of the MM/PBSA and MM/GBSA methods. 10. Impacts of enhanced sampling and variable dielectric model on protein–protein interactions”, *Phys. Chem. Chem. Phys.*, **21**, 18958–18969 (2019).
- [293] C. Wang, D. Greene, L. Xiao, R. Qi, and R. Luo, “Recent developments and applications of the MMPBSA method”, *Front. Mol. Biosci.*, **4**, 87:1–18 (2018).
- [294] S. Genheden and U. Ryde, “The MM/PBSA and MM/GBSA methods to estimate ligand-binding affinities”, *Expert Opin. Drug Dis.*, **10**, 449–461 (2015).
- [295] E. Wang, H. Sun, J. Wang, Z. Wang, H. Liu, J. Z. H. Zhang, and T. Hou, “End-point binding free energy calculation with MM/PBSA and MM/GBSA: Strategies and applications in drug design”, *Chem. Rev.*, **119**, 9478–9508 (2019).
- [296] G. Poli, C. Granchi, F. Rizzolio, and T. Tuccinardi, “Applications of MM-PBSA methods in virtual screening”, *Molecules*, **25**, 1971:1–19 (2020).
- [297] J. Li, T. Zhu, C. J. Cramer, and D. G. Truhlar, “New class IV charge model for extracting accurate partial charges from wave functions”, *J. Phys. Chem. A*, **102**, 1820–1831 (1998).
- [298] P. Winget, J. D. Thompson, J. D. Xidos, C. J. Cramer, and D. G. Truhlar, “Charge model 3: A class IV charge model based on hybrid density functional theory with variable exchange”, *J. Phys. Chem. A*, **106**, 10707–10717 (2002).
- [299] R. M. Olson, A. V. Marenich, C. J. Cramer, and D. G. Truhlar, “Charge model 4 and intramolecular charge polarization”, *J. Chem. Theory Comput.*, **3**, 2046–2054 (2007).
- [300] A. V. Marenich, S. V. Jerome, C. J. Cramer, and D. G. Truhlar, “Charge model 5: An extension of Hirshfeld population analysis for the accurate description of molecular interactions in gaseous and condensed phases”, *J. Chem. Theory Comput.*, **8**, 527–541 (2012).

- [301] E. R. Davidson and S. Chakravorty, “A test of the Hirshfeld definition of atomic charges and moments”, *Theor. Chem. Acc.*, **83**, 319–330 (1992).
- [302] M. H. Abraham, “Scales of solute hydrogen-bonding: Their construction and application to physicochemical and biochemical processes”, *Chem. Soc. Rev.*, **22**, 73–83 (1993).
- [303] A. C. Chamberlin, C. J. Cramer, and D. G. Truhlar, “Predicting aqueous free energies of solvation as functions of temperature”, *J. Phys. Chem. B*, **110**, 5665–5675 (2006).
- [304] A. C. Chamberlin, C. J. Cramer, and D. G. Truhlar, “Extension of a temperature-dependent aqueous solvation model to compounds containing nitrogen, fluorine, chlorine, bromine, and sulfur”, *J. Phys. Chem. B*, **112**, 3024–3039 (2008).
- [305] J. C. Dearden, “Partitioning and lipophilicity in quantitative structure–activity relationships”, *Environ. Health Persp.*, **61**, 203–228 (1985).
- [306] S. Amézqueta, X. Subirats, E. Fuguet, M. Rosés, and C. Ràfols, “Octanol–water partition constant”, in *Liquid-Phase Extraction*, C. F. Poole, Ed.; Elsevier: Amsterdam, 2020; chapter 6, pages 183–208.
- [307] T. Ginex, J. Vazquez, E. Gilbert, E. Herrero, and F. J. Luque, “Lipophilicity in drug design: An overview of lipophilicity descriptors in 3D-QSAR studies”, *Future Med. Chem.*, **11**, 1177–1193 (2019).
- [308] S. Sahoo, C. Adhikari, M. Kuanar, and B. K. Mishra, “A short review of the generation of molecular descriptors and their applications in quantitative structure property/activity relationships”, *Curr. Comput. Aided Drug Des.*, **12**, 181–205 (2016).
- [309] F. Tsopelas, C. Giaginis, and A. Tsantili-Kakoulidou, “Lipophilicity and biomimetic properties to support drug discovery”, *Expert Opin. Drug Dis.*, **12**, 885–896 (2017).
- [310] J. L. M. Hermens, J. H. M. de Brujin, and D. N. Brooke, “The octanol–water partition coefficient: Strengths and limitations”, *Environ. Toxicol. Chem.*, **32**, 732–733 (2013).
- [311] M. Işık, T. D. Bergazin, T. Fox, A. Rizzi, J. D. Chodera, and D. L. Mobley, “Assessing the accuracy of octanol–water partition coefficient predictions in the SAMPL6 part II $\log P$ challenge”, *J. Comput.-Aided Mol. Des.*, **34**, 335–370 (2020).
- [312] J. A. Ouimet and A. S. Paluch, “Predicting octanol/water partition coefficients for the SAMPL6 challenge using the SM12, SM8, and SMD solvation models”, *J. Comput.-Aided Mol. Des.*, **34**, 575–588 (2020).
- [313] J. R. Pliego Jr. and J. M. Riveros, “Gibbs energy of solvation of organic ions in aqueous and dimethyl sulfoxide solutions”, *Phys. Chem. Chem. Phys.*, **4**, 1622–1627 (2002).
- [314] C. Amovilli, “Calculation of the dispersion energy contribution to the solvation free energy”, *Chem. Phys. Lett.*, **229**, 244–249 (1994).
- [315] C. Amovilli and B. Mennucci, “Self-consistent-field calculation of Pauli repulsion and dispersion contributions to the solvation free energy in the polarizable continuum model”, *J. Phys. Chem. B*, **101**, 1051–1057 (1997).
- [316] V. Weijo, B. Mennucci, and L. Frediani, “Toward a general formulation of dispersion effects for solvation continuum models”, *J. Chem. Theory Comput.*, **6**, 3358–3364 (2010).

- [317] L. Cupellini, C. Amovilli, and B. Mennucci, “Electronic excitations in nonpolar solvents: Can the polarizable continuum model accurately reproduce solvent effects?”, *J. Phys. Chem. B*, **119**, 8984–8991 (2015).
- [318] A. Pomogaeva, D. W. Thompson, and D. M. Chipman, “Modeling short-range contributions to hydration energies with minimal parameterization”, *Chem. Phys. Lett.*, **511**, 161–165 (2011).
- [319] A. Pomogaeva and D. M. Chipman, “Field-extremum model for short-range contributions to hydration free energy”, *J. Chem. Theory Comput.*, **7**, 3952–3960 (2011).
- [320] A. Pomogaeva and D. M. Chipman, “New implicit solvation models for dispersion and exchange energies”, *J. Phys. Chem. A*, **117**, 5812–5820 (2013).
- [321] A. Pomogaeva and D. M. Chipman, “Hydration energy from a composite method for implicit representation of the solvent”, *J. Chem. Theory Comput.*, **10**, 211–219 (2014).
- [322] A. Pomogaeva and D. M. Chipman, “Composite method for implicit representation of solvent in dimethyl sulfoxide and acetonitrile”, *J. Phys. Chem. A*, **119**, 5173–5180 (2015).
- [323] T. T. Duignan, D. F. Parsons, and B. W. Ninham, “A continuum solvent model of the multipolar dispersion solvation energy”, *J. Phys. Chem. B*, **117**, 9412–9420 (2013).
- [324] T. T. Duignan, D. F. Parsons, and B. W. Ninham, “A continuum model of solvation energies including electrostatic, dispersion, and cavity contributions”, *J. Phys. Chem. B*, **117**, 9421–9429 (2013).
- [325] M.-J. Huron and P. Claverie, “Calculation of the interaction energy of one molecule with its whole surrounding. I. Method and application to pure nonpolar compounds”, *J. Phys. Chem.*, **76**, 2123–2133 (1972).
- [326] F. Floris and J. Tomasi, “Evaluation of the dispersion contribution to the solvation energy. A simple computational model in the continuum approximation”, *J. Comput. Chem.*, **10**, 616–627 (1989).
- [327] F. M. Floris, J. Tomasi, and J. L. P. Ahuir, “Dispersion and repulsion contributions to the solvation energy: Refinements to a simple computational model in the continuum approximation”, *J. Comput. Chem.*, **12**, 784–791 (1991).
- [328] F. M. Floris, A. Tani, and J. Tomasi, “Evaluation of dispersion–repulsion contributions to the solvation energy. Calibration of the uniform approximation with the aid of RISM calculations”, *Chem. Phys.*, **169**, 11–20 (1993).
- [329] T. N. Truong, “Quantum modelling of reactions in solution: An overview of the dielectric continuum methodology”, *Int. Rev. Phys. Chem.*, **17**, 525–546 (1998).
- [330] A. D. McLachlan, “Retarded dispersion forces between molecules”, *Proc. R. Soc. Lond. A*, **271**, 387–401 (1963).
- [331] R. McWeeny, “Weak interactions between molecules”, *Croatica Chem. Acta*, **57**, 865–878 (1984).
- [332] M. Jaszunski and R. McWeeny, “Time-dependent Hartree–Fock calculations of dispersion energy”, *Mol. Phys.*, **55**, 1275–1286 (1985).

- [333] R. McWeeny, “Electron density and response theory”, *J. Mol. Struct. (Theochem)*, **123**, 231–242 (1985).
- [334] C. Amovilli and M. McWeeny, “A matrix partitioning approach to the calculation of intermolecular potentials. General theory and some examples”, *Chem. Phys.*, **140**, 343–361 (1990).
- [335] R. McWeeny, *Methods of Molecular Quantum Mechanics*, Academic Press: New York, 2nd ed., 1992.
- [336] K. T. Tang, “Dynamic polarizabilities and van der Waals coefficients”, *Phys. Rev.*, **177**, 108–114 (1969).
- [337] P. W. Langhoff and M. Karplus, “Application of Padé approximants to dispersion force and optical polarizability computations”, in *The Padé Approximant in Theoretical Physics*, G. A. Baker Jr. and J. L. Gammel, Eds., Vol. 71 of *Mathematics in Science and Engineering*; Academic Press: New York, 1970; chapter 2, pages 41–97.
- [338] A. Szabo and N. S. Ostlund, “The correlation energy in the random phase approximation: Intermolecular forces between closed-shell systems”, *J. Chem. Phys.*, **67**, 4351–4360 (1977).
- [339] I. G. Kaplan and O. B. Rodimova, “Intermolecular interactions”, *Sov. Phys. Usp.*, **21**, 918–943 (1978).
- [340] S. Y. Buhmann and D.-G. Welsch, “Dispersion forces in macroscopic quantum electrodynamics”, *Prog. Quantum Electron.*, **31**, 51–130 (2007).
- [341] F. London, “Zur Theorie und Systematik der Molekularkräfte”, *Z. Phys.*, **63**, 245–279 (1930).
- [342] H. C. Longuet-Higgins, “Intermolecular forces”, *Discuss. Faraday Soc.*, **40**, 7–18 (1965).
- [343] P. Norman and K. Ruud, “Microscopic theory of nonlinear optics”, in *Non-Linear Optical Properties of Matter*, M. G. Papadopoulos, A. J. Sadlej, and J. Leszczynski, Eds., Vol. 1 of *Challenges and Advances in Computational Chemistry and Physics*; Springer: Dordrecht, 2006; chapter 1, pages 1–49.
- [344] I. E. Dyzaloshinskii, E. M. Lifshitz, and L. P. Pitaevskii, “The general theory of van der Waals forces”, *Adv. Phys.*, **10**, 165–209 (1961).
- [345] E. Zaremba and W. Kohn, “Van der Waals interaction between an atom and a solid surface”, *Phys. Rev. B*, **13**, 2270–2285 (1976).
- [346] V. A. Parsegian, *Van der Waals Forces: A Handbook for Biologists, Chemists, Engineers, and Physicists*, Cambridge University Press: New York, 2006.
- [347] O. A. Vydrov and T. Van Voorhis, “Improving the accuracy of the nonlocal van der Waals density functional with minimal empiricism”, *J. Chem. Phys.*, **130**, 104105:1–7 (2009).
- [348] O. A. Vydrov and T. Van Voorhis, “Nonlocal van der Waals density functional theory made simple”, *Phys. Rev. Lett.*, **103**, 063004:1–4 (2009).
- [349] O. A. Vydrov and T. Van Voorhis, “Nonlocal van der Waals density functional: The simpler the better”, *J. Chem. Phys.*, **133**, 244103:1–9 (2010).

- [350] O. A. Vydrov and T. Van Voorhis, “Nonlocal van der Waals density functionals based on local response models”, in *Fundamentals of Time-Dependent Density Functional Theory*, M. A. L. Marques, N. T. Maitra, F. M. S. Nogueira, E. K. U. Gross, and A. Rubio, Eds., Vol. 837 of *Lecture Notes in Physics*; Springer-Verlag: Berlin, 2012; chapter 23, pages 443–456.
- [351] J. Calbo, E. Ortí, J. C. Sancho-García, and J. Aragó, “The nonlocal correlation density function VV10: A successful attempt to accurately capture noncovalent interactions”, *Annu. Rep. Comput. Chem.*, **11**, 37–102 (2015).
- [352] D. C. Langreth, M. Dion, H. Rydberg, E. Schröder, P. Hyldgaard, and B. I. Lundqvist, “Van der Waals density functional theory with applications”, *Int. J. Quantum Chem.*, **101**, 599–610 (2005).
- [353] M. Dion, H. Rydberg, E. Schröder, D. C. Langreth, and B. I. Lundqvist, “Van der Waals density functional for general geometries”, *Phys. Rev. Lett.*, **92**, 246401:1–4 (2004).
- [354] D. C. Langreth, B. I. Lundqvist, S. D. Chakarova-Käck, V. R. Cooper, M. Dion, P. Hyldgaard, A. Kelkkanen, J. Kleis, L. Kong, S. Li, P. G. Moses, E. Murray, A. Puzder, H. Rydberg, E. Schröder, and T. Thonhauser, “A density functional for sparse matter”, *J. Phys.: Condens. Matt.*, **21**, 084203:1–15 (2009).
- [355] K. Lee, É. D. Murray, L. Kong, B. I. Lundqvist, and D. C. Langreth, “Higher-accuracy van der Waals density functional”, *Phys. Rev. B*, **82**, 081101:1–4 (2010).
- [356] C. Herring and M. Flicker, “Asymptotic exchange coupling of two hydrogen atoms”, *Phys. Rev.*, **134**, A362–A366 (1964).
- [357] R. Cammi, V. Verdolino, B. Mennucci, and J. Tomasi, “Towards the elaboration of a QM method to describe molecular solutes under the effect of a very high pressure”, *Chem. Phys.*, **344**, 135–141 (2008).
- [358] R. Cammi, C. Cappelli, B. Mennucci, and J. Tomasi, “Calculation and analysis of the harmonic vibrational frequencies in molecules at extreme pressure: Methodology and diborane as a test case”, *J. Chem. Phys.*, **137**, 154112:1–16 (2012).
- [359] B. Chen, R. Hoffmann, and R. Cammi, “The effect of pressure on organic reactions in fluids—a new theoretical perspective”, *Angew. Chem. Int. Ed. Engl.*, **56**, 11126–11142 (2017).
- [360] R. Cammi, “Quantum chemistry at the high pressures: The eXtreme pressure polarizable continuum model (XP-PCM)”, in *Frontiers of Quantum Chemistry*, M. J. Wójcik, H. Nakatsuji, B. Kirtman, and Y. Ozaki, Eds.; Springer Nature: Singapore, 2018; chapter 12, pages 273–288.
- [361] C. J. Fecko, J. D. Eaves, J. J. Loparo, A. Tokmakoff, and P. L. Geissler, “Ultrafast hydrogen-bond dynamics in the infrared spectroscopy of water”, *Science*, **301**, 1698–1702 (2003).
- [362] S. A. Corcelli, C. P. Lawrence, and J. L. Skinner, “Combined electronic structure/molecular dynamics approach for ultrafast infrared spectroscopy of dilute HOD in liquid H₂O and D₂O”, *J. Chem. Phys.*, **120**, 8107–8117 (2004).
- [363] J. D. Smith, C. D. Cappa, K. R. Wilson, R. C. Cohen, P. L. Geissler, and R. J. Saykally, “Unified description of temperature-dependent hydrogen-bond rearrangements in liquid water”, *Proc. Natl. Acad. Sci. USA*, **102**, 14171–14174 (2005).

- [364] N. M. Silva, P. Deglmann, and J. R. Pliego, Jr., “CMIRS solvation model for methanol: Parameterization, testing, and comparison with SMD, SM8, and COSMO-RS”, *J. Phys. Chem. B*, **120**, 12660–12668 (2016).
- [365] S. He, F. Biedermann, N. Vankova, L. Zhechkov, T. Heine, R. E. Hoffman, A. De Simone, T. T. Duignan, and W. M. Nau, “Cavitation energies can outperform dispersion interactions”, *Nat. Chem.*, **10**, 1252–1257 (2018).
- [366] N. Ansari, A. Laio, and A. Hassanali, “Spontaneously forming dendritic voids in liquid water can host small polymers”, *J. Phys. Chem. Lett.*, **10**, 5585–5591 (2019).
- [367] C. J. F. Böttcher and P. Bordewijk, *Theory of Electric Polarization*, Vol. 2, Elsevier: Amsterdam, 1978.
- [368] W. E. Vaughan, “Dielectric relaxation”, *Annu. Rev. Phys. Chem.*, **30**, 103–124 (1979).
- [369] Y. Feldman, A. Puzenko, and Y. Ryabov, “Dielectric relaxation phenomena in complex materials”, *Adv. Chem. Phys.*, **133**, 1–125 (2006).
- [370] Y. Feldman, P. B. Ishai, A. Puzenko, and V. Raicu, “Elementary theory of the interaction of electromagnetic fields with dielectric materials”, in *Dielectric Relaxation in Biological Systems*, V. Raicu and Y. Feldman, Eds.; Oxford University Press: Oxford, first ed., 2015; pages 33–59.
- [371] U. Kaatze, “Complex permittivity of water as a function of frequency and temperature”, *J. Chem. Eng. Data*, **34**, 371–374 (1989).
- [372] U. Kaatze, “Dielectric spectroscopy of aqueous solutions. Hydration phenomena and hydrogen-bonded networks”, *J. Mol. Liq.*, **56**, 95–115 (1993).
- [373] U. Kaatze, “Dielectric relaxation of water”, in *Dielectric Relaxation in Biological Systems*, V. Raicu and Y. Feldman, Eds.; Oxford University Press: Oxford, first ed., 2015; pages 189–227.
- [374] C.-P. Hsu, X. Song, and R. A. Marcus, “Time-dependent Stokes shift and its calculation from solvent dielectric dispersion data”, *J. Phys. Chem. B*, **101**, 2546–2551 (1997).
- [375] F. Ingrosso, B. Mennucci, and J. Tomasi, “Quantum mechanical calculations coupled with a dynamical continuum model for the description of dielectric relaxation: Time dependent Stokes shift of coumarin C153 in polar solvents”, *J. Mol. Liq.*, **108**, 21–46 (2003).
- [376] M. Caricato, B. Mennucci, J. Tomasi, F. Ingrosso, R. Cammi, S. Corni, and G. Scalmani, “Formation and relaxation of excited states in solution: A new time dependent polarizable continuum model based on time dependent density functional theory”, *J. Chem. Phys.*, **124**, 124520:1–13 (2006).
- [377] F. Ding, D. B. Lingerfelt, B. Mennucci, and X. Li, “Time-dependent non-equilibrium dielectric response in QM/continuum approaches”, *J. Chem. Phys.*, **142**, 034120:1–8 (2015).
- [378] A. Wildman, G. Donati, F. Lippalini, B. Mennucci, and X. Li, “Nonequilibrium environment dynamics in a frequency-dependent polarizable embedding model”, *J. Chem. Theory Comput.*, **15**, 43–51 (2019).

- [379] P. J. W. Debye, *Polar Molecules*, The Chemical Catalog Company: New York, 1929.
- [380] J. J. Goings, P. J. Lestrange, and X. Li, “Real-time time-dependent electronic structure theory”, *WIREs Comput. Mol. Sci.*, **8**, e1341:1–19 (2018).
- [381] X. Li, N. Govind, C. Isborn, A. E. DePrince III, and K. Lopata, “Real-time time-dependent electronic structure theory”, *Chem. Rev.*, **120**, 9951–9993 (2020).
- [382] J. Mistrik, S. Kasap, H. E. Ruda, C. Koughia, and J. Singh, “Optical properties of electronic materials: Fundamentals and characterization”, in *Springer Handbook of Electronic and Photonic Materials*, S. Kasap and P. Capper, Eds.; Springer International Publishing: Cham, Switzerland, 2017; chapter 3, pages 47–83.
- [383] C. Wohlfarth and B. Wohlfarth, *Refractive Indices of Organic Liquids*, Vol. 38B of *Group III Condensed Matter*, Landolt-Börnstein, Springer-Verlag: Berlin, 1996.
- [384] G. M. Hale and M. R. Querry, “Optical constants of water in the 200-nm to 200- μ m wavelength region”, *Appl. Opt.*, **12**, 555–563 (1973).
- [385] M. Cossi and V. Barone, “Separation between fast and slow polarizations in continuum solvation models”, *J. Phys. Chem. A*, **104**, 10614–10622 (2000).
- [386] M. Dinpajoh, M. D. Newton, and D. V. Matyushov, “Free energy functionals for polarization fluctuations: Pekar factor revisited”, *J. Chem. Phys.*, **146**, 064504:1–18 (2017).
- [387] C. H. Collie, J. B. Hasted, and D. M. Ritson, “The dielectric properties of water and heavy water”, *Proc. Phys. Soc.*, **60**, 145–160 (1948).
- [388] C. Rønne, L. Thrane, P.-O. Åstrand, A. Wallqvist, K. V. Mikkelsen, and S. R. Keiding, “Investigation of the temperature dependence of dielectric relaxation in liquid water by THz reflection spectroscopy and molecular dynamics simulation”, *J. Chem. Phys.*, **107**, 5319–5331 (1997).
- [389] C. Rønne and S. R. Keiding, “Low frequency spectroscopy of liquid water using THz-time domain spectroscopy”, *J. Mol. Liq.*, **101**, 199–218 (2002).
- [390] M. Nagai, H. Yada, T. Arikawa, and K. Tanaka, “Terahertz time-domain attenuated total reflection spectroscopy in water and biological solution”, *Int. J. Infrared Milli.*, **27**, 505–515 (2006).
- [391] J. Zhou, X. Rao, X. Liu, T. Li, L. Zhou, Y. Zheng, and Z. Zhu, “Temperature dependent optical and dielectric properties of liquid water studied by terahertz time-domain spectroscopy”, *AIP Adv.*, **9**, 035346:1–7 (2019).
- [392] I. Popov, P. B. Ishai, A. Khamzin, and Y. Feldman, “The mechanism of the dielectric relaxation of water”, *Phys. Chem. Chem. Phys.*, **18**, 13941–13953 (2016).
- [393] D. C. Elton, “The origin of the Debye relaxation in liquid water and fitting the high frequency excess response”, *Phys. Chem. Chem. Phys.*, **19**, 18739–18749 (2017).
- [394] U. Kaatze and V. Uhlendorf, “The dielectric properties of water at microwave frequencies”, *Z. Phys. Chem. Neue Folge*, **126**, 151–165 (1981).

- [395] C. Wohlfarth, *Static Dielectric Constants of Pure Liquids and Binary Liquid Mixtures*, Vol. 6 of *Landolt-Börnstein, New Series IV*, Springer Science + Business Media, 1991.
- [396] L. W. Tilton and J. K. Taylor, “Refractive index and dispersion of distilled water for visible radiation, at temperatures 0 to 60° C”, *J. Res. Nat. Bur. Stand.*, **20**, 419–477 (1938).
- [397] C. Kittel, *Introduction to Solid State Physics*, John Wiley & Sons: Hoboken, 8th ed., 2005.
- [398] S. H. Wemple, M. Didomenico Jr., and I. Camlibel, “Dielectric and optical properties of melt-grown BaTiO₃”, *J. Phys. Chem. Solids*, **29**, 1797–1803 (1968).
- [399] N. Mataga, Y. Kaifu, and M. Koizumi, “Solvent effects upon fluorescence spectra and the dipole moments of excited molecules”, *Bull. Chem. Soc. Jpn.*, **29**, 465–470 (1956).
- [400] E. Lippert, “Spektroskopische Bestimmung des Dipolmomentes aromatischer Verbindungen im ersten angeregten Singulettzustand”, *Z. Electrochem.*, **61**, 962–975 (1957).
- [401] N. Mataga, H. Chosrowjan, and S. Taniguchi, “Ultrafast charge transfer in excited electronic states and investigations into fundamental problems of exciplex chemistry: Our early studies and recent developments”, *J. Photoch. Photobio. C*, **6**, 37–79 (2005).
- [402] N. S. Bayliss, “The effect of the electrostatic polarization of the solvent on electronic absorption spectra in solution”, *J. Chem. Phys.*, **18**, 292–296 (1950).
- [403] Y. Ooshika, “Absorption spectra of dyes in solution”, *J. Phys. Soc. Jpn.*, **9**, 594–602 (1954).
- [404] E. G. McRae, “Theory of solvent effects on molecular electronic spectra. Frequency shifts”, *J. Phys. Chem.*, **61**, 562–572 (1957).
- [405] L. Bilot and A. Kawski, “Zue Theorie des Einflusses von Lösungsmitteln auf die Electronenspektren der Moleküle”, *Z. Naturforsch. A*, **17**, 621–627 (1962).
- [406] N. G. Bakshiev, “Universal intermolecular interactions and their effect on the position of the electronic spectra of molecules in two component solutions”, *Opt. Spectrosc.*, **16**, 821–832 (1964).
- [407] W. Liptay, “Dipole moments of molecules in excited states and the effect of external electric fields on the optical absorption of molecules in solution”, in *Modern Quantum Chemistry: Istanbul Lectures. Part III. Action of Light and Organic Crystals*, O. Sinanoğlu, Ed.; Academic Press: New York, 1965; pages 45–66.
- [408] T. Abe, “Theory of solvent effects on molecular electronic spectra. Frequency shifts”, *Bull. Chem. Soc. Jpn.*, **38**, 1314–1318 (1965).
- [409] A. Chamma and P. Viallet, “Determination du moment dipolaire d'une molecule dans un etat excite singulet”, *Sci. Paris Ser. C*, **270**, 1901–1904 (1970).
- [410] J. E. Brady and P. W. Carr, “An analysis of dielectric models of solvatochromism”, *J. Phys. Chem.*, **89**, 5759–5766 (1985).
- [411] M. Józefowicz, P. Milart, and J. R. Heldt, “Determination of ground and excited state dipole moments of 4,5'-diamino[1,1':3',1''-terphenyl]-4',6'-dicarbonitrile using solvatochromic method and quantum-chemical calculations”, *Spectrochim. Acta A*, **74**, 959–963 (2009).

- [412] R. Siddlingeshwar and S. M. Hanagodimath, “Estimation of the ground and the first excited singlet-state dipole moments of 1,4-disubstituted anthraquinone dyes by the solvatochromic method”, *Spectrochim. Acta A*, **75**, 1203–1210 (2010).
- [413] S. R. Manohara, V. U. Kumar, Shivakumaraiah, and G. Gerward, “Estimation of ground and excited-state dipole moments of 1,2-diazines by solvatochromic method and quantum-chemical calculation”, *J. Mol. Liq.*, **181**, 97–104 (2013).
- [414] E. G. Demissie, E. T. Mengesha, and G. W. Woyessa, “Modified solvatochromic equations for better determination of ground and excited state dipole moments of *p*-aminobenzoic acid (PABA): Accounting for real shape over hypothetical spherical solvent shell”, *J. Photochem. Photobiol. A*, **337**, 184–191 (2017).
- [415] R. Kumari, A. Varghese, L. George, and Y. N. Sudhaker, “Effect of solvent polarity on the photophysical properties of chalcone derivatives”, *RSC Adv.*, **7**, 24204:1–11 (2017).
- [416] C. G. Renuka, Y. F. Nadaf, G. Sripakash, and S. R. Prasad, “Solvent dependence on structure and electronic properties of 7-(diethylamino)-2H-1-benzopyran-2-one (C-466) laser dye”, *J. Fluoresc.*, **28**, 839–854 (2018).
- [417] V. M. Divac, D. Šakić, T. Weitner, and M. Gabrićević, “Solvent effects on the absorption and fluorescence spectra of Zaleplon: Determination of ground and excited state dipole moments”, *Spectrochim. Acta A*, **212**, 356–362 (2019).
- [418] R. A. Marcus, “On the theory of oxidation-reduction reactions involving electron transfer. I.”, *J. Chem. Phys.*, **24**, 966–978 (1956).
- [419] R. A. Marcus, “Chemical and electrochemical electron-transfer theory”, *Annu. Rev. Phys. Chem.*, **15**, 155–196 (1964).
- [420] R. A. Marcus and N. Sutin, “Electron transfers in chemistry and biology”, *Biochim. Biophys. Acta*, **811**, 265–322 (1985).
- [421] M. D. Newton, “The role of solvation in electron transfer: Theoretical and computational aspects”, in *Continuum Solvation Models in Chemical Physics*, B. Mennucci and R. Cammi, Eds.; Wiley: Chichester, UK, 2007; pages 389–413.
- [422] X.-Y. Li, “An overview of continuum models for nonequilibrium solvation: Popular theories and new challenge”, *Int. J. Quantum Chem.*, **115**, 700–721 (2015).
- [423] C.-P. Hsu, “Reorganization energies and spectral densities for electron transfer problems in charge transporting materials”, *Phys. Chem. Chem. Phys.*, **22**, 21630–21641 (2020).
- [424] C. J. Cramer and D. G. Truhlar, “Implicit solvation models: Equilibria, structure, spectra, and dynamics”, *Chem. Rev.*, **99**, 2161–2200 (1999).
- [425] H. J. Kim and J. T. Hynes, “Equilibrium and nonequilibrium solvation and solute electronic structure. I. Formulation”, *J. Chem. Phys.*, **93**, 5194–5210 (1990).
- [426] M. A. Aguilar, F. J. Olivares del Valle, and J. Tomasi, “Nonequilibrium solvation: An *ab initio* quantum-mechanical method in the continuum cavity model approximation”, *J. Chem. Phys.*, **98**, 7375–7384 (1993).

- [427] B. Mennucci, “Continuum models for excited states”, in *Continuum Solvation Models in Chemical Physics*, B. Mennucci and R. Cammi, Eds.; Wiley: Chichester, UK, 2007; pages 110–123.
- [428] C. A. Guido and S. Caprasecca, “On the description of the environment polarization response to electronic transitions”, *Int. J. Quantum Chem.*, **119**, e25711:1–11 (2019).
- [429] B. Mennucci, R. Cammi, and J. Tomasi, “Excited states and solvatochromatic shifts within a nonequilibrium solvation approach: A new formulation of the integral equation formalism method at the self-consistent field, configuration interaction, and multiconfiguration self-consistent field level”, *J. Chem. Phys.*, **109**, 2798–2807 (1998).
- [430] M. Cossi and V. Barone, “Solvent effect on vertical electronic transitions by the polarizable continuum model”, *J. Chem. Phys.*, **112**, 2427–2435 (2000).
- [431] D. M. Chipman, “Vertical electronic excitation with a dielectric continuum model of solvation including volume polarization. I. Theory”, *J. Chem. Phys.*, **131**, 014103:1–10 (2009).
- [432] J.-M. Mewes, Z.-Q. You, M. Wormit, T. Kriesche, J. M. Herbert, and A. Dreuw, “Experimental benchmark data and systematic evaluation of two *a posteriori*, polarizable-continuum corrections for vertical excitation energies in solution”, *J. Phys. Chem. A*, **119**, 5446–5464 (2015).
- [433] J.-M. Mewes, J. M. Herbert, and A. Dreuw, “On the accuracy of the general, state-specific polarizable-continuum model for the description of correlated ground- and excited states in solution”, *Phys. Chem. Chem. Phys.*, **19**, 1644–1654 (2017).
- [434] M. P. Coons, Z.-Q. You, and J. M. Herbert, “The hydrated electron at the surface of neat liquid water appears to be indistinguishable from the bulk species”, *J. Am. Chem. Soc.*, **138**, 10879–10886 (2016).
- [435] R. Cammi and J. Tomasi, “Nonequilibrium solvation theory for the polarizable continuum model: A new formulation at the SCF level with application to the case of the frequency-dependent linear electric response function”, *Int. J. Quantum Chem. Symp.*, **29**, 465–474 (1995).
- [436] M. A. Aguilar, “Separation of the electric polarization into fast and slow components: A comparison of two partition schemes”, *J. Phys. Chem. A*, **105**, 10393–10396 (2001).
- [437] S. I. Pekar, *Untersuchungen über die Elektronentheorie der Kristalle*, Akademie-Verlag: Berlin, 1954.
- [438] S. I. Pekar “Research in Electron Theory of Crystals” Technical Report AEC-tr-5575, U.S. Atomic Energy Commission, Division of Technical Information, (1963).
- [439] N. S. Bayliss and E. G. McRae, “Solvent effects in organic spectra: Dipole forces and the Franck-Condon principle”, *J. Phys. Chem.*, **58**, 1002–1006 (1954).
- [440] M. V. Basilevsky and G. E. Chudinov, “Dynamics of charge transfer chemical reactions in a polar medium within the scope of the Born-Kirkwood-Onsager model”, *Chem. Phys.*, **157**, 327–344 (1991).

- [441] H. Houjou, M. Sakurai, and Y. Inoue, “Theoretical evaluation of medium effects on absorption maxima of molecular solutes. I. Formulation of a new method based on the self-consistent reaction field theory”, *J. Chem. Phys.*, **107**, 5652–5660 (1997).
- [442] R. Cammi, L. Frediani, B. Mennucci, J. Tomasi, K. Ruud, and K. V. Mikkelsen, “A second-order, quadratically convergent multiconfigurational self-consistent field polarizable continuum model for equilibrium and nonequilibrium solvation”, *J. Chem. Phys.*, **117**, 13–26 (2002).
- [443] A. V. Marenich, C. J. Cramer, D. G. Truhlar, C. A. Guido, B. Mennucci, G. Scalmani, and M. J. Frisch, “Practical computation of electronic excitation in solution: Vertical excitation model”, *Chem. Sci.*, **2**, 2143–2161 (2011).
- [444] L. D. Jacobson and J. M. Herbert, “A simple algorithm for determining orthogonal, self-consistent excited-state wave functions for a state-specific Hamiltonian: Application to the optical spectrum of the aqueous electron”, *J. Chem. Theory Comput.*, **7**, 2085–2093 (2011).
- [445] B. Lunkenheimer and A. Köhn, “Solvent effects on electronically excited states using the conductor-like screening model and the second-order correlated method ADC(2)”, *J. Chem. Theory Comput.*, **9**, 977–994 (2013).
- [446] B. Winter and M. Faubel, “Photoemission from liquid aqueous solutions”, *Chem. Rev.*, **106**, 1176–1211 (2006).
- [447] R. Seidel, S. Thürmer, and B. Winter, “Photoelectron spectroscopy meets aqueous solution: Studies from a vacuum liquid microjet”, *J. Phys. Chem. Lett.*, **2**, 633–641 (2011).
- [448] R. Seidel, B. Winter, and S. E. Bradforth, “Valence electronic structure of aqueous solutions: Insights from photoelectron spectroscopy”, *Annu. Rev. Phys. Chem.*, **67**, 283–305 (2016).
- [449] B. Winter, R. Weber, I. V. Hertel, M. Faubel, P. Jungwirth, E. C. Brown, and S. E. Bradforth, “Electron binding energies of aqueous alkali and halide ions: EUV photoelectron spectroscopy of liquid solutions and combined ab initio and molecular dynamics calculations”, *J. Am. Chem. Soc.*, **127**, 7203–7214 (2005).
- [450] L. D. Jacobson and J. M. Herbert, “A one-electron model for the aqueous electron that includes many-body electron-water polarization: Bulk equilibrium structure, vertical electron binding energy, and optical absorption spectrum”, *J. Chem. Phys.*, **133**, 154506:1–19 (2010).
- [451] D. Ghosh, O. Isayev, L. V. Slipchenko, and A. I. Krylov, “Effect of solvation on the vertical ionization energy of thymine: From microhydration to bulk”, *J. Phys. Chem. A*, **115**, 6028–6038 (2011).
- [452] D. Ghosh, A. Roy, R. Seidel, B. Winter, S. Bradforth, and A. I. Krylov, “First-principle protocol for calculating ionization energies and redox potentials of solvated molecules and ions: Theory and application to aqueous phenol and phenolate”, *J. Phys. Chem. B*, **116**, 7269–7280 (2012).
- [453] R. N. Tazhigulov, P. K. Gurunathan, Y. Kim, L. V. Slipchenko, and K. B. Bravaya, “Polarizable embedding for simulating redox potentials of biomolecules”, *Phys. Chem. Chem. Phys.*, **21**, 11642–11650 (2019).
- [454] Z. Tóth, J. Kubečka, E. Muchová, and P. Slaviček, “Ionization energies in solution with the QM:QM approach”, *Phys. Chem. Chem. Phys.*, **22**, 10550–10560 (2020).

- [455] M. R. Provorose, T. Peev, C. Xiong, and C. M. Isborn, “Convergence of excitation energies in mixed quantum and classical solvent: Comparison of continuum and point charge models”, *J. Phys. Chem. B*, **120**, 12148–12159 (2016). Erratum: *J. Phys. Chem. B*, **121**, 2372 (2017).
- [456] S. K. Paul, M. P. Coons, and J. M. Herbert, “Erratum: ‘Quantum chemistry in arbitrary dielectric environments: Theory and implementation of nonequilibrium Poisson boundary conditions and application to compute vertical ionization energies at the air/water interface’”, *J. Chem. Phys.*, **151**, 189901:1–2 (2019).
- [457] C. F. Perry, P. Zhang, F. B. Nunes, I. Jordan, A. von Conta, and H. J. Wörner, “Ionization energy of liquid water revisited”, *J. Phys. Chem. Lett.*, **11**, 1789–1794 (2020).
- [458] D. Luckhaus, Y. Yamamoto, T. Suzuki, and R. Signorell, “Genuine binding energy of the hydrated electron”, *Sci. Adv.*, **3**, e1603224:1–5 (2017).
- [459] J. M. Herbert, “Structure of the aqueous electron”, *Phys. Chem. Chem. Phys.*, **21**, 20538–20565 (2019).
- [460] A. Muñoz-Losa, D. Markovitsi, and R. Improta, “A state-specific PCM-DFT method to include dynamic solvent effects in the calculation of ionization energies: Application to DNA bases”, *Chem. Phys. Lett.*, **634**, 20–24 (2015).
- [461] S. K. Khani, A. M. Khah, and C. Hättig, “Comparison of reaction field schemes for coupling continuum solvation models with wave function methods for excitation energies”, *J. Chem. Theory Comput.*, **16**, 4554–4564 (2020).
- [462] M. A. Thompson and G. K. Schenter, “Excited states of the bacteriochlorophyll *b* dimer of *Rhodopseudomonas viridis*: A QM/MM study of the photosynthetic reaction center that includes MM polarization”, *J. Phys. Chem.*, **99**, 6374–6386 (1995).
- [463] R. Cammi, S. Corni, B. Mennucci, and J. Tomasi, “Electronic excitation energies of molecules in solution: State specific and linear response methods for nonequilibrium continuum solvation models”, *J. Chem. Phys.*, **122**, 104513:1–12 (2005).
- [464] R. Improta, V. Barone, G. Scalmani, and M. J. Frisch, “A state-specific polarizable continuum model time dependent density functional method for excited state calculations in solution”, *J. Chem. Phys.*, **125**, 054103:1–9 (2006).
- [465] R. Improta, G. Scalmani, M. J. Frisch, and V. Barone, “Toward effective and reliable fluorescence energies in solution by a new state specific polarizable continuum model time dependent density functional theory approach”, *J. Chem. Phys.*, **127**, 074504:1–9 (2007).
- [466] F. Furche and R. Ahlrichs, “Adiabatic time-dependent density functional methods for excited state properties”, *J. Chem. Phys.*, **117**, 7433–7447 (2002). Erratum, *J. Chem. Phys.*, **121**, 12772–12773 (2004).
- [467] E. Ronca, C. Angeli, L. Belpassi, F. De Angelis, F. Tarantelli, and M. Pastore, “Density relaxation in time-dependent density functional theory: Combining relaxed density natural orbitals and multireference perturbation theories for an improved description of excited states”, *J. Chem. Theory Comput.*, **10**, 4014–4024 (2014).

- [468] F. Maschietto, M. Campetella, M. J. Frisch, G. Scalmani, C. Adamo, and I. Ciofini, “How are the charge transfer descriptors affected by the quality of the underpinning electronic density?”, *J. Comput. Chem.*, **39**, 735–742 (2018).
- [469] B. Mennucci, C. Cappelli, C. A. Guido, R. Cammi, and J. Tomasi, “Structures and properties of electronically excited chromophores in solution from the polarizable continuum model coupled to the time-dependent density functional theory”, *J. Phys. Chem. A*, **113**, 3009–3020 (2009).
- [470] A. T. Amos and B. L. Burrows, “Solvent-shift effects on electronic spectra and excited-state dipole moments and polarizabilities”, *Adv. Quantum Chem.*, **7**, 289–313 (1973).
- [471] P. Suppan, “Solvent effects on the energy of electronic transitions: Experimental observations and applications to structural problems of excited molecules”, *J. Chem. Soc. A*, pages 3125–3133 (1968).
- [472] P. Suppan, “Polarizability of excited molecules from spectroscopic studies”, *Spectrochim. Acta A*, **24**, 1161–1165 (1968).
- [473] A. T. Amos and B. L. Burrows, “Dispersion interactions and solvent-shift effects”, *Theor. Chem. Acc.*, **29**, 139–150 (1973).
- [474] A. V. Marenich, C. J. Cramer, and D. G. Truhlar, “Uniform treatment of solute–solvent dispersion in the ground and excited electronic states of the solute based on a solvation model with state-specific polarizability”, *J. Chem. Theory Comput.*, **9**, 3649–3659 (2013).
- [475] A. V. Marenich, C. J. Cramer, and D. G. Truhlar, “Electronic absorption spectra and solvatochromic shifts by the vertical excitation model: Solvated clusters and molecular dynamics sampling”, *J. Phys. Chem. B*, **119**, 958–967 (2015).
- [476] D. Jacquemin, A. Planchat, C. Adamo, and B. Mennucci, “TD-DFT assessment of functionals for optical 0–0 transitions in solvated dyes”, *J. Chem. Theory Comput.*, **8**, 2359–2372 (2012).
- [477] F. J. Olivares del Valle and J. Tomasi, “Electron correlation and solvation effects. I. Basic formulation and preliminary attempt to include the electron correlation in the quantum mechanical polarizable continuum model so as to study solvation phenomena”, *Chem. Phys.*, **150**, 139–150 (1991).
- [478] M. A. Aguilar, F. J. Olivares del Valle, and J. Tomasi, “Electron correlation and solvation effects. II. The description of the vibrational properties of a water molecule in a dielectric given by the application of the polarizable continuum model with inclusion of correlation effects”, *Chem. Phys.*, **150**, 151–161 (1991).
- [479] J. Ángyán, “Choosing between alternative MP2 algorithms in the self-consistent reaction field theory of solvent effects”, *Chem. Phys. Lett.*, **241**, 51–56 (1995).
- [480] F. Lipparini, G. Scalmani, and B. Mennucci, “Non covalent interactions in RNA and DNA base pairs: A quantum-mechanical study of the coupling between solvent and electronic density”, *Phys. Chem. Chem. Phys.*, **11**, 11617–11623 (2009).
- [481] R. Cammi, “Quantum cluster theory for the polarizable continuum model. I. The CCSD level with analytical first and second derivatives”, *J. Chem. Phys.*, **131**, 164104:1–14 (2009).

- [482] R. Cammi and J. Tomasi, “Quantum cluster theory for the polarizable continuum model (PCM)”, in *Handbook of Computational Chemistry*, J. Leszczynski, A. Kaczmarek-Kedziera, T. Puzyn, M. G. Papadopoulos, H. Reis, and M. K. Shukla, Eds.; Springer International Publishing: Switzerland, 2nd ed., 2017; chapter 34, pages 1517–1556.
- [483] M. Caricato, B. Mennucci, G. Scalmani, G. W. Trucks, and M. J. Frisch, “Electronic excitation energies in solution at equation of motion CCSD level within a state specific polarizable continuum model approach”, *J. Chem. Phys.*, **132**, 084102:1–7 (2010).
- [484] M. Caricato, “CCSD-PCM: Improving upon the reference reaction field approximation at no cost”, *J. Chem. Phys.*, **135**, 074113:1–11 (2011).
- [485] M. Caricato, “Coupled cluster theory in the condensed phase within the singles-T density scheme for the environment response”, *WIREs Comput. Mol. Sci.*, **10**, e1463:1–27 (2020).
- [486] S. K. Khani, A. M. Khah, and C. Hättig, “COSMO-RI-ADC(2) excitation energies and excited state gradients”, *Phys. Chem. Chem. Phys.*, **20**, 16354–16363 (2018).
- [487] A. Dreuw and M. Wormit, “The algebraic diagrammatic construction scheme for the polarization propagator for the calculation of excited states”, *WIREs Comput. Mol. Sci.*, **5**, 82–95 (2015).
- [488] M. De Vetta, M. F. S. J. Menger, J. J. Nogueira, and L. González, “Solvent effects on electronically excited states: QM/continuum versus QM/explicit models”, *J. Phys. Chem. B*, **122**, 2975–2984 (2018).
- [489] M. Cossi and V. Barone, “Time-dependent density functional theory for molecules in liquid solutions”, *J. Chem. Phys.*, **115**, 4708–4717 (2001).
- [490] R. Cammi and B. Mennucci, “Linear response theory for the polarizable continuum model”, *J. Chem. Phys.*, **110**, 9877–9886 (1999).
- [491] R. Cammi, B. Mennucci, and J. Tomasi, “Fast evaluation of geometries and properties of excited molecules in solution: A Tamm-Dancoff model with application to 4-dimethylaminobenzonitrile”, *J. Phys. Chem. A*, **104**, 5631–5637 (2000).
- [492] S. Corni and J. Tomasi, “Excitation energies of a molecule close to a metal surface”, *J. Chem. Phys.*, **117**, 7266–7278 (2002).
- [493] M. F. Iozzi, B. Mennucci, J. Tomasi, and R. Cammi, “Excitation energy transfer (EET) between molecules in condensed matter: A novel application of the polarizable continuum model (PCM)”, *J. Chem. Phys.*, **120**, 7029–7040 (2004).
- [494] R. Cammi, M. Cossi, B. Mennucci, and J. Tomasi, “Analytical Hartree–Fock calculation of the dynamical polarizabilities α , β , and γ of molecules in solution”, *J. Chem. Phys.*, **105**, 10556–10564 (1996).
- [495] I. Duchemin, C. A. Guido, D. Jacquemin, and X. Blase, “The Bethe–Salpeter formalism with polarisable continuum embedding: Reconciling linear-response and state-specific features”, *Chem. Sci.*, **9**, 4430–4443 (2018).
- [496] R. Cammi, “Coupled-cluster theories for the polarizable continuum model. II. Analytical gradients for excited states of molecular solutes by the equation of motion coupled-cluster method”, *Int. J. Quantum Chem.*, **110**, 3040–3052 (2010).

- [497] R. Cammi, “Coupled-cluster theory for the polarizable continuum model. III. A response theory for molecules in solution”, *Int. J. Quantum Chem.*, **112**, 2547–2560 (2012).
- [498] M. Caricato, “A comparison between state-specific and linear-response formalisms for the calculation of vertical electronic transition energy in solution with the CCSD-PCM method”, *J. Chem. Phys.*, **139**, 044116:1–9 (2013).
- [499] M. Caricato, “Linear response coupled cluster theory with the polarizable continuum model within the singles approximation for the solvent response”, *J. Chem. Phys.*, **148**, 134113:1–9 (2018).
- [500] M. Caricato, “CCSD-PCM excited state energy gradients with the linear response singles approximation to study the photochemistry of molecules in solution”, *ChemPhotoChem*, **3**, 747–754 (2019).
- [501] T. Helgaker, P. Jørgensen, and J. Olsen, *Molecular Electronic-Structure Theory*, Wiley: New York, 2000.
- [502] S. Corni, R. Cammi, B. Mennucci, and J. Tomasi, “Electronic excitation energies of molecules in solution within continuum solvation models: Investigating the discrepancy between state-specific and linear-response methods”, *J. Chem. Phys.*, **123**, 134512:1–10 (2005).
- [503] A. Pedone, “Role of solvent on charge transfer in 7-aminocoumarin dyes: New hints from TD-CAM-B3LYP and state specific PCM calculations”, *J. Chem. Theory Comput.*, **9**, 4087–4096 (2013).
- [504] N. Minezawa, “State-specific solvation effect on the intramolecular charge transfer reaction in solution: A linear-response free energy TDDFT method”, *Chem. Phys. Lett.*, **608**, 140–144 (2014).
- [505] C. Bernini, L. Zani, M. Calamante, G. Reginato, A. Mordini, M. Taddei, R. Basosi, and A. Sinicropi, “Excited state geometries and vertical emission energies of solvated dyes for DSSC: A PCM/TD-DFT benchmark study”, *J. Chem. Theory Comput.*, **10**, 3925–3933 (2014).
- [506] Š. Budzák, P. Mach, M. Medved’, and O. Kysel’, “Critical analysis of spectral solvent shifts calculated by the contemporary PCM approaches of a representative series of charge-transfer methylated benzenes”, *Phys. Chem. Chem. Phys.*, **17**, 17618–17627 (2015).
- [507] C. A. Guido, D. Jacquemin, C. Adamo, and B. Mennucci, “Electronic excitations in solution: The interplay between state specific approaches and a time-dependent density functional theory description”, *J. Chem. Theory Comput.*, **11**, 5782–5790 (2015).
- [508] C. A. Guido, B. Mennucci, G. Scalmani, and D. Jacquemin, “Excited state dipole moments in solution: Comparison between state-specific and linear-response TD-DFT values”, *J. Chem. Theory Comput.*, **14**, 1544–1553 (2018).
- [509] B. Klaumünzer, D. Kröner, and P. Saalfrank, “(TD-)DFT calculation of vibrational and vibronic spectra of riboflavin in solution”, *J. Phys. Chem. B*, **114**, 10826–10834 (2010).
- [510] J. Bloino, A. Baiardi, and M. Biczysko, “Aiming at an accurate prediction of vibrational and electronic spectra for medium-to-large molecules: An overview”, *Int. J. Quantum Chem.*, **116**, 1543–1574 (2016).

- [511] C. García-Irieapa, M. Zemmouche, M. Ponce-Vargas, and I. Navizet, “The role of solvation models on the computed absorption and emission spectra: The case of fireflies oxyluciferin”, *Phys. Chem. Chem. Phys.*, **21**, 4613–4623 (2019).
- [512] S. Chibani, Š. Budzák, M. Medved', B. Mennucci, and D. Jacquemin, “Full cLR-PCM calculations of the solvatochromic effects on emission energies”, *Phys. Chem. Chem. Phys.*, **16**, 26024–26029 (2014).
- [513] T. Schwabe, “General theory for environmental effects on (vertical) electron excitation energies”, *J. Chem. Phys.*, **145**, 154105:1–7 (2016).
- [514] B. Mennucci and R. Cammi, “Ab initio model to predict NMR shielding tensors for solutes in liquid crystals”, *Int. J. Quantum Chem.*, **93**, 121–130 (2003).
- [515] H. Hoshi, M. Sakurai, Y. Inoue, and R. Chûjô, “Medium effects on the molecular electronic structure. I. The formulation of a theory for the estimation of a molecular electronic structure surrounded by an anisotropic medium”, *J. Chem. Phys.*, **87**, 1107–1115 (1987).
- [516] L. Frediani, B. Mennucci, and R. Cammi, “Quantum-mechanical continuum solvation study of the polarizability of halides at the water/air interface”, *J. Phys. Chem. B*, **108**, 13796–13806 (2004).
- [517] L. Frediani, R. Cammi, S. Corni, and J. Tomasi, “A polarizable continuum model for molecules at diffuse interfaces”, *J. Chem. Phys.*, **120**, 3893–3907 (2004).
- [518] L. Bondesson, L. Frediani, H. Ågren, and B. Mennucci, “Solvation of N_3^- at the water surface: The polarizable continuum model approach”, *J. Phys. Chem. B*, **110**, 11361–11368 (2006).
- [519] M. F. Iozzi, M. Cossi, R. Imrota, N. Rega, and V. Barone, “A polarizable continuum approach for the study of heterogeneous dielectric environments”, *J. Chem. Phys.*, **124**, 184103 (2006).
- [520] D. Si and H. Li, “Heterogeneous conductorlike solvation model”, *J. Chem. Phys.*, **131**, 044123:1–8 (2009).
- [521] J.-B. Wang, J.-Y. Ma, and X.-Y. Li, “Polarizable continuum model associated with the self-consistent-reaction field for molecular adsorbates at the interface”, *Phys. Chem. Chem. Phys.*, **12**, 207–214 (2010).
- [522] K. Mozgawa, B. Mennucci, and L. Frediani, “Solvation at surfaces and interfaces: A quantum-mechanical/continuum approach including nonelectrostatic contributions”, *J. Phys. Chem. C*, **118**, 4715–4725 (2014).
- [523] K. Mozgawa and L. Frediani, “Electronic structure of small surfactants: A continuum solvation study”, *J. Phys. Chem. C*, **120**, 17501–17513 (2016).
- [524] P. Jungwirth and D. J. Tobias, “Ions at the air/water interface”, *J. Phys. Chem. B*, **106**, 6361–6373 (2002).
- [525] P. Jungwirth and D. J. Tobias, “Specific ion effects at the air/water interface”, *Chem. Rev.*, **106**, 1259–1281 (2006).
- [526] T. T. Duignan and X. S. Zhao, “The Born model can accurately describe electrostatic ion solvation”, *Phys. Chem. Chem. Phys.*, **22**, 25126–25135 (2020).

- [527] M. Chaplin, “Theory vs experiment: What is the surface charge of water?”, *Water*, **1**, 1–28 (2009).
- [528] T. T. Duignan, D. F. Parsons, and B. W. Ninham, “Ion interactions with the air–water interface using a continuum solvent model”, *J. Phys. Chem. B*, **118**, 8700–8710 (2014).
- [529] T. T. Duignan, D. F. Parsons, and B. W. Ninham, “Hydronium and hydroxide at the air–water interface with a continuum solvent model”, *Chem. Phys. Lett.*, **635**, 1–12 (2015).
- [530] H. Aksu, S. K. Paul, J. M. Herbert, and B. D. Dunietz, “How well does a solvated octa-acid capsule shield the embedded chromophore? A computational analysis based on an anisotropic dielectric continuum model”, *J. Phys. Chem. B*, **124**, 6998–7004 (2020).
- [531] J. M. Herbert and M. P. Coons, “The hydrated electron”, *Annu. Rev. Phys. Chem.*, **68**, 447–472 (2017).
- [532] J. M. J. Swanson, J. Mongan, and J. A. McCammon, “Limitations of atom-centered dielectric functions in implicit solvent models”, *J. Phys. Chem. B*, **109**, 14769–14772 (2005).
- [533] H.-X. Zhou, S. Qin, and H. Tjong, “Modeling protein–protein and protein–nucleic acid interactions: Structure, thermodynamics, and kinetics”, *Annu. Rep. Comput. Chem.*, **4**, 67–87 (2008).
- [534] X. Pang and H.-X. Zhou, “Poisson-Boltzmann calculations: van der Waals or molecular surface?”, *Commun. Comput. Phys.*, **13**, 1–12 (2013).
- [535] S. Decherchi, J. Colmenares, C. E. Catalano, M. Spagnuolo, E. Alexov, and W. Rocchia, “Between algorithm and model: Different molecular surface definitions for the Poisson-Boltzmann based electrostatic characterization of biomolecules in solution”, *Commun. Comput. Phys.*, **13**, 61–89 (2013).
- [536] W. J. Hehre, L. Radom, P. v. R. Schleyer, and J. A. Pople, *Ab Initio Molecular Orbital Theory*, Wiley-Interscience: New York, 1986.